AN ION MODE REENTRY COMMUNICATION SYSTEM

By

ROBERT BYRON BUCHANAN

Bachelor of Science
Wichita State University
Wichita, Kansas
1963

Master of Science
Oklahoma State University
Stillwater, Oklahoma
1965

Submitted to the Faculty of the Graduate College
of the Oklahoma State University
in partial fulfillment of the requirements
for the Degree of
DOCTOR OF PHILOSOPHY
May, 1968

AN ION MODE REENTRY COMMUNICATION

SYSTEM

Thesis Approved:

Kenneth R. Cook
Thesis Adviser

Arthur M. Breipohl

Kenneth A. McCollom

W. Ellis Jr. Lewis

Wm. L. Hughes

N. Durham
Dean of the Graduate College

PREFACE

The advent of spacecraft and ICBM's has made the problem of reentry communications blackout a very important one. This thesis proposes a novel approach to alleviate this problem. The preliminary evaluation of the system is done theoretically, because of the difficulty in duplicating a reentry plasma in a laboratory. It is found that the proposed communications system has some promising aspects, but that experimentation is needed to define some portions of the problem sufficiently for engineering purposes.

I wish to express my gratitude to my thesis adviser, Dr. K. R. Cook, for his valuable assistance and guidance which continued even when he no longer was with Oklahoma State University. Others who have helped me are P. T. Bauer, of the University of Dayton, and Dr. R. L. Gallawa, of the Institute of Telecommunication Sciences and Aeronomy, with a number of illuminating conversations. Finally, I express my gratitude to the National Aeronautics and Space Administration for the Predoctoral Traineeship which provided financial support of my graduate program.

TABLE OF CONTENTS

LIST OF TABLES

LIST OF FIGURES

CHAPTER I

INTRODUCTION

1.1 Statement of the Problem

The region of ionized gas which envelops a space vehicle during hypersonic entry into an atmosphere interrupts radio communication, thereby creating a "blackout" condition. Such communication blackout gives rise to many problems in space technology, and, therefore, much research has been directed toward defining and alleviating the blackout condition. For example, because of loss of ground support during blackout periods, additional vehicle payload may be needed for navigation, guidance, and redundancy in case of an onboard system failure. Real-time terminal-phase systems may be compromised, such as altimeters, ICBM homing devices, and decoy discrimination systems. The cause of blackout is now understood in a large measure, and progress is being made in preventing it.

The intense heating that occurs in the bow shock wave ionizes the gas in the shock layer between the bow shock and the vehicle surface. Because of the high temperatures and nonzero chemical reaction times, this ionization may persist as the gas flows over the vehicle and into the wake region, thus engulfing the vehicle in a layer of high concentration of free charge which can impair electromagnetic transmission from either direction because of attenuation and reflection. The following model of the interaction of an electromagnetic wave with a

plasma has usually been used to explain the blackout process.

Given a plane wave propagating in a plasma with a space variation of e^{-ikx}, a knowledge of the wave number, k, in terms of the parameters of the plasma will determine whether or not the wave is attenuated. If k is a real number, the wave propagates unattenuated in space; however, if k has an imaginary component, the exponential term is of the form $e^{-\alpha x}$ and the wave is attenuated, perhaps severely. A fashionable theory predicts that the wave number for a wave of frequency ω in a plasma is given by

$$k = k_o\left(1 - \frac{\omega_p^2/\omega^2}{1 - i\upsilon/\omega}\right)^{\frac{1}{2}} \qquad (1.1.1)$$

where ω_p is the electron plasma frequency, υ is the average collision frequency of electrons with other particles in the plasma and k_o is the wave number in free space.

The plasma frequency is the characteristic oscillating frequency of a charged particle in a plasma, and is determined by

$$\omega_p = \sqrt{\frac{N_o e^2}{m\epsilon_o}} \qquad (1.1.2)$$

where N_o is the density of charges, e and m are the charge and mass of the particle, and ϵ_o is the free space permittivity. An heuristic explanation of the plasma frequency may be visualized by first assuming that the plasma contains an equal number of positive and negative charges and may be considered macroscopically neutral. Consider, for simplicity, that the average spacing maintained by these particles due to their electrostatic fields is an equilibrium spacing. If one of the charged particles were perturbed from its equilibrium position and all other charges remained fixed, the electrostatic force of the neighboring

charges would tend to restore the perturbed charge to its equilibrium position. If the perturbed charge were released, the restoring electrostatic force would cause the charged particle to oscillate about its position of equilibrium at the characteristic oscillating frequency like a mass on a spring. The collision of the oscillating particle with other particles provides a damping force.

If collisions are neglected, the wave number for the plasma becomes

$$k = k_o\left(1 - \frac{\omega_p^2}{\omega^2}\right)^{\frac{1}{2}} \qquad (1.1.3)$$

Note that if ω_p is less than the signal frequency ω, the term in parentheses is positive, and k is real. From e^{-ikx}, one sees that the wave will propagate for this condition. However, if the plasma frequency is greater than the signal frequency, the wave number is imaginary and propagation is cut off. This is the blackout condition.

By considering Equation 1.1.2 for the electron plasma frequency, one sees that it is proportional to the square root of the average electron density. The mechanism of blackout is now apparent. The increase in temperature in the shock layer causes an increase in charged particle density, which raises the plasma frequency, thereby bringing conditions closer to the cutoff at $\omega_p = \omega$. Blackout becomes more severe as electron densities go even higher.

1.2 Previous Work in the Area

The literature related to the reentry blackout problem is much too voluminous for detailed listing in this thesis. However, the general approaches being taken toward alleviation have been summarized by Huber and Sims (1964). The research approaches discussed in their paper are:

(1) signal frequency selection, (2) aerodynamic shaping, (3) imposed magnetic fields, (4) material addition, and (5) laser communication. All of these schemes are directed at modifying the wave number k in a beneficial manner. Strictly speaking, the imposition of a static magnetic field creates an anisotropic plasma with two distinct wave numbers, one of which may allow propagation under conditions that would normally cause blackout; however, the assumptions used in developing the theory for magnetoplasmas are the same as those used in deriving the wave number k in Equation 1.1.1. In fact, Equation 1.1.1 results from magnetoplasma theory if the magnitude of the imposed static magnetic field is set equal to zero. Therefore, all of the above research approaches rely upon the same theoretical model of an electromagnetic wave in a plasma. In 1967 Dunphy, Kahn, and Mintzer wrote a paper on energy coupling at a plasma density discontinuity and mentioned the possibility of using electroacoustic modes to penetrate the plasma sheath; however, the idea is not developed.

1.3 Outline of the Method of Solution

The subsequent text will present some basic material on electromagnetic phenomena in plasmas in an attempt to show that the usual set of simplifying assumptions concerning reentry plasmas appear to have obscured the existence of a mode of energy propagation through the reentry sheath which will, in theory, propagate for all signal frequencies and electron densities. If two of these assumptions are eliminated, the theoretical model is a better approximation to an actual reentry plasma. Some interesting phenomena are predicted by the more general theory which might be employed in a reentry communication system. The

development of the more general theoretical model of a reentry plasma, the proposal of a communication system based on this model, and a theoretical investigation of the practicality of the system comprise the remainder of this thesis.

CHAPTER II

THE HOT TWO-FLUID PLASMA MODEL OF A REENTRY SHEATH

2.1 Basic Equations and Plane Wave Propagation

If an equilibrium plasma is assumed to be an ideal isotropic gas composed of equal numbers of electrons and singly-charged ions, both of which are free to move in the presence of a force field, and, if local perturbations of the field quantities are assumed to be time-harmonic and small with respect to the overall average, one may derive the following equations to describe the behavior of a collisionless plasma. These equations are derived in Appendix A and are due to Oster (1960):

$$\nabla\times\vec{H} = i\omega\epsilon_o\vec{E} + Ne(\vec{v}_i - \vec{v}_e) \qquad \nabla\cdot\vec{H} = 0 \tag{2.1.1}$$

$$\nabla\times\vec{E} + i\omega\mu_o\vec{H} = 0 \qquad \nabla\cdot\vec{E} = \frac{e}{\epsilon_o}(n_i - n_e) \tag{2.1.2}$$

$$im_i\omega N_o\vec{v}_i = N_o e\vec{E} - m_i u_i^2 \nabla n_i \tag{2.1.3}$$

$$im_e\omega N_o\vec{v}_e = -N_o e\vec{E} - m_e u_e^2 \nabla n_e \tag{2.1.4}$$

$$i\omega n_i + N_o\nabla\cdot\vec{v}_i = 0 \tag{2.1.5}$$

$$i\omega n_e + N_o\nabla\cdot\vec{v}_e = 0 \tag{2.1.6}$$

where,

$\vec{E}$, $\vec{H}$ = electric and magnetic fields,

$\vec{v}$ = particle velocity,

m = particle mass,

n = variation in particle density,

e = magnitude of electronic charge,

ϵ_o, μ_o = permittivity and permeability of free space,

ω = radian frequency,

u = mean thermal velocity in particle gas = $(3kT/m)^{\frac{1}{2}}$,

N_o = steady state particle density,

and the subscripts "e" and "i" refer to electron and ion quantities, respectively.

Equations 2.1.3 and 2.1.4 may be rewritten using the linearized equation of state for an ideal gas, $P = mnu^2$.

We then have

$$im_i\omega N_o\vec{v}_i = N_oe\vec{E} - \nabla P_i \tag{2.1.7}$$

$$im_e\omega N_o\vec{v}_e = -N_oe\vec{E} - \nabla P_e \tag{2.1.8}$$

where P is the variation in pressure in the particle gas.

Likewise, Equations 2.1.5 and 2.1.6 may be written as

$$-u_i^2m_iN_o\nabla\cdot\vec{v}_i = i\omega P_i \tag{2.1.9}$$

$$-u_e^2m_eN_o\nabla\cdot\vec{v}_e = i\omega P_e \tag{2.1.10}$$

The basic equations will now be arranged to show that a compressible, two-fluid plasma will support three modes of propagation, an optical or electromagnetic mode and two plasma or electroacoustic modes. The basic procedure to be followed is due to Cohen (1961), and begins by applying the Helmholtz Principle to decompose the fields into solenoidal and irrotational fields. All necessary constraints are assumed to be satisfied.

Assume

$$\vec{E} = \vec{E}_o + \vec{E}_p \quad , \quad \nabla\cdot\vec{E}_o = 0 \quad , \quad \nabla x\vec{E}_p = 0$$

$$\vec{H} = \vec{H}_o + \vec{H}_p \quad , \quad \nabla\cdot\vec{H}_o = 0 \quad , \quad \nabla x\vec{H}_p = 0$$

$$\vec{v}_e = \vec{v}_{oe} + \vec{v}_{pe}, \ \nabla\cdot\vec{v}_{oe} = 0 \quad , \quad \nabla x\vec{v}_{pe} = 0$$

$$\vec{v}_i = \vec{v}_{oi} + \vec{v}_{pi}, \ \nabla\cdot\vec{v}_{oi} = 0 \quad , \quad \nabla x\vec{v}_{pi} = 0$$

By substituting these relations into Equations 2.1.1 through 2.1.10 and following procedures similar to those involved in deriving the wave equation in free space, the following result is obtained:

$$\vec{H} = \vec{H}_o \quad , \quad \vec{E} = \vec{E}_o + \vec{E}_p \tag{2.1.11}$$

where

$$\nabla^2\vec{H}_o + K_o^2\vec{H}_o = 0 \tag{2.1.12}$$

$$\nabla^2\vec{E}_o + K_o^2\vec{E}_o = 0 \tag{2.1.13}$$

$$\vec{E}_p = \frac{1}{N_o e(1 - x_e - x_i)} [x_e \nabla P_e - x_i \nabla P_i] \tag{2.1.14}$$

and

$$K_o^2 = \omega^2 \mu_o \epsilon_o (1 - x_e - x_i)$$

$$x_e = \omega_{pe}^2/\omega^2$$

$$x_i = \omega_{pi}^2/\omega^2$$

$$\omega_{pe}^2 = N_o e^2/m_e \epsilon_o \quad \text{(electron plasma frequency)}$$

$$\omega_{pi}^2 = N_o e^2/m_i \epsilon_o \quad \text{(ion plasma frequency)}$$

The optical or electromagnetic mode fields are given by $\vec{E}_o$ and $\vec{H}_o$

which satisfy the familiar wave equation with wave number k_o. The plasma mode field is determined from the pressure gradients ∇P_e and ∇P_i; if P_e and P_i are determined, a solution may be obtained for the plasma field $\vec{E}_p$. It is interesting to note at this point that the magnetic field, $\vec{H}$, is entirely associated with the optical mode and that the free charge density is entirely associated with the plasma modes ($\nabla \cdot \vec{E}_o = 0$). The optical mode is, of course, transverse; however, the plasma mode is a longitudinal field, hence the designation "electroacoustic".

To determine the pressure terms, Equations 2.1.11 and 2.1.14 are substituted into Equations 2.1.7 and 2.1.8 to yield

$$\vec{v}_i = \vec{v}_{oi} + \vec{v}_{pi} \quad , \quad \vec{v}_e = \vec{v}_{oe} + \vec{v}_{pe} \tag{2.1.15}$$

where

$$\vec{v}_{oi} = -\frac{ie}{\omega m_i}\vec{E}_o \quad , \quad \vec{v}_{oe} = \frac{ie}{\omega m_e}\vec{E}_o \tag{2.1.16}$$

$$\begin{bmatrix} \vec{v}_{pe} \\ \vec{v}_{pi} \end{bmatrix} = -\frac{i}{\omega N_o \epsilon}\begin{bmatrix} \frac{x_i - 1}{m_e} & \frac{x_i}{m_e} \\ \frac{x_e}{m_i} & \frac{x_e - 1}{m_i} \end{bmatrix} \nabla \begin{bmatrix} P_e \\ P_i \end{bmatrix} \tag{2.1.17}$$

where

$$\epsilon = 1 - x_e - x_i$$

or,

$$\begin{bmatrix} \vec{v}_{pe} \\ \vec{v}_{pi} \end{bmatrix} = -\frac{i}{\omega N_o \epsilon}\hat{A}\nabla\vec{P} \tag{2.1.18}$$

From the continuity Equations 2.1.9 and 2.1.10 we have

$$\nabla \cdot \begin{bmatrix} \vec{v}_{pe} \\ \vec{v}_{pi} \end{bmatrix} = - \frac{i\omega}{N_o u_e^2 m_e} \begin{bmatrix} P_e \\ P_i \end{bmatrix} \tag{2.1.19}$$

where the relationship

$$u_e^2 m_e = u_i^2 m_i = 3kT$$

has been used.

Now, Equations 2.1.17 and 2.1.19 may be combined to yield

$$\nabla^2 \vec{P} - \frac{\epsilon \omega^2}{u_e^2 m_e} \hat{A}^{-1} \vec{P} = \vec{0} \tag{2.1.20}$$

or

$$\nabla^2 \begin{bmatrix} P_e \\ P_i \end{bmatrix} + \frac{\omega^2 m_i}{u_e^2} \begin{bmatrix} \frac{1 - x_e}{m_i} & \frac{x_i}{m_e} \\ \frac{x_e}{m_i} & \frac{1 - x_i}{m_e} \end{bmatrix} \begin{bmatrix} P_e \\ P_i \end{bmatrix} = \vec{0} \tag{2.1.21}$$

Therefore, the pressure terms P_e and P_i satisfy two coupled wave equations (see Equation 2.1.21). It is interesting to note that if the assumption $m_i = m_e$ is made, both equations in Equation 2.1.21 reduce to the equation describing pressure in a one-fluid electron plasma.

Writing Equation 2.1.21 as

$$\nabla^2 \vec{P} + \hat{T} \vec{P} = \vec{0} \tag{2.1.22}$$

It is noted that $\hat{T}$ is real and symmetric. This is because

$$\frac{x_i}{m_e} = \frac{x_e}{m_i} = \frac{N_o e^2}{m_e m_i \omega^2 \epsilon_o}$$

Therefore, the matrix $\hat{T}$ may be diagonalized by a unitary transformation which will decouple the two wave equations. Losses caused by particle

collisions were not included in the plasma equations, because in that case $\hat{T}$ would not be symmetric. The equations for the lossy case follow from Equation 2.1.21 by substituting

$$x_e = \frac{x_e}{1 - i\upsilon_e/\omega} \quad , \quad x_i = \frac{x_i}{1 - i\upsilon_i/\omega}$$

where υ_e = electron collision frequency

υ_i = ion collision frequency.

Generally speaking, υ_e and υ_i are quite a bit different in a plasma so the resulting matrix in the lossy case will not be symmetric. For this reason, losses are ignored. Some consideration of losses is given in Chapter VI.

To diagonalize $\hat{T}$, define the following transformation

$$\vec{P} = \hat{M}\,\vec{\vec{P}} = \begin{bmatrix} m_{11} & m_{12} \\ m_{21} & m_{22} \end{bmatrix} \begin{bmatrix} P_1 \\ P_2 \end{bmatrix} \tag{2.1.23}$$

Then,

$$\nabla^2\vec{\vec{P}} + (\hat{M}^{-1}\hat{T}\hat{M})\,\vec{\vec{P}} = \vec{0}$$

The matrix $\hat{M}$ is chosen so that

$$\hat{M}^{-1}\hat{T}\hat{M} = D[\lambda_1, \lambda_2]$$

where λ_1 and λ_2 are the eigenvalues of $\hat{T}$, found by solving the determinantal equation $\det(\hat{T} - \lambda\hat{I}) = 0$. After some algebra, the eigenvalues of $\hat{T}$ are found to be

$$\lambda_1 = \frac{\omega^2 m_i}{2u_e^2}\left\{\frac{1 - x_e}{m_i} + \frac{1 - x_i}{m_e} + \left[\left(\frac{1 - x_e}{m_i} + \frac{1 - x_i}{m_e}\right)^2 - \frac{4(1 - x_e - x_i)}{m_e m_i}\right]^{\frac{1}{2}}\right\}$$

$$\lambda_2 = \frac{\omega^2 m_i}{2u_e^2}\left\{\frac{1 - x_e}{m_i} + \frac{1 - x_i}{m_e} - \left[\left(\frac{1 - x_e}{m_i} + \frac{1 - x_i}{m_e}\right)^2 - \frac{4(1 - x_e - x_i)}{m_e m_i}\right]^{\frac{1}{2}}\right\} \tag{2.1.24}$$

Thus, for source free regions,

$$\nabla^2 P_1 + K_1^2 P_1 = 0$$
$$\nabla^2 P_2 + K_2^2 P_2 = 0 \qquad (2.1.25)$$

where $K_1^2 = \lambda_1$, $K_2^2 = \lambda_2$.

Note that $K_2 = 0$ at $1 - x_e - x_i = 0$, which means that the mode of propagation described by P_2 is evanescent or nonpropagating for frequencies less than the plasma frequency. However, K_1^2 is always real and positive, so the P_1 mode always propagates.

Thus, we have seen that a warm, two-fluid plasma will support three modes of propagation: (1) the optical or electromagnetic mode, (2) the P_1 mode, and (3) the P_2 mode. The P modes are called electroacoustic or plasma modes. The optical field may be found from a vector potential $\vec{\Pi}$, and the field due to plasma modes may be found from the transformed pressures P_1 and P_2 which may be considered as scalar potentials. The fields are thus determined by solution of the three simultaneous Helmholtz equation:

$$\nabla^2 \vec{\Pi} + K_o^2 \vec{\Pi} = 0$$
$$\nabla^2 P_1 + K_1^2 P_1 = 0$$
$$\nabla^2 P_2 + K_2^2 P_2 = 0$$

together with boundary conditions that remain to be presented.

Seshadri (1965) has investigated the phase velocity of the three modes with wave numbers K_o, K_1, and K_2. Figure 1 illustrates his results. It is seen that although the optical and P_2 mode suffer cutoff at the electron plasma frequency, the P_1 mode propagates for all signal

frequencies. In the limiting case of high signal frequency, the P_2 mode phase velocity approaches the mean electron thermal velocity, and the P_1 mode velocity approaches the ion thermal velocity; therefore, the P_1 and P_2 modes will be called the ion and electron modes, respectively. However, it is pointed out that the ion and electron modes are actually both linear combinations of electron and ion waves and are not purely due to the motion of one specie of particle as the names might imply.

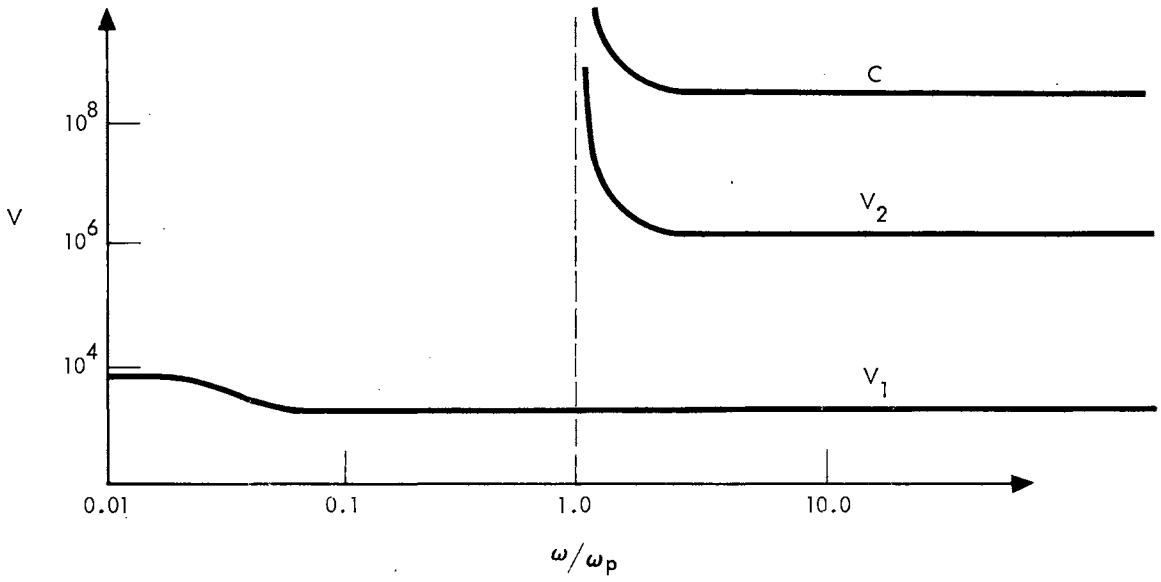

Figure 1. Phase Velocity in a Two-Fluid Plasma

Application of boundary conditions in later work will require expression of $\vec{E}_p$ in terms of P_1 and P_2. To accomplish this, recall that

$$\begin{bmatrix} P_e \\ P_i \end{bmatrix} = \begin{bmatrix} m_{11} & m_{12} \\ m_{21} & m_{22} \end{bmatrix} \begin{bmatrix} P_1 \\ P_2 \end{bmatrix}$$

and the m_{ij} are chosen such that

$$\hat{M}^{-1}\hat{T}\hat{M} = D[\lambda_1, \lambda_2]$$

where

$$\hat{T} = \frac{\omega^2 m_i}{u_e^2} \begin{bmatrix} \frac{1 - x_e}{m_i} & \frac{x_i}{m_e} \\ \frac{x_e}{m_i} & \frac{1 - x_i}{m_e} \end{bmatrix}$$

Now,

$$\hat{T}\hat{M} = \hat{M}D[\lambda_1, \lambda_2]$$

$$\begin{bmatrix} t_{11} & t_{12} \\ t_{21} & t_{22} \end{bmatrix} \begin{bmatrix} m_{11} & m_{12} \\ m_{21} & m_{22} \end{bmatrix} = \begin{bmatrix} m_{11} & m_{12} \\ m_{21} & m_{22} \end{bmatrix} \begin{bmatrix} \lambda_1 & 0 \\ 0 & \lambda_2 \end{bmatrix}$$

or,

$$\begin{bmatrix} t_{11} & t_{12} \\ t_{21} & t_{22} \end{bmatrix} \begin{bmatrix} m_{11} \\ m_{21} \end{bmatrix} = \lambda_1 \begin{bmatrix} m_{11} \\ m_{21} \end{bmatrix} \tag{2.1.27}$$

and

$$\begin{bmatrix} t_{11} & t_{12} \\ t_{21} & t_{22} \end{bmatrix} \begin{bmatrix} m_{12} \\ m_{22} \end{bmatrix} = \lambda_2 \begin{bmatrix} m_{12} \\ m_{22} \end{bmatrix} \tag{2.1.28}$$

Considering the matrix $\hat{T}$ as an operator, the vector (m_{11}, m_{21}) is an

eigenvector of $\hat{T}$ corresponding to the eigenvalue λ_1. Likewise, the vector (m_{12}, m_{22}) is an eigenvector of the operator $\hat{T}$ corresponding to the eigenvalue λ_2.

It may be shown that a real self-adjoint matrix can be transformed into a diagonal matrix by an orthogonal transformation (Friedman, 1956). The transformation for $\hat{T}$ may be determined by finding an eigenvector of $\hat{T}$ from Equation 2.1.27. Because the eigenvectors of a self-adjoint operator which correspond to different eigenvalues are orthogonal, a vector orthogonal to the eigenvector for λ_1 will be an eigenvector corresponding to λ_2.

Therefore, from Equation 2.1.27

$$\begin{aligned} (t_{11} - \lambda_1)m_{11} + t_{12}m_{21} &= 0 \\ t_{21}m_{11} + (t_{22} - \lambda_1)m_{21} &= 0 \end{aligned} \tag{2.1.29}$$

These equations have nontrivial solutions for m_{11} and m_{21} since λ_1 is an eigenvalue of $\hat{T}$. One such solution will be taken for the first column of $\hat{M}$ and normalized. A unit vector orthogonal to the first vector will be chosen for the second column of $\hat{M}$.

Thus, from Equation 2.1.29,

$$m_{21} = \frac{\lambda_1 - t_{11}}{t_{12}} m_{11}$$

To normalize,

$$m_{11}^2 + m_{21}^2 = 1$$

or,

$$m_{11}^2 + \left[\frac{\lambda_1 - t_{11}}{t_{12}}\right]^2 m_{11}^2 = 1$$

Therefore,

$$m_{11} = \frac{t_{12}}{[t_{12}^2 + (\lambda_1 - t_{11})^2]^{\frac{1}{2}}}$$

$$m_{21} = \frac{\lambda_1 - t_{11}}{[t_{12}^2 + (\lambda_1 - t_{11})^2]^{\frac{1}{2}}}$$

And the first normalized eigenvector is

$$M_1 = \left\{ \frac{t_{12}}{[t_{12}^2 + (\lambda_1 - t_{11})^2]^{\frac{1}{2}}} \quad , \quad \frac{\lambda_1 - t_{11}}{[t_{12}^2 + (\lambda_1 - t_{11})^2]^{\frac{1}{2}}} \right\}$$

The second eigenvector must satisfy

$$m_{11}m_{12} + m_{21}m_{22} = 0$$

or

$$\frac{t_{12}}{[t_{12}^2 + (\lambda_1 - t_{11})^2]^{\frac{1}{2}}} m_{12} + \frac{(\lambda_1 - t_{11})}{[t_{12}^2 + (\lambda_1 - t_{11})^2]^{\frac{1}{2}}} m_{22} = 0$$

Solving,

$$m_{12} = \frac{t_{11} - \lambda_1}{t_{12}}$$

After normalizing, the second eigenvector is

$$M_2 = \left\{ \frac{t_{11} - \lambda_1}{[t_{12}^2 + (\lambda_1 - t_{11})^2]^{\frac{1}{2}}} \quad , \quad \frac{t_{12}}{[t_{12}^2 + (\lambda_1 - t_{11})^2]^{\frac{1}{2}}} \right\}$$

so,

$$\overset{\frown}{M} = [t_{12}^2 + (\lambda_1 - t_{11})^2]^{\frac{1}{2}} \begin{bmatrix} t_{12} & t_{11} - \lambda_1 \\ \lambda_1 - t_{11} & t_{12} \end{bmatrix}$$

where λ_1 is given by Equation 2.1.24 and

$$t_{11} = \frac{\omega^2}{u_e^2}(1 - x_e)$$

$$t_{12} = \frac{\omega^2 x_e}{u_e^2}$$

Note that

$$\det \hat{M} = 1$$

$$M_1 \cdot M_2 = 0$$

From the definition

$$\begin{bmatrix} P_e \\ P_i \end{bmatrix} = \begin{bmatrix} m_{11} & m_{12} \\ m_{21} & m_{22} \end{bmatrix} \begin{bmatrix} P_1 \\ P_2 \end{bmatrix}$$

we have

$$\nabla P_e = m_{11}\nabla P_1 + m_{12}\nabla P_2$$

$$\nabla P_i = m_{21}\nabla P_1 + m_{22}\nabla P_2$$

Substitution into

$$\vec{E}_p = \frac{1}{\epsilon N_o e}\left[x_e \nabla P_e - x_i \nabla P_i\right]$$

reveals the desired result

$$\vec{E}_p = \frac{1}{\epsilon N_o e}\left[(x_e m_{11} - x_i m_{21})\nabla P_1 - (x_i m_{22} - x_e m_{12})\nabla P_2\right] \qquad (2.1.32)$$

or,

$$\vec{E}_p = \alpha_1 \nabla P_1 - \alpha_2 \nabla P_2 \qquad (2.1.33)$$

where

$$\alpha_1 = (x_e m_{11} - x_i m_{21})/\epsilon N_o e$$

$$\alpha_2 = (x_i m_{22} - x_e m_{12})/\epsilon N_o e$$

To determine the velocities in terms of P_1 and P_2, recall

$$\begin{bmatrix} \vec{v}_{pe} \\ \\ \vec{v}_{pi} \end{bmatrix} = \frac{-i}{\epsilon\omega N_o} \begin{bmatrix} A_{11} & A_{12} \\ \\ A_{21} & A_{22} \end{bmatrix} \nabla \begin{bmatrix} P_e \\ \\ P_i \end{bmatrix}$$

where

$$A_{11} = \frac{x_i - 1}{m_e} \qquad A_{12} = \frac{x_i}{m_e}$$

$$A_{21} = \frac{x_e}{m_i} \qquad A_{22} = \frac{x_e - 1}{m_i}$$

Substitution for (P_e, P_i) reveals

$$\begin{bmatrix} \vec{v}_{pe} \\ \\ \vec{v}_{pi} \end{bmatrix} = - \frac{i}{\epsilon\omega N_o} \begin{bmatrix} (A_{11}m_{11} + A_{12}m_{21}) & (A_{11}m_{12} + A_{12}m_{22}) \\ \\ (A_{21}m_{11} + A_{22}m_{21}) & (A_{21}m_{12} + A_{22}m_{22}) \end{bmatrix} \nabla \begin{bmatrix} P_1 \\ \\ P_2 \end{bmatrix} \quad (2.1.34)$$

or,

$$\begin{bmatrix} \vec{v}_{pe} \\ \\ \vec{v}_{pi} \end{bmatrix} = \begin{bmatrix} \beta_{11} & \beta_{12} \\ \\ \beta_{21} & \beta_{22} \end{bmatrix} \nabla \begin{bmatrix} P_1 \\ \\ P_2 \end{bmatrix} \quad (2.1.35)$$

2.2 Boundary Conditions and Mode Coupling

By including the effects of ion motion and a nonzero plasma temperature, it is seen that three modes of propagation may exist, one of which is electromagnetic, the others, electroacoustic. To apply this model of a plasma to a reentry sheath, two types of boundaries must be considered: (1) the solid boundary between the surface of the space vehicle and the plasma, and (2) the boundary between plasma and air

defined by the bow shock wave.

The physics of actual boundaries is a complicated matter, and the boundary conditions commonly used in the theory of compressible plasmas are, regrettably, not entirely realistic. However, in the interest of having a tractable mathematical model, and for lack of a more realistic understanding of boundary processes, the following boundary conditions are adopted for the case of two continuous plasmas. The derivation of these boundary conditions is given in Appendix B.

$$\begin{aligned} \hat{n}\times[\vec{E}_1 - \vec{E}_2] &= 0 \\ \hat{n}\times[\vec{H}_1 - \vec{H}_2] &= 0 \\ \hat{n}\cdot[n_{o1}\vec{v}_{i1} - n_{o2}\vec{v}_{i2}] &= 0 \\ \hat{n}\cdot[n_{o1}\vec{v}_{e1} - n_{o2}\vec{v}_{e2}] &= 0 \end{aligned} \qquad (2.2.1)$$

For the case of a boundary between a perfect conductor and the compressible two-fluid plasma, we have:

$$\begin{aligned} \hat{n}\times\vec{E} &= 0 \\ \hat{n}\cdot\vec{v}_e &= 0 \\ \hat{n}\cdot\vec{v}_i &= 0 \end{aligned} \qquad (2.2.2)$$

For the boundary between the plasma and air, $n_{o2} = 0$, and the conditions are:

$$\begin{aligned} \hat{n}\times[\vec{E}_1 - \vec{E}_2] &= 0 \\ \hat{n}\times[\vec{H}_1 - H_2] &= 0 \\ \hat{n}\cdot\vec{v}_i &= 0 \\ \hat{n}\cdot\vec{v}_e &= 0 \end{aligned}$$

If one recalls that the total electric field $\vec{E}$ and velocity field $\vec{v}$ are composed of terms from both the optical and plasma modes, it is apparent that a discontinuity in the plasma will allow coupling between the modes. From a mathematical standpoint, the solutions of the three wave equations must be adjusted so that the boundary conditions on the total field are satisfied. This coupling between modes has been studied for the one-fluid plasma by a number of workers. Gallawa (1965, 1966) has studied the case of a plasma mode wave incident upon a plasma-free space interface; and, it is noted that the incident plasma mode converts partially into an optical mode on the free space side of the boundary. The plasma in Gallawa's investigation did not include ion motion; however, the principle of mode conversion should hold true for the case of an ion mode wave incident upon a plasma-air interface. That is, one would expect that a portion of the power in the incident ion mode would be transmitted through the boundary in the form of an optical mode; the magnitude of this conversion is the subject of Chapter V.

2.3 Justification of Assumptions

The preceding material on compressible two-fluid plasmas has been presented with the intent of applying the theory to the reentry plasma sheath. Before doing so, it seems fitting to examine the assumptions involved in terms of what is known about reentry plasma.

Considering the assumption of a compressible plasma, recall that the basic differential equations showed compressibility to become more significant as the temperature was increased. Whale (1963, 1964) published results of rocket soundings that indicate that the ionosphere is significantly compressible. Electroacoustic waves in warm plasmas also

appear to have been demonstrated experimentally by Chen, Judson, and Lin (1967); Sessler (1967); and Aksornkitti, Hsuan, and Lonngren (1967). Because a typical reentry sheath is very much hotter than the plasmas in these experiments, one would expect the reentry plasma to be compressible.

Inclusion of ion motion may be justified by recalling that the ion plasma frequency is actually the characteristic oscillation frequency of an ion in the plasma, and is given by

$$\omega_{pi} = \sqrt{\frac{N_o e^2}{m_i \epsilon_o}} \qquad (2.3.1)$$

In the case of the ionosphere, N_o is low enough so that ω_{pi} is of the order of 100 to 1000 Hz.; the signal frequency is usually well above the ion plasma frequency, and the ions should not respond to the signal. However, for a reentry plasma, the blackout problem itself results from the fact that charge densities are much too high - say on the order of 10^{14} cm^{-3}. Under these conditions, the characteristic response frequency of the ions is in the microwave spectrum, i.e., usual communications frequencies are near the ion frequency, and significant ion motion will probably occur.

CHAPTER III

THE ION MODE REENTRY COMMUNICATION SYSTEM

3.1 Theory of Operation

It has been shown to this point that a reentry plasma may support an ion mode which will propagate for all signal frequencies and that an ion mode incident on the bow shock will convert partially to an electromagnetic wave on the outside of the sheath. The possibility of an ion mode reentry communication system is now apparent: place an antenna on the reentry body which will radiate significantly in the ion mode in such a manner that acceptable conversion to electromagnetic radiation takes place at the boundary of the sheath.

Because of the intense aerodynamic heating during the reentry phase one would expect that the antenna would be of the aperture type in order to survive. The technology of antenna survivability is probably well-developed by now, so this factor will not be considered further.

The problem of antenna location must be studied, because the ion mode is essentially acoustical and, therefore, sensitive to motion of the supporting medium. In most cases, the phase velocity of the ion mode is of the same order of magnitude as the vehicle reentry velocity. Figure 2 illustrates a simplified description of the flow field surrounding two common reentry shapes (Pope and Goin, 1965). Note that the plasma is hypersonic in most of the sheath and quite turbulent in the

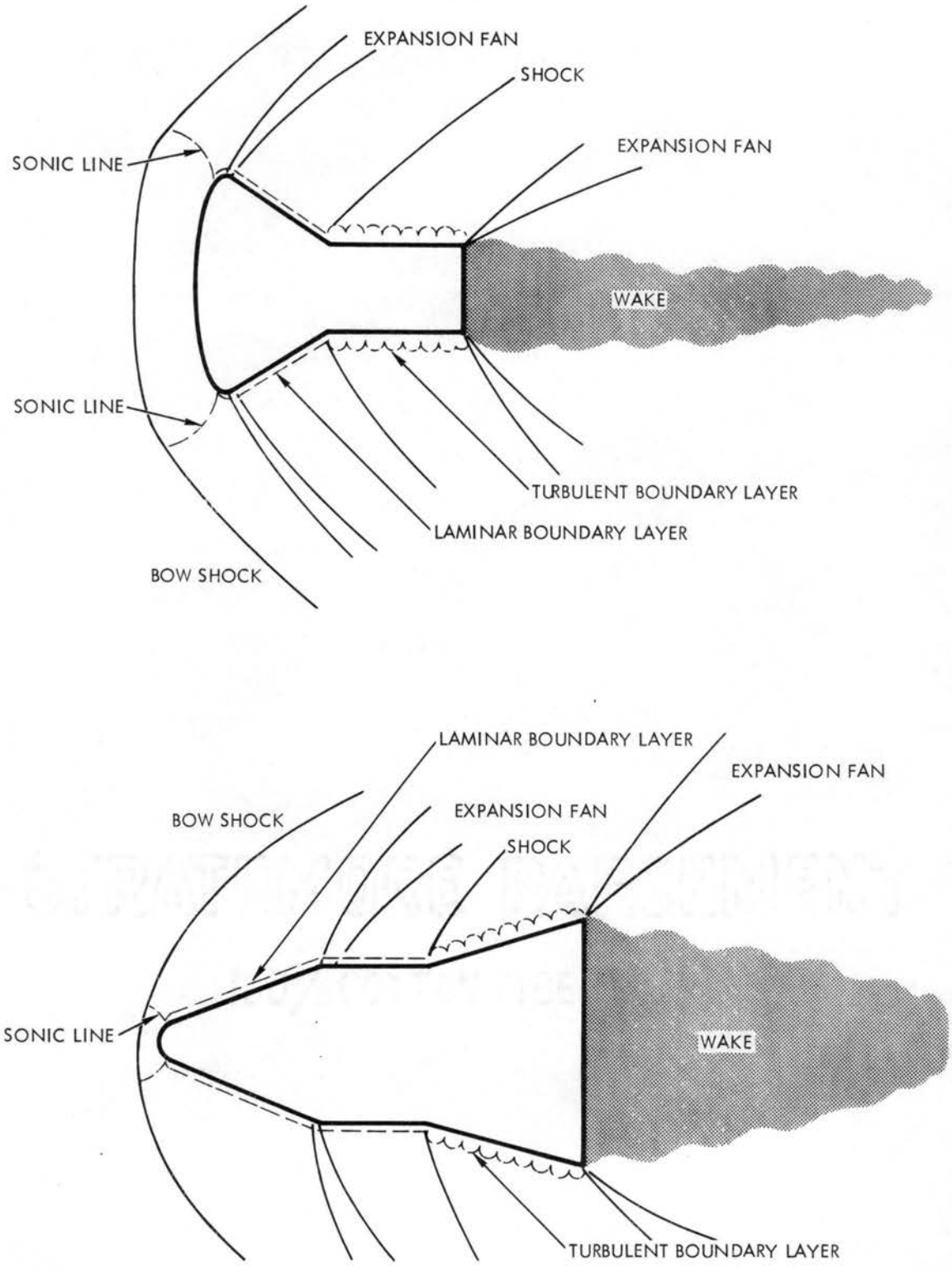

Figure 2. Typical Reentry Flow Fields

wake; one would therefore expect that an ion mode signal propagating in such a plasma would suffer wholesale destruction of phase fronts and become unintelligible. Therefore, unless the hypersonic regions can be avoided, the ion mode cannot be used.

Fortunately, the bow region of the sheath is close to the stagnation point, and the plasma velocity in this region is low subsonic. The plasma remains subsonic until it crosses the sonic line (see Figure 2) where a rapid transition to hypersonic flow occurs. Therefore, an ion mode signal should propagate with little interference in the bow region.

Because the ion mode is not driven into cutoff by high electron density, the fact that the bow region has the highest electron density of any location in the sheath is not important. Moreover, two factors in addition to low gas velocity make the bow region attractive. First, the bow region has the highest temperature, and thus, the greatest compressible plasma behavior. Second, the shape of the normal bow shock is usually not extremely sensitive to changing angle of attack during reentry; this has implications on the mode conversion at the shock front (see Chapter V).

3.2 Formulation of the Theoretical Model

Having discussed the theory of operation of the ion mode reentry communication system, a theoretical performance study will now be made. A sketch of a blunt reentry body with a detached bow shock wave is shown in Figure 3. The antenna aperture operates into the hot stagnation region of the plasma.

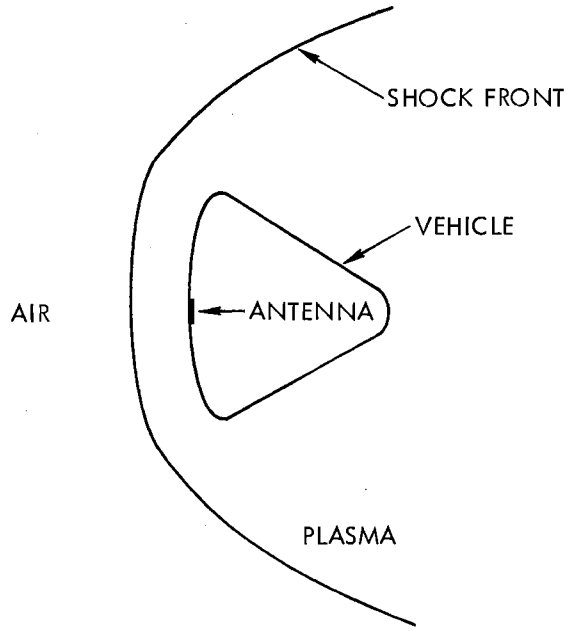

Figure 3. A Blunt Reentry Vehicle with Ion Mode System

Because the stagnation region gas velocity is at least an order of magnitude below the phase velocity of the ion mode, the plasma in the theoretical model is assumed to be stationary. The great portion of the previous work in plasma theory has neglected the motion of ions, mainly because the inclusion of ion motion greatly increases the amount of tedious algebra. In order to compensate for the inclusion of ion motion in the present problem, a simple geometry will be chosen.

Because the wave length of the ion mode is usually very short, it is probably not a bad approximation to neglect curvature of the reentry

vehicle and shock wave; therefore, a rectangular coordinate system is chosen and the boundaries are assumed to be planar and infinite in extent.

A first step in the investigation of radiation in a compressible plasma is to consider elemental sources such as a Hertzian dipole (Seshadri, 1965) or a slot of infinitesimal width (Wait, 1964 a & b). Therefore, to gain understanding of the basic phenomena of aperture radiation into a two-fluid plasma, the problem of an infinitesimal slot will be considered. Assuming that the heat shield can be made conductive within several wavelengths of the aperture, the slot will be assumed to be situated in a perfectly conducting ground plane of infinite extent. The solution of this problem may be taken as the radiation from an aperture of very narrow width or as the Green's function for treating more complicated apertures.

Because of the need for a tractable theoretical model, the shock front forming the outer boundary of the plasma sheath will be assumed to be a sharp discontinuity between equilibrium plasma and free space. Furthermore, a rigid boundary condition will be used (vanishing normal particle velocity). Although this assumption seems necessary to be able to handle the mathematics, it is not realistic. Chapter V discusses the physics of real hypersonic shock fronts and the qualitative behavior of an ion mode wave encountering the shock.

The geometry of the theoretical model at this point is shown in Figure 4.

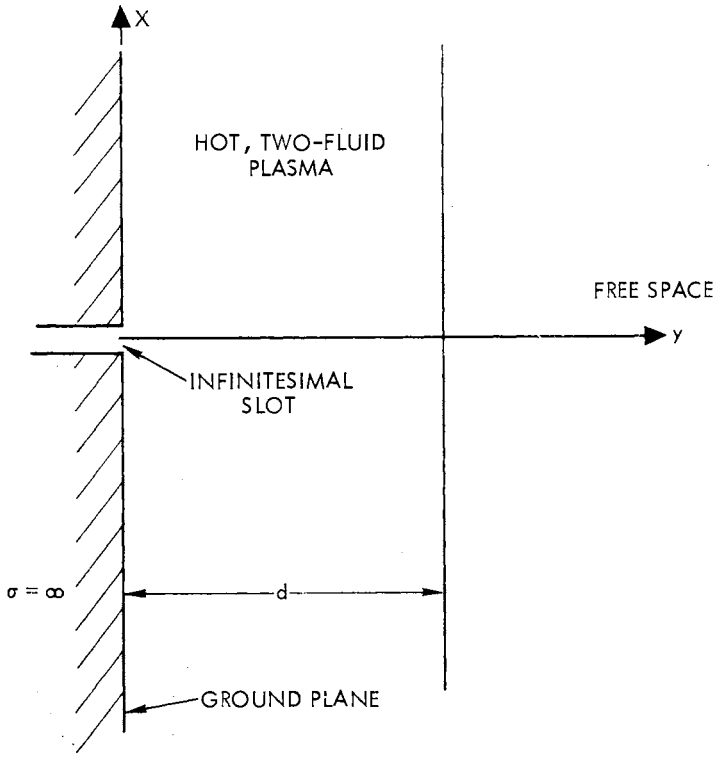

Figure 4. Slab of Plasma Over a Ground Plane

While the geometry of a homogeneous slab of plasma over a perfectly conducting ground plane certainly seems simple, the mathematics involved in the evaluation of the radiation pattern is quite burdensome. To elaborate, the above problem was formulated using Fourier transform techniques. The field potentials were expressed as integrals of the form

$$\Pi_j(x_1 y) = \int_{-\infty}^{\infty} A_j(\lambda) e^{-i(K_j^2 - \lambda^2)^{\frac{1}{2}} y} e^{-i\lambda x} d\lambda$$

where the $A_j(\lambda)$ are determined from the boundary conditions at $y = 0$ and $y = d$. Because the plasma region supports outgoing and reflected waves

in all three modes and the free space region supports a single outward traveling mode, seven coefficients must be determined. Application of the boundary conditions yields a 7x7 matrix equation of the form

$$[a_{ij}]_{7x7} \cdot (A_j(\lambda)) = (e)$$

The solution for the transmitted field coefficient will be of the form

$$A_k(\lambda) = \frac{N(\lambda)}{D(\lambda)}$$

where $D(\lambda) = \det [a_{ij}]$. Because the determinant of a 7x7 matrix has 7! or 5,040 terms, a formal solution for $A_k(\lambda)$ seems almost unmanageable. This does not consider the difficulties in evaluation of the Fourier inversion integral. Therefore, further approximations will be made to arrive at a reasonable problem.

To be more exact, the problem of the plasma slab over a ground plane should be solved; however, conditions in an actual reentry sheath during communications blackout support to some extent the division into two simpler problems: (1) radiation by a slot into a plasma half-space, and (2) mode conversion at a plasma-vacuum boundary.

It is likely that physical processes existing in the actual reentry sheath will produce attenuation of the ion mode signal which is not predicted by the linearized, collisionless plasma model used in the present analysis. Because the wavelength of the ion mode at radio frequencies is short, a typical plasma sheath will be many wavelengths thick for a reasonable shock detachment of ten centimeters. If a moderate amount of attenuation occurs over the distance to the shock, then ion mode reflections from the plasma boundary will not interfere with radiation

from the aperture. Because the electron and optical modes are highly attenuated under blackout conditions, these fields will not be significant at the boundary; this statement was tested by calculating attenuation at d = 10 cm for electron and optical mode wave numbers in the blackout spectrum. Therefore, relying on the heuristic argument of ion mode losses due to the nonideal character of an actual reentry plasma, the aperture will radiate very nearly as it would into an infinite half-space of hot, two-fluid plasma. The approximation of lossy materials by an infinite region of the material has been used with success in waveguide measurement of dielectric properties and in calculation of radar cross section of lossy dielectric bodies. In evaluating practicality of the ion mode communication system, the attenuation over the path through the sheath must be included; however, this must be determined by experiment.

In retrospect, the solution of the problem of the aperture radiating into a plasma half space revealed the possibility of a surface wave bound to the ground plane with wave number close to the ion mode number. However, calculations showed that the amplitude of the surface wave was severely attenuated at typical shock detachment distances. Therefore, in blackout conditions, the illumination of the plasma-vacuum boundary may be essentially due to the ion mode space wave. This being the case, the slab problem has been separated into two simpler problems. The ion mode radiation from the aperture into a half-space can be assumed to illuminate the plasma boundary, and the fields in the free space region will approximate those in the original slab problem.

Because the boundary is separated from the aperture by a large number of ion mode wave lengths, the constant phase surfaces will be nearly

planar; thus, it will be assumed that the plasma boundary is illuminated by ion mode plane waves with phase and amplitude origin at the aperture and an angular variation given by the radiation pattern of the aperture in the plasma half space (see Figure 5).

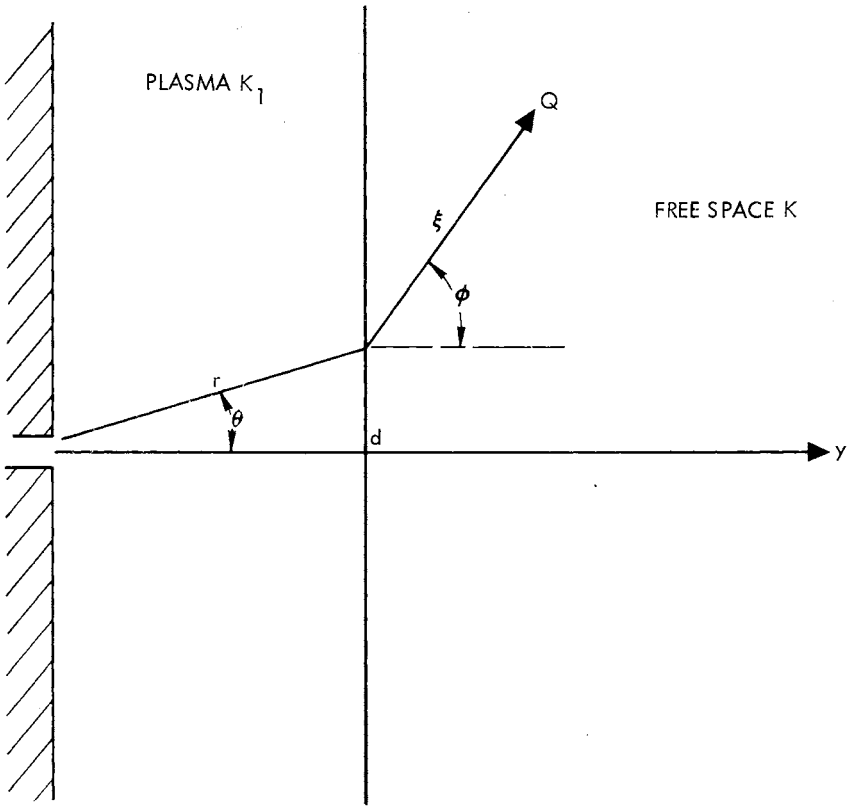

Figure 5. Ray Path Through Plasma Slab

Assume that the ion radiation pattern in the half-space of plasma is given by

$$P_1(R,\theta) = F(K,\theta)e^{-i\bar{K}_1\cdot\bar{r}}$$

with attenuation included in the ion mode wave number as

$$K_1 = \beta_1 - i\alpha_1$$

Therefore, the boundary illumination is

$$P_1 = F(K,\theta)e^{-\alpha_1 r}e^{-i\beta_1 r}$$

where it is apparent that the phase and amplitude of the field distribution on the boundary will vary as a function of both the aperture radiation pattern $F(K,\theta)$ and the distance, r, from the aperture to the boundary point. The radiation pattern in the optical mode may be found approximately using the above ion mode illumination.

Generally speaking, the conversion from ion to optical mode will depend on the wave number and angle of incidence of the illuminating waves. Moreover, the conversion process will produce a change in amplitude and direction of the energy density; let this change in energy density distribution be represented by the operator $\hat{L}(K,\theta)$ such that the electric field at a typical free-space point Q (see Figure 5) is given by

$$E(R,\Phi) = \hat{L}(K,\theta)F(K,\theta)e^{-\alpha_1 r}e^{-i(\beta_1 r + k\xi)}$$

Solution of the boundary problem (see Chapter V) yields the Snell's law relation

$$K_1 \sin \theta_i = K \sin \Phi$$

where

K_1 = ion mode wave number

θ_i = angle of incidence for ion mode

K = free space wave number

Φ = angle of optical mode transmission.

In the reentry plasma, K_1 is orders of magnitude greater than K. Due to familiar Brewster angle effects, conversion to the optical mode at a sharp boundary will not occur if θ_1 exceeds

$$\theta_c = \sin^{-1}\left(\frac{K}{K_1}\right)$$

which is a very small angle. Because no optical mode radiation field will be produced by ion mode radiation that impinges on the boundary at angles greater than θ_c, it may be assumed that the boundary is not illuminated at angles greater than θ_c without affecting the radiation field distribution in free space. This assumption is represented by

$$E(R,\Phi) = \begin{cases} L(K,\theta_i)F(K,\theta_i)e^{-\alpha_1 r}e^{-i(\beta_1 r + K\xi)} & |\theta_i| < \theta_c \\ 0 & \text{Otherwise} \end{cases}$$

Because θ_c is so small, r is essentially invariant in the range $|\theta_i| < \theta_c$, and may be closely approximated by r = d. Thus,

$$E(r,\Phi) = \hat{L}(K,\theta)F(K,\theta)e^{-\alpha_1 d}e^{-i\beta_1 d}e^{-iK\xi}$$

Letting $E_o = e^{-\alpha_1 d}e^{-i\beta_1 d}$

$$E(r,\Phi) = E_o\hat{L}(K,\theta)F(K,\theta)e^{-iK\xi}$$

Therefore, the very burdensome problem of radiation from the aperture covered by the plasma slab may be treated approximately by considering the two simpler problems of radiation into the half-space to determine $F(K,\theta)$ and mode conversion at the boundary to find $\hat{L}(K,\theta)$. These two problems will now be treated in detail, and engineering

recommendations will be based on the results.

CHAPTER IV

RADIATION FROM A SLOTTED GROUND PLANE INTO A TWO-FLUID, COMPRESSIBLE PLASMA HALF SPACE

4.1 The Formal Solution

The geometry chosen for the ground plane problem is shown in Figure 6.

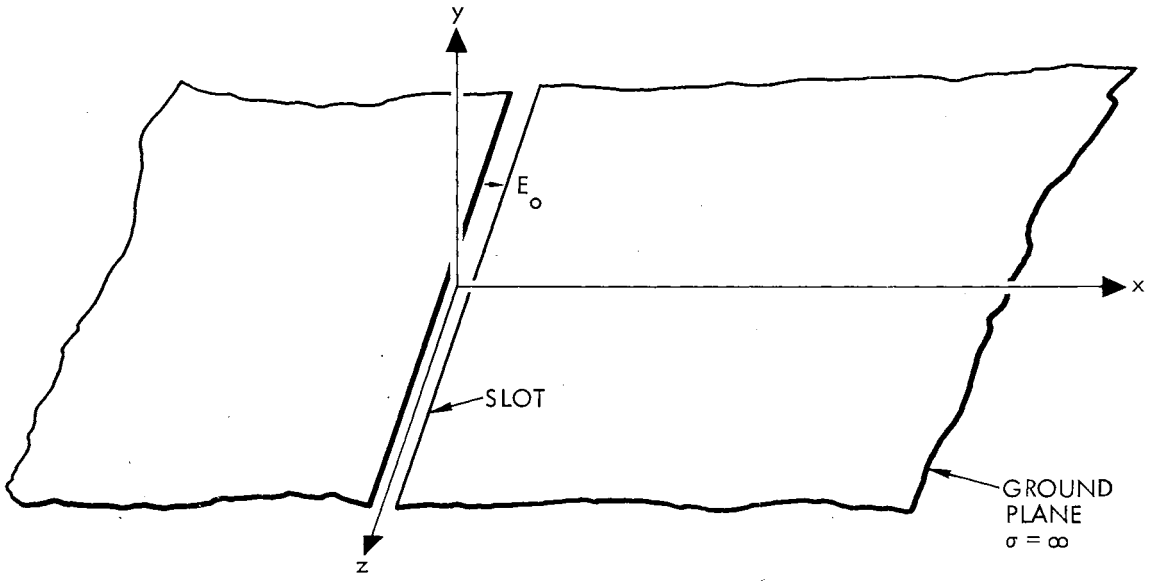

Figure 6. Geometry of the Ground Plane Problem

The region $y > 0$ is filled with a compressible two-fluid plasma, and the excitation slot is assumed to be rigid and of infinitesimal width.

The excitation is assumed to be

$$\vec{E}^i = E_o \delta(x) \hat{u}_x \text{ on } y = 0$$

From earlier sections, the following equations must be solved in the region $y > 0$.

$$\nabla^2 \vec{\Pi} + K_o^2 \vec{\Pi} = 0$$
$$\nabla^2 P_1 + K_1^2 P_1 = 0$$
$$\nabla^2 P_2 + K_2^2 P_2 = 0$$

such that the following boundary conditions are met at $y = 0$:

$$\begin{aligned} \hat{n} \times (\vec{E}_o + \vec{E}_p) &= \hat{n} \times \vec{E}^i \\ \hat{n} \cdot (\vec{v}_{oe} + \vec{v}_{pe}) &= 0 \\ \hat{n} \cdot (\vec{v}_{oi} + \vec{v}_{pi}) &= 0 \end{aligned} \qquad (4.1.1)$$

and such that the fields behave properly at infinity.

There is no field variation in the z-direction and $E_z = 0$ over the entire ground plane, therefore the solution for the optical mode will be constructed TE to z.

Let $\vec{\Pi} = \Pi \hat{u}_z$ be chosen as the vector potential so that

$$\vec{E}_o = - \nabla \times \vec{\Pi} \quad , \quad \vec{H}_o = - i\omega\varepsilon \vec{\Pi} + \frac{1}{i\omega\mu_o} \nabla(\nabla \cdot \vec{\Pi}) \qquad (4.1.2)$$

Expanding in rectangular coordinates,

$$E_{ox} = - \frac{\partial \Pi}{\partial y} \quad , \quad E_{oy} = \frac{\partial \Pi}{\partial x} \quad , \quad E_{oz} = 0$$

The total field is

$$\vec{E} = \vec{E}_o + \vec{E}_p \quad , \quad \vec{v} = \vec{v}_o + \vec{v}_p$$

or

$$\begin{aligned}
E_x &= -\frac{\partial \Pi}{\partial y} + \alpha_1 \frac{\partial P_1}{\partial x} - \alpha_2 \frac{\partial P_2}{\partial x} \\
E_y &= \frac{\partial \Pi}{\partial x} + \alpha_1 \frac{\partial P_1}{\partial y} - \alpha_2 \frac{\partial P_2}{\partial y} \\
v_{iy} &= -\frac{ie}{\omega m_i} \frac{\partial \Pi}{\partial x} + \beta_{21} \frac{\partial P_1}{\partial y} + \beta_{22} \frac{\partial P_2}{\partial y} \\
v_{ey} &= \frac{ie}{\omega m_e} \frac{\partial \Pi}{\partial x} + \beta_{11} \frac{\partial P_1}{\partial y} + \beta_{12} \frac{\partial P_2}{\partial y}
\end{aligned} \tag{4.1.3}$$

With no z-variation, the potentials must satisfy

$$\left(\frac{\partial^2}{\partial x^2} + \frac{\partial^2}{\partial y^2} + K_o^2\right)\Pi(x,y) = 0$$

$$\left(\frac{\partial^2}{\partial x^2} + \frac{\partial^2}{\partial y^2} + K_1^2\right) P_1(x,y) = 0$$

$$\left(\frac{\partial^2}{\partial x^2} + \frac{\partial^2}{\partial y^2} + K_2^2\right) P_2(x,y) = 0$$

If the basic solution is taken to be of the form

$$\psi = F(y)e^{-i\lambda x}$$

substitution into $\nabla^2\psi + K^2\psi = 0$ shows that $F(y) \sim e^{\pm i\sqrt{K^2 - \lambda^2}\, y}$.

Choosing the minus sign to ensure outgoing waves, the general solutions for the three potentials are taken to be superpositions of the basic solutions, or

$$\begin{aligned}
\Pi(x,y) &= \int_{-\infty}^{\infty} A_o(\lambda) e^{-i\sqrt{K_o^2 - \lambda^2}\, y} e^{-i\lambda x} d\lambda \\
P_1(x,y) &= \int_{-\infty}^{\infty} A_1(\lambda) e^{-i\sqrt{K_1^2 - \lambda^2}\, y} e^{-i\lambda x} d\lambda
\end{aligned} \tag{4.1.4}$$

$$P_2(x,y) = \int_{-\infty}^{\infty} A_2(\lambda) e^{-i\sqrt{K_2^2 - \lambda^2}\, y} e^{-i\lambda x} d\lambda$$

where the $A_j(\lambda)$ are determined from the boundary conditions at y = 0:

$$- \frac{ie}{\omega m_i} \frac{\partial \Pi}{\partial x} + \beta_{21} \frac{\partial P_1}{\partial y} + \beta_{22} \frac{\partial P_2}{\partial y} = 0 \qquad (4.1.5)$$

$$\frac{ie}{\omega m_e} \frac{\partial \Pi}{\partial x} + \beta_{11} \frac{\partial P_1}{\partial y} + \beta_{12} \frac{\partial P_2}{\partial y} = 0 \qquad (4.1.6)$$

$$- \frac{\partial \Pi}{\partial y} + \alpha_1 \frac{\partial P_1}{\partial x} - \alpha_2 \frac{\partial P_2}{\partial x} = E_o \delta(x) = E_o \int_{-\infty}^{\infty} e^{-i\lambda x} d\lambda \qquad (4.1.7)$$

Substituting Equation 4.1.4 into Equation 4.1.5

$$- \frac{ie}{\omega m_i} \int_{-\infty}^{\infty} (-i\lambda) A_o(\lambda) e^{-i\lambda x} d\lambda + \beta_{21} \int_{-\infty}^{\infty} (-i\sqrt{K_1^2 - \lambda^2}) A_1(\lambda) e^{i\lambda x} d\lambda$$

$$+ \beta_{22} \int_{-\infty}^{\infty} (-i\sqrt{K_2^2 - \lambda^2}) A_2(\lambda) e^{-i\lambda x} d\lambda = 0$$

It follows that the sum of the integrands must be zero, and

$$- \frac{ie}{\omega m_i} \lambda A_o(\lambda) + \beta_{21} \sqrt{K_1^2 - \lambda^2}\, A_1(\lambda) + \beta_{22} \sqrt{K_2^2 - \lambda^2}\, A_2(\lambda) = 0 \qquad (4.1.8)$$

From Equation 4.1.6

$$\frac{ie}{\omega m_e} \int_{-\infty}^{\infty} (-i\lambda) A_o(\lambda) e^{-i\lambda x} d\lambda + \beta_{11} \int_{-\infty}^{\infty} (-i\sqrt{K_1^2 - \lambda^2}) A_1(\lambda) e^{-i\lambda x} d\lambda$$

$$+ \beta_{12} \int_{-\infty}^{\infty} (-i\sqrt{K_2^2 - \lambda^2}) A_2(\lambda) e^{i\lambda x} d\lambda = 0$$

or,

$$\frac{ie}{\omega m_e} \lambda A_o(\lambda) + \beta_{11} \sqrt{K_1^2 - \lambda^2}\, A_1(\lambda) + \beta_{12} \sqrt{K_2^2 - \lambda^2}\, A_2(\lambda) = 0 \qquad (4.1.8)$$

And, from Equation 4.1.7

$$-\int_{-\infty}^{\infty}(-i\sqrt{K_o^2-\lambda^2})A_o(\lambda)e^{-\lambda x}d\lambda+\alpha_1\int_{-\infty}^{\infty}(-i\lambda)A_1e^{-i\lambda x}d\lambda-\alpha_2\int_{-\infty}^{\infty}(-i\lambda)A_2e^{-\lambda x}d\lambda=$$

$$E_o\int_{-\infty}^{\infty}e^{i\lambda x}d\lambda$$

or,

$$-\sqrt{K_o^2-\lambda^2}\,A_o(\lambda)+\alpha_1\lambda A_1(\lambda)-\alpha_2\lambda A_2(\lambda)=iE_o \qquad (4.1.9)$$

Therefore, the three $A_j(\lambda)$ may be found by solving

$$\begin{bmatrix} -\frac{ie\lambda}{\omega m_i} & \beta_{21}\sqrt{K_1^2-\lambda^2} & \beta_{22}\sqrt{K_2^2-\lambda^2} \\ \frac{ie}{\omega m_e}\lambda & \beta_{11}\sqrt{K_1^2-\lambda^2} & \beta_{12}\sqrt{K_2^2-\lambda^2} \\ -\sqrt{K_o^2-\lambda^2} & \alpha_1\lambda & -\alpha_2\lambda \end{bmatrix}\begin{bmatrix} A_o(\lambda) \\ A_1(\lambda) \\ A_2(\lambda) \end{bmatrix}=\begin{bmatrix} 0 \\ 0 \\ iE_o \end{bmatrix} \qquad (4.1.10)$$

Straightforward use of Cramer's Rule reveals:

$$A_o(\lambda)=-iE_o\frac{C_3\sqrt{K_1^2-\lambda^2}\,\sqrt{K_2^2-\lambda^2}}{C_1\lambda^2\sqrt{K_1^2-\lambda^2}+C_2\lambda^2\sqrt{K_2^2-\lambda^2}+C_3\sqrt{K_o^2-\lambda^2}\,\sqrt{K_1^2-\lambda^2}\,\sqrt{K_2^2-\lambda^2}} \qquad (4.1.11)$$

$$A_1(\lambda)=-E_o\frac{C_4\lambda\sqrt{K_2^2-\lambda^2}}{C_1\lambda^2\sqrt{K_1^2-\lambda^2}+C_2\lambda^2\sqrt{K_2^2-\lambda^2}+C_3\sqrt{K_o^2-\lambda^2}\,\sqrt{K_1^2-\lambda^2}\,\sqrt{K_2^2-\lambda^2}} \qquad (4.1.12)$$

$$A_2(\lambda)=E_o\frac{C_5\lambda\sqrt{K_1^2-\lambda^2}}{C_1\lambda^2\sqrt{K_1^2-\lambda^2}+C_2\lambda^2\sqrt{K_2^2-\lambda^2}+C_3\sqrt{K_o^2-\lambda^2}\,\sqrt{K_1^2-\lambda^2}\,\sqrt{K_2^2-\lambda^2}} \qquad (4.1.13)$$

where

$$C_1=\frac{ie}{\omega m_i}\alpha_2\beta_{11}+\frac{ie}{\omega m_e}\alpha_2\beta_{21}$$

$$C_2=\frac{ie}{\omega m_i}\alpha_1\beta_{12}+\frac{ie}{\omega m_e}\alpha_1\beta_{22}$$

$$C_3 = \beta_{11}\beta_{22} - \beta_{21}\beta_{12}$$

$$C_4 = \frac{e\beta_{12}}{\omega m_i} + \frac{e\beta_{22}}{\omega m_e}$$

$$C_5 = \frac{e\beta_{11}}{\omega m_i} + \frac{e\beta_{21}}{\omega m_e}$$

Recall the integral solutions for the three mode potentials:

$$\Pi(x,y) = \int_{-\infty}^{\infty} A_o(\lambda) e^{-i\sqrt{K_o^2-\lambda^2}\, y_e - i\lambda x} d\lambda$$

$$P_1(x,y) = \int_{-\infty}^{\infty} A_1(\lambda) e^{-i\sqrt{K_1^2-\lambda^2}\, y_e - i\lambda x} d\lambda$$

$$P_2(x,y) = \int_{-\infty}^{\infty} A_2(\lambda) e^{-i\sqrt{K_2^2-\lambda^2}\, y_e - i\lambda x} d\lambda$$

where the A_j have been determined.

In cylindrical coordinates,

$$x = R \cos\theta$$

$$y = R \sin\theta$$

Therefore,

$$\Pi(R,\theta) = \int_{-\infty}^{\infty} A_o(\lambda) e^{-iR\left[\sqrt{K_o^2-\lambda^2} \sin\theta + \lambda\cos\theta\right]} d\lambda$$

$$P_1(R,\theta) = \int_{-\infty}^{\infty} A_1(\lambda) e^{-iR\left[\sqrt{K_1^2-\lambda^2} \sin\theta + \lambda\cos\theta\right]} d\lambda$$

$$P_2(R,\theta) = \int_{-\infty}^{\infty} A_2(\lambda) e^{-iR\left[\sqrt{K_2^2-\lambda^2} \sin\theta + \lambda\cos\theta\right]} d\lambda$$

The contributions to the above integrals will arise from the poles of the A_j which may indicate surface waves, and from the saddle points, which give the space waves. The space waves are the only ones that contribute to the desired radiation; therefore, they will be given greater emphasis.

4.2 Evaluation of Integrals

The formal solution of the ground plane problem has produced three integrals of the form

$$I(R,\theta) = \int_{-\infty}^{\infty} G(\lambda) e^{R\Phi(\lambda)} d\lambda$$

where $\Phi(\lambda) = -i[(K^2-\lambda^2)^{\frac{1}{2}}\sin\theta + \lambda\cos\theta]$.

Because $G(\lambda)$ has branch points at $\pm K_1$, $\pm K_2$, $\pm K_o$, representation of all values of $G(\lambda)$ requires a Riemann surface of eight sheets. The eight sheets represent all values of $G(\lambda)$ by including all possible combinations of values of the $(K_j^2 - \lambda^2)^{\frac{1}{2}}$. These are given in detail in the table below.

TABLE I

ARGUMENTS OF RADICALS ON THE RIEMANN SURFACE

Sheet	Sign of $(K_o^2-\lambda^2)^{\frac{1}{2}}$	Sign of $(K_1^2-\lambda^2)^{\frac{1}{2}}$	Sign of $(K_2^2-\lambda^2)^{\frac{1}{2}}$
1	+	+	+
2	+	+	-
3	+	-	+
4	-	+	+
5	-	-	+
6	+	-	-
7	-	-	-
8	-	+	-

However, the integration must be performed on a sheet where the integrals converge, that is, on a sheet where $\Phi(\lambda)$ has a negative real part. Therefore, we require

$$\left.\begin{aligned} &\text{Im } \lambda < 0 \\ &\text{Im}(K^2-\lambda^2)^{\frac{1}{2}} < 0 \end{aligned}\right\} \text{ for } 0 \le \theta \le \frac{\pi}{2}$$

$$\left.\begin{aligned} &\text{Im } \lambda > 0 \\ &\text{Im}(K^2-\lambda^2)^{\frac{1}{2}} < 0 \end{aligned}\right\} \text{ for } \frac{\pi}{2} \le \theta \le \pi$$

All integrations will be performed on the spectral sheet where the above conditions hold for $K^2 = K_o^2, K_1^2, K_2^2$; therefore, all three integrals will converge on the spectral sheet.

The branch cuts in the λ-plane may be located by the loci $\text{Im}(K^2-\lambda^2)^{\frac{1}{2}} = 0$, where $K^2 = K_o^2, K_1^2, K_2^2$. Consider the branch cuts for K_1^2. Letting $\lambda = \sigma + i\omega$,

$$(K_1^2-\lambda^2)^{\frac{1}{2}} = (K_1^2 - \sigma^2 + \omega^2 - i2\sigma\omega)^{\frac{1}{2}}$$

Assuming small losses, $K_1 = K_1' - iK_1''$ where K_1' and K_1'' are positive,

$$(K_1^2-\lambda^2)^{\frac{1}{2}} = \left\{K_1'^2 - K_1''^2 - \sigma^2 + \omega^2 - i2(\sigma\omega + K_1'K_1'')\right\}^{\frac{1}{2}}$$

Therefore, the branch cut is the hyperbola $\sigma\omega = -K_1'K_1''$. Similar results occur for the K_o and K_2 branch cuts as shown in Figure 7. As losses approach zero, the branch cuts approach the dotted lines on the axes. In the blackout spectrum, K_o and K_2 are imaginary, and their branch cuts coincide with the imaginary axis.

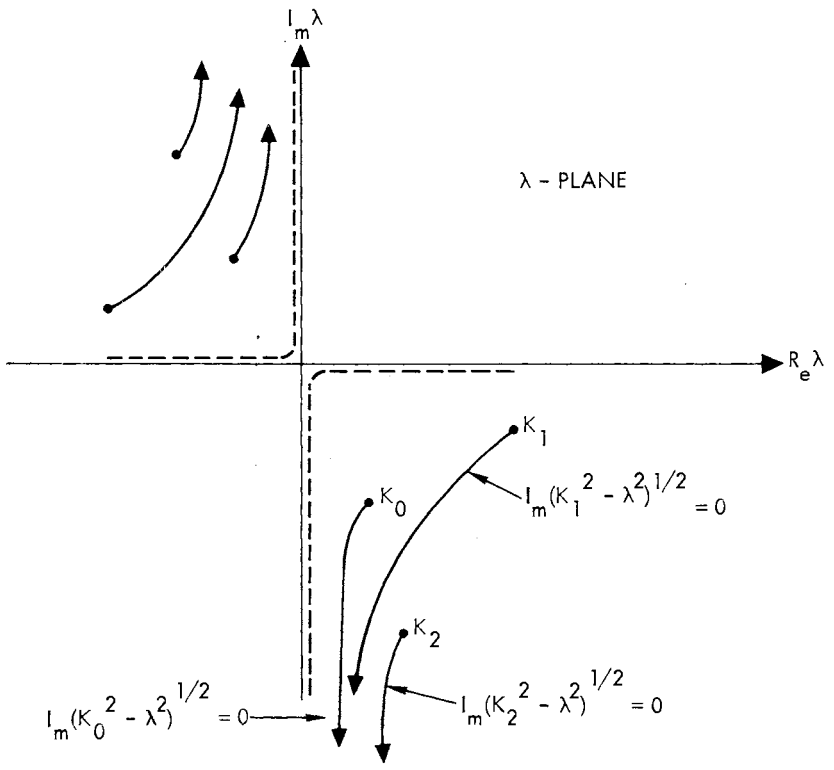

Figure 7. Branch Cuts in the λ-Plane

The singularities of the integrands must be known to complete the picture of the λ-plane. Recall that all three integrands are of the form

$$G(\lambda) = \frac{N(\lambda)}{D(\lambda)}$$

where

$$D(\lambda) = C_1\lambda^2(K_1^2-\lambda^2)^{\frac{1}{2}} + C_2\lambda^2(K_2^2-\lambda^2)^{\frac{1}{2}} + C_3(K_0^2-\lambda^2)^{\frac{1}{2}}(K_1^2-\lambda^2)^{\frac{1}{2}}(K_2^2-\lambda^2)^{\frac{1}{2}}$$

The singularities of the integrand occur where $D(\lambda) = 0$. Locating the

zeros of $D(\lambda)$ requires a great deal of algebraic detail; in fact, a complete formal solution is probably impossible. However, the general character of the zeros was determined by using a specific numerical calculation in the blackout spectrum. The numerical method involved: (1) expanding $D(\lambda)$ into a polynomial equation in λ, (2) evaluating all roots of the polynomial using a standard computer method, and (3) testing the roots to see which ones were actual poles on the spectral sheet and would therefore contribute to the field structure.

The polynomial equation was of the form

$$A_6\lambda^{12} + A_5\lambda^{10} + A_4\lambda^8 + A_3\lambda^6 + A_2\lambda^4 + A_1\lambda^2 + A_0 = 0$$

where the coefficients are complicated functions of the wave numbers and the C_j. The high degree of many of the terms in the A_j expressions required that great pains be taken in precise computation. All possible roots were computed for $\omega = 10^{10}$ where

$$C_1 = 0.29346661 \times 10^{-3}$$

$$C_2 = -.71670240 \times 10^{-7}$$

$$C_3 = 0.61530723 \times 10^{-7}$$

$$K_0^2 = -.52964758 \times 10^{7}$$

$$K_1^2 = .50224426 \times 10^{12}$$

$$K_2^2 = -.43657346 \times 10^{13}$$

The value $\omega = 10^{10}$ was chosen because it is close to both the assumed ion plasma frequency and the usual microwave voice communication frequencies. The resulting roots of the polynomial equation were directly substituted into the original expression $D(\lambda) = 0$ to determine if they were roots on the spectral sheet where $\mathrm{Im}(K^2-\lambda^2)^{\frac{1}{2}} < 0$. Only one of the

roots was found to be a true pole of the integrand on the spectral sheet, with the remaining roots corresponding to virtual poles. The computed true pole was

$$\lambda_p^2 = 0.50224456 \times 10^{12}$$

The solution for $P_1(R,\theta)$ includes the residue at this pole which describes the field structure of a surface wave propagating along the ground plane with a wave number slightly greater than K_1. This seems quite plausible from a physical standpoint; however, in order to prove that a surface wave indeed exists, we must demonstrate that the group velocity (energy flow) is directed away from the aperture. This was not done because a surface wave would not contribute to the radiation; the wave number was used only to show that the wave amplitude would be highly attenuated at typical shock detachment distances. This being so for the example, illumination of the plasma-air boundary may not be affected by a surface wave. The complexity of the integrand of

$$I(R,\theta) = \int_{-\infty}^{\infty} G(\lambda) e^{R\Phi(\lambda)} d\lambda$$

forces exact solution to be abandoned in favor of a useful approximation. If the function $G(\lambda)$ is well behaved in the region of integration, $I(R,\theta)$ may be approximated in the radiation zone by the saddle point method of analysis, which is generally accredited to Debye. A detailed development of the saddle point technique is omitted here, because excellent discussions have appeared elsewhere (Felsen and Marcuvitz, 1959).

If $G(\lambda)$ is well behaved, the saddle point of the integrand is given

by λ_o such that

$$\frac{d\Phi(\lambda)}{d\lambda}\Big|_{\lambda = \lambda_o} = 0$$

Assume that the original path of integration is transformed to the contour of steepest descent on which $Im\Phi(\lambda) = Im\Phi(\lambda_o)$. By expanding $G(\lambda)$ in a power series on the contour and evaluating the resulting integral term-by-term, a power series expression for $I(R,\theta)$ may be developed. Provided $G(\lambda)$ is well behaved near λ_o, $I(R,\theta)$ may be approximated by the first term in the series, namely:

$$\lim_{R \to \infty} I(R,\theta) \cong G(\lambda_o) e^{R\Phi(\lambda_o)} \left[\frac{-\pi}{2R\Phi''(\lambda_o)}\right]^{\frac{1}{2}}$$

If, however, $G(\lambda)$ has unusual behavior near the saddle point, more terms of the series must be retained; the reader is referred to Felsen and Marcuvitz for a detailed discussion of such special cases. Because the blackout spectrum is of primary interest, the ion mode integral will be studied in detail. We have

$$P_1(R,\theta) = \int_{-\infty}^{\infty} G(\lambda) e^{R\Phi(\lambda)} d\lambda$$

where

$$\Phi(\lambda) = -i[(K_1^2-\lambda^2)^{\frac{1}{2}} \sin\theta + \lambda \cos\theta]$$

and

$$G(\lambda) = -C_4 \frac{\lambda(K_2^2-\lambda^2)^{\frac{1}{2}}}{C_1\lambda^2(K_1^2-\lambda^2)^{\frac{1}{2}} + C_2\lambda^2(K_2^2-\lambda^2)^{\frac{1}{2}} + C_3(K_o^2-\lambda^2)^{\frac{1}{2}}(K_1^2-\lambda^2)^{\frac{1}{2}}(K_2^2-\lambda^2)^{\frac{1}{2}}}$$

The integration will be simpler if we make the transformation

$$\lambda = K_1 \sin \Phi$$

so that

$$P_1(R,\theta) = \int_C G(\Phi) e^{-iK_1 R \sin(\theta + \Phi)} K_1 \cos \Phi \, d\Phi$$

To study the transformation in some detail, let $\Phi = \sigma + i\omega$, then

$$\lambda = K_1[\sin \sigma \cosh \omega + i \sinh \omega \cos \sigma] \qquad (4.2.1)$$

The imaginary axis of the λ-plane maps onto the imaginary axis of the Φ-plane, and the real axis is mapped as

$$\lambda = K_1 \sin \sigma \cosh \omega.$$

If $0 < \theta < \pi/2$, Im $\lambda < 0$ is required for convergence and the contour of integration is indented around the poles so that the pole on the positive real axis is enclosed in the first quadrant of the λ-plane and the pole on the negative axis is not enclosed. This ensures that the residue of the enclosed pole describes an outward traveling wave. For $\pi/2 < \theta < \pi$, the opposite indentation is chosen.

By considering the signs of the trigonometric and hyperbolic functions in Equation 4.2.1, it is seen that the λ-plane is mapped onto the fundamental strip of the Φ-plane $-\pi < \sigma < \pi$, $-\infty < \omega < \infty$ in the following manner.

TABLE II

MAPPING OF THE λ-PLANE

λ-plane		Φ-plane
First Quadrant	$0 < \sigma < \pi/2$	$\pi/2 < \sigma < \pi$
	$0 < \omega < \infty$	$-\infty < \omega < 0$
Second Quadrant	$-\pi/2 < \sigma < 0$	$-\pi < \sigma < -\pi/2$
	$0 < \omega < \infty$	$-\infty < \omega < 0$
Third Quadrant	$-\pi/2 < \sigma < 0$	$-\pi < \sigma < -\pi/2$
	$-\infty < \omega < 0$	$0 < \omega < \infty$
Fourth Quadrant	$0 < \sigma < \pi/2$	$\pi/2 < \sigma < \pi$
	$-\infty < \omega < 0$	$0 < \omega < \infty$

Because sin Φ is periodic with period 2π, the λ-plane maps similarly onto any vertical strip of width 2π centered at $\sigma = 2K\pi$ $K = \pm 1, \pm 2, \ldots$ in the Φ-plane. However, only the fundamental strip is of interest for the integration.

The transformed contour C is shown in the Φ-plane in Figure 8.

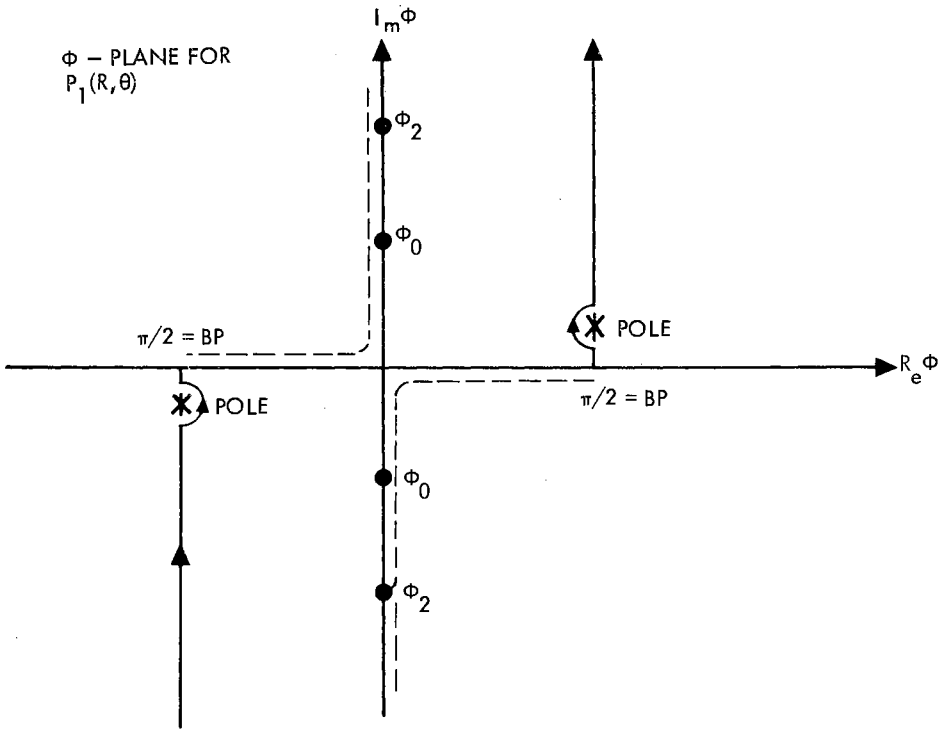

Figure 8. Φ-plane for Ion Mode Integration

Branch points are located at

$$\Phi_1 = \pm \frac{\pi}{2}$$

$$\Phi_2 = \sin^{-1}\left(\pm \frac{K_2}{K_1}\right)$$

$$\Phi_o = \sin^{-1}\left(\pm \frac{K_o}{K_1}\right)$$

with branch cuts following the axes as in the λ-plane. The poles are at

$$\lambda_p = \pm (K_1 + \delta) \qquad \delta \ll K_1$$

or, in the Φ-plane

$$\Phi_p = \pm \left(\frac{\pi}{2} + i\epsilon \right) \qquad \text{where } \epsilon \text{ is a small quantity.}$$

The saddle point is located at Φ_{sp} where

$$\frac{d\Phi(\Phi)}{d\Phi} = K_1 \cos (\theta + \Phi) = 0$$

Therefore,

$$\Phi_{sp} = \pm \frac{\pi}{2} - \theta \qquad 0 < \theta < \pi$$

Hence for

$$0 < \theta < \frac{\pi}{2} \, , \; 0 < \Phi_{sp} < \frac{\pi}{2}$$

for

$$\frac{\pi}{2} < \theta < \pi \, , \; -\frac{\pi}{2} < \Phi_{sp} < 0$$

The path of steepest descent is found from

$$\text{Im} \left\{ -iK_1 R \sin (\theta + \Phi) \right\} = \text{Im} \left\{ -iK_1 R \right\}$$

or,

$$\text{Im} \left\{ -iK_1 R [\sin \theta \cos \Phi + \cos \theta \sin \Phi] \right\} = -K_1 R$$

$$\text{Im} \left\{ -iK_1 R [\sin \theta \cos (\sigma + i\omega) + \cos \theta \sin (\sigma + i\omega)] \right\} = -K_1 R$$

Therefore, the path of steepest descent is

$$\cosh \omega \sin (\sigma + \theta) = 1$$

which is a much simpler expression than would be derived in the λ-plane.

Investigating the behavior of the steepest descent contour (SDC), the imaginary axis crossing occurs at ω_c where $\sigma = 0$, or

$$\cosh \omega_c = \frac{1}{\sin \theta}$$

We see that

$$\lim_{\theta \to \pi/2} \omega_c = 0$$

$$\lim_{\theta \to 0} \omega_c = -\infty$$

As θ varies from 0 to $\pi/2$, the imaginary axis crossing of the SDC varies over the entire negative axis. Therefore, branch cuts are crossed and must be accounted for in the saddle point evaluation. By letting $\omega = 0$, it is easily seen that the real axis crossing is at the saddle point. To investigate the asymptotic behavior,

$$\lim_{\omega \to \pm \infty} \sigma = \begin{cases} -\theta \\ \pi - \theta \end{cases}$$

Choose

$$\lim_{\omega \to -\infty} \sigma = -\theta$$

$$\lim_{\omega \to \infty} \sigma = \pi - \theta$$

The steepest descent contour may be shown as in Figure 9.

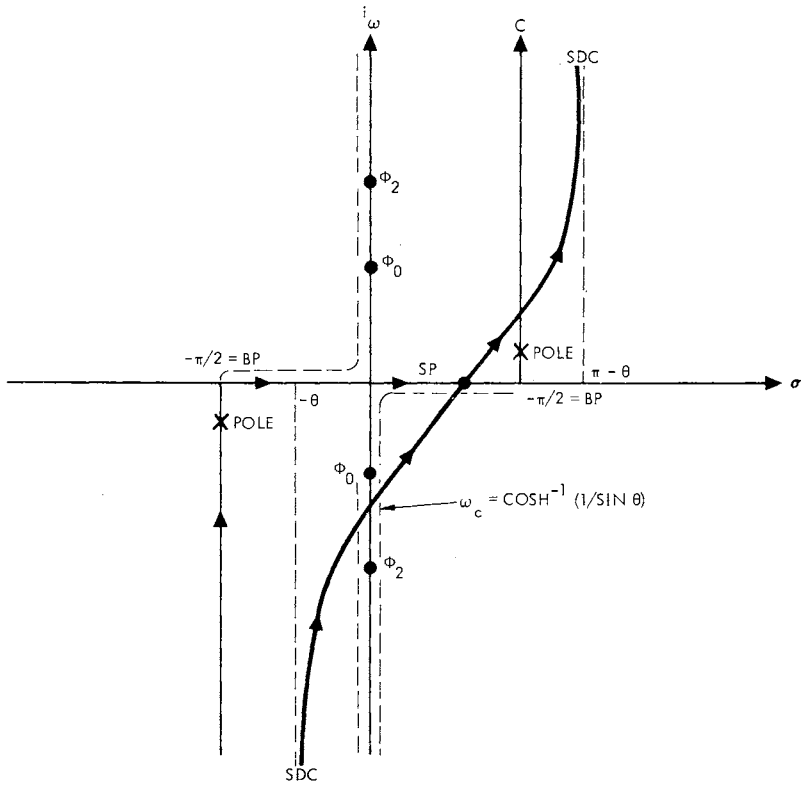

Figure 9. Steepest Descent Path in Φ-plane for the Ion Mode

Because of the pole, special consideration must be given to the point where the SDC crosses the line $\sigma = \pi/2$. By letting $\sigma = \pi/2$, the expression for the SDC reveals a crossing at

$$\cosh \omega = \frac{1}{\cos \theta}$$

As θ approaches zero, both the saddle point and the SDC approach the pole, which is very slightly removed from $\sigma = \pi/2$. In this limit, the assumption of regularity of $G(\lambda)$ in the region of the saddle point is violated and the usual first-order asymptotic evaluation will be

inaccurate. Although the literature includes methods for dealing with poles near the saddle point through inclusion of higher order terms (Felsen and Marcuvitz, 1959), the radiation at angles near $\theta = 0$ is not of much practical interest for the communication system; therefore, little concern will be shown for this inaccuracy. As θ approaches $\pi/2$, the saddle point approaches the origin and is well removed from the pole; therefore, the first-order evaluation should suffice in this region.

Consider the effect of the branch cuts on

$$G(\Phi) = \frac{C_4 \sin \Phi \Gamma_2(\Phi)}{K_1 [C_1 \sin^2\Phi \cos \Phi + C_2 \sin^2\Phi \Gamma_2(\Phi) + C_3 \cos \Phi \Gamma_o(\Phi)\Gamma_2(\Phi)]}$$

where

$$\Gamma_j(\Phi) = \left(\frac{K_j^2}{K_1^2} - \sin^2\Phi\right)^{\frac{1}{2}}$$

On the spectral sheet, all the radicals $(K^2-\lambda^2)^{\frac{1}{2}}$ have a positive sign; however, if the SDC crosses a branch cut, the associated radical changes sign, (see Figure 9). In the blackout spectrum, K_1 lies on the real axis and the SDC crosses the associated branch cut twice before reaching the saddle point; therefore, no change in sign occurs for the $\Gamma_1(\Phi)$ terms. For θ near $\pi/2$, the SDC crosses the imaginary axis well above either the $-K_o$ and $-K_2$ branch points; thus, the $\Gamma_o(\Phi)$ and $\Gamma_2(\Phi)$ terms are positive for these angles. However, as θ decreases from $\pi/2$ the SDC will eventually cross the $-K_o$ and the $-K_2$ branch cuts, changing the sign of the $\Gamma_o(\Phi)$ and $\Gamma_2(\Phi)$ terms.

In order to locate the critical values of θ for which the SDC crosses the branch cut for K_j, recall that the imaginary axis crossing

is at

$$\cosh \omega_c = \frac{1}{\sin \theta}$$

and the branch point in the blackout spectrum is at

$$-\sinh \omega_j = \left|\frac{K_j}{K_1}\right|$$

Form the difference

$$\cosh^2\omega_c - \sinh^2\omega_j = \csc^2\theta - \left|\frac{K_j}{K_1}\right|^2$$

Since $\omega_c = \omega_j$ at the critical θ_j,

$$\cosh^2\omega_j - \sinh^2\omega_j = \csc^2\theta_j - \left|\frac{K_j}{K_1}\right|^2 = 1$$

and we find

$$\theta_j = \sin^{-1}\left[\frac{K_1}{(K_1^2 + |K_j|^2)^{\frac{1}{2}}}\right]$$

Recalling that $\Gamma_j(\Phi) = \left(\frac{K_j^2}{K_1^2} - \sin^2\Phi\right)^{\frac{1}{2}}$, we have the ion mode radiation integral

$$P_1(R,\theta) = C_4 \int_{SDC} \frac{\sin \Phi \cos \Phi \Gamma_2(\Phi) e^{-iK_1R \sin(\Phi + \theta)} d\Phi}{C_1 \sin^2\Phi \cos \Phi + C_2 \sin^2\Phi \Gamma_2(\Phi) + C_3 \cos \Phi \Gamma_o(\Phi)\Gamma_2(\Phi)}$$

where the signs of the $\Gamma_j(\Phi)$ are given in Table I.

TABLE III

SIGNS FOR THE ION MODE RADIATION INTEGRAL

Range of θ	$\Gamma_0(\Phi)$	$\Gamma_2(\Phi)$
$0 \le \theta < \sin^{-1} \frac{K_1}{(K_1^2 + \lvert K_2^2 \rvert)^{\frac{1}{2}}}$	-	-
$\sin^{-1} \frac{K_1}{(K_1^2 + \lvert K_2 \rvert^2)^{\frac{1}{2}}} < \theta < \sin^{-1} \frac{K_1}{(K_1^2 + \lvert K_0 \rvert^2)^{\frac{1}{2}}}$	-	+
$\sin^{-1} \frac{K_1}{(K_1^2 + \lvert K_0 \rvert^2)^{\frac{1}{2}}} < \theta < \frac{\pi}{2}$	+	+

Recalling that the first-order asymptotic evaluation of

$$I(R,\theta) = \int_{-\infty}^{\infty} G(\lambda) e^{R\Phi(\lambda)} d\lambda$$

is

$$\lim_{R \to \infty} I(R,\theta) \cong G(\lambda_o) e^{R\Phi(\lambda_o)} \left[\frac{-\pi}{2R\Phi''(\lambda_o)}\right]^{\frac{1}{2}}$$

the radiation zone solution for the ion mode is

$$P_1(R,\theta) \cong - \left[\frac{\pi K_1}{2R}\right] \cdot$$

$$\frac{C_4 \cos\theta \sin\theta (K_2^2 - K_1^2\cos^2\theta)^{\frac{1}{2}} e^{-iK_1R} e^{i\pi/4}}{C_1 K_1^2 \cos^2\theta \sin\theta + C_2 K_1 \cos^2\theta (K_2^2 - K_1^2\cos^2\theta)^{\frac{1}{2}} + C_3 \sin\theta (K_o^2 - K_1^2\cos^2\theta)^{\frac{1}{2}} (K_2^2 - K_1^2\cos^2\theta)^{\frac{1}{2}}}$$

where the signs on the radicals depend on θ as given in Table I.

The time-average power density (Seshadri, 1965) is

$$\vec{S}_1 = \frac{-i\omega}{u_e^2 m_e N_o} \frac{P_1 \nabla P_1^*}{K_1^2}$$

Finally, writing $P_1 = F_1(K,\theta) \frac{e^{-iK_1R}}{R^{\frac{1}{2}}}$, we have

$$\vec{S}_1 = \frac{\omega |F_1|^2}{u_e^2 m_e N_o K_1} \frac{1}{R} \hat{u}_r$$

For $\omega > \omega_p$, we have electron mode radiation given by

$$P_2(R,\theta) = \int_{-\infty}^{\infty} G(\lambda) e^{R\Phi(\lambda)} d\lambda$$

where

$$\Phi(\lambda) = -i[(K_2^2 - \lambda^2)^{\frac{1}{2}} \sin\theta + \lambda \cos\theta]$$

$$G(\lambda) = \frac{C_5 \lambda (K_1^2-\lambda^2)^{\frac{1}{2}}}{C_1\lambda^2(K_1^2-\lambda^2)^{\frac{1}{2}} + C_2\lambda^2(K_2^2-\lambda^2)^{\frac{1}{2}} + C_3(K_o^2-\lambda^2)^{\frac{1}{2}}(K_1^2-\lambda^2)^{\frac{1}{2}}(K_2^2-\lambda^2)^{\frac{1}{2}}}$$

Choose the mapping

$$\lambda = K_2 \sin\Phi$$

so that

$$P_2(R,\theta) = \int_C G(\Phi) e^{-iK_2R \sin(\theta+\Phi)} K_2 \cos\Phi \, d\Phi$$

The mapping is essentially that studied previously for the ion mode integral. The real axis is now mapped as

$$\lambda = K_2 \sin\sigma \cosh\omega$$

and branch points occur at

$$\Phi_o = \sin^{-1}\left(\pm \frac{K_o}{K_2}\right)$$

$$\Phi_1 = \sin^{-1}\left(\pm \frac{K_1}{K_2}\right)$$

$$\Phi_2 = \pm \frac{\pi}{2}$$

Since for $\omega > \omega_p$, $K_1 > K_2 > K_o$, the Φ-plane is now as shown in Figure 10.

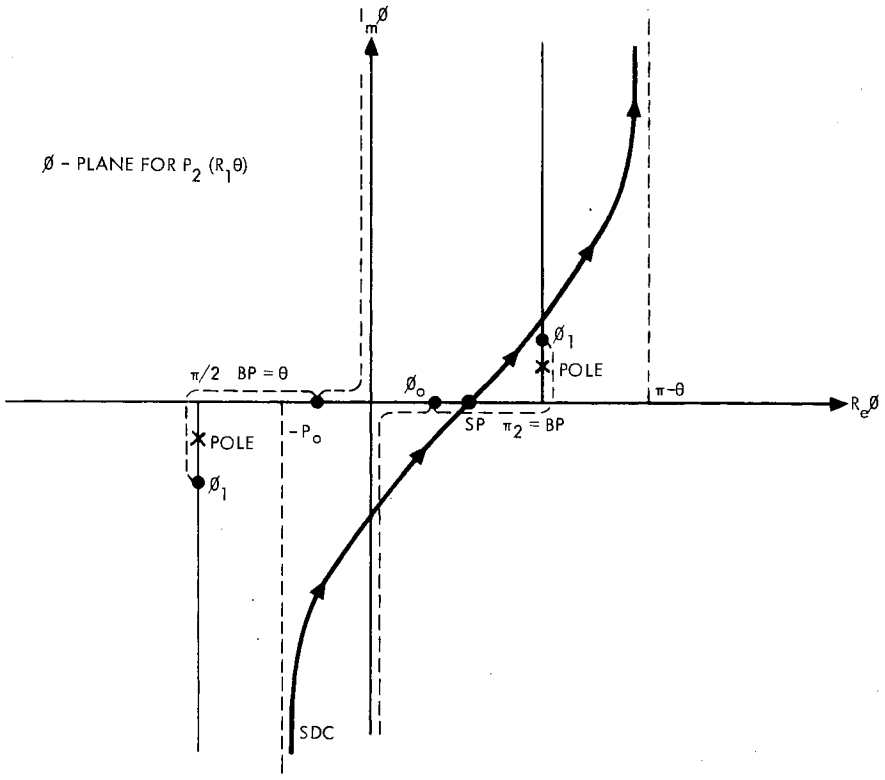

Figure 10. Φ-plane for Electron Mode Integration

The saddle point is again at $\Phi_{sp} = \frac{\pi}{2} - \theta$ with the SDC being

$$\cosh \omega \sin(\sigma + \theta) = 1$$

Again the first-order asymptotic evaluation is inaccurate for $\theta \approx 0$.

To consider branch cuts, the SDC always crosses the cuts for K_1 and K_2 twice before encountering the saddle point, so no net effect on the associated radicals takes place. However, the branch cut for K_o may be crossed either once or twice, depending upon θ. Investigating this, the branch point satisfies

$$\sin \Phi_o = \frac{K_o}{K_2}$$

and the real axis crossover is the saddle point $\Phi_{sp} = \frac{\pi}{2} - \theta$. The crossover coincides with the branch point Φ_o when $\sin \Phi_o = \sin \Phi_{sp}$ or,

$$\frac{K_o}{K_2} = \cos \theta_o$$

Therefore, in the $P_2(R,\theta)$ integral, the term $(K_o^2-\lambda^2)^{\frac{1}{2}}$ has the sign denoted in Table II.

TABLE IV

ELECTRON MODE RADIATION INTEGRAL

Range of θ	Sign of $(K_o^2-\lambda)^{\frac{1}{2}}$
$0 \leq \theta \leq \cos^{-1} \frac{K_o}{K_2}$	-
$\cos^{-1} \frac{K_o}{K_2} < \theta < \frac{\pi}{2}$	+

Using the same method employed for the ion mode integral, the saddle point evaluation for the electron mode is

$$P_2(R,\theta) = \left(\frac{\pi K_2}{2R}\right)^{\frac{1}{2}} \cdot$$

$$\frac{C_5 \sin\theta\cos\theta(K_1^2-K_2^2\cos^2\theta)^{\frac{1}{2}} e^{-iK_2R} e^{i\pi/4}}{C_1K_2\cos^2\theta(K_1^2-K_2^2\cos^2\theta)^{\frac{1}{2}}+C_2K_2^2\cos^2\theta\sin\theta+C_3(K_o^2-K_2^2\cos^2\theta)^{\frac{1}{2}}(K_1^2-K_2^2\cos^2\theta)^{\frac{1}{2}}\sin\theta}$$

where the sign on $(K_o^2 - K_2^2\cos^2\theta)^{\frac{1}{2}}$ is chosen according to Table II.

The time-average power density vector is

$$\vec{S}_2 = \frac{-i\omega}{u_e^2 m_e N_o} \frac{P_2 \nabla P_2^*}{K_2^2}$$

Finally, writing $P_2 = F_2(K,\theta) \frac{e^{-iK_2R}}{R^{\frac{1}{2}}}$, we have

$$\vec{S}_2 = \frac{\omega |F_2|^2}{u_e^2 m_e N_o K_2} \frac{1}{R} \hat{u}_r$$

For $\omega > \omega_p$, the optical mode radiation potential is

$$\prod (R,\theta) = \int_{-\infty}^{\infty} G(\lambda) e^{R\Phi(\lambda)} d\lambda$$

where

$$\Phi(\lambda) = -i[(K_o^2-\lambda^2)^{\frac{1}{2}}\sin\theta + \lambda\cos\theta]$$

and

$$G(\lambda) = \frac{-i\, C_3(K_1^2-\lambda^2)^{\frac{1}{2}}(K_2^2-\lambda^2)^{\frac{1}{2}}}{C_1\lambda^2(K_1^2-\lambda^2)^{\frac{1}{2}} + C_2\lambda^2(K_2^2-\lambda^2)^{\frac{1}{2}} + C_3(K_o^2-\lambda^2)^{\frac{1}{2}}(K_1^2-\lambda^2)^{\frac{1}{2}}(K_2^2-\lambda^2)^{\frac{1}{2}}}$$

With the transformation

$$\lambda = K_o \sin \Phi$$

we have

$$\prod (R,\theta) = \int_C G(\Phi) e^{-iK_o R \sin (\theta + \Phi) K_o \cos \Phi} d\Phi$$

Branch points occur at

$$\Phi_o = \pm \frac{\pi}{2}$$

$$\Phi_1 = \sin^{-1} \left(\pm \frac{K_1}{K_o} \right)$$

$$\Phi_2 = \sin^{-1} \left(\pm \frac{K_2}{K_o} \right)$$

The saddle point and SDC are the same as before, so the integration plane for the optical mode is shown in Figure 11.

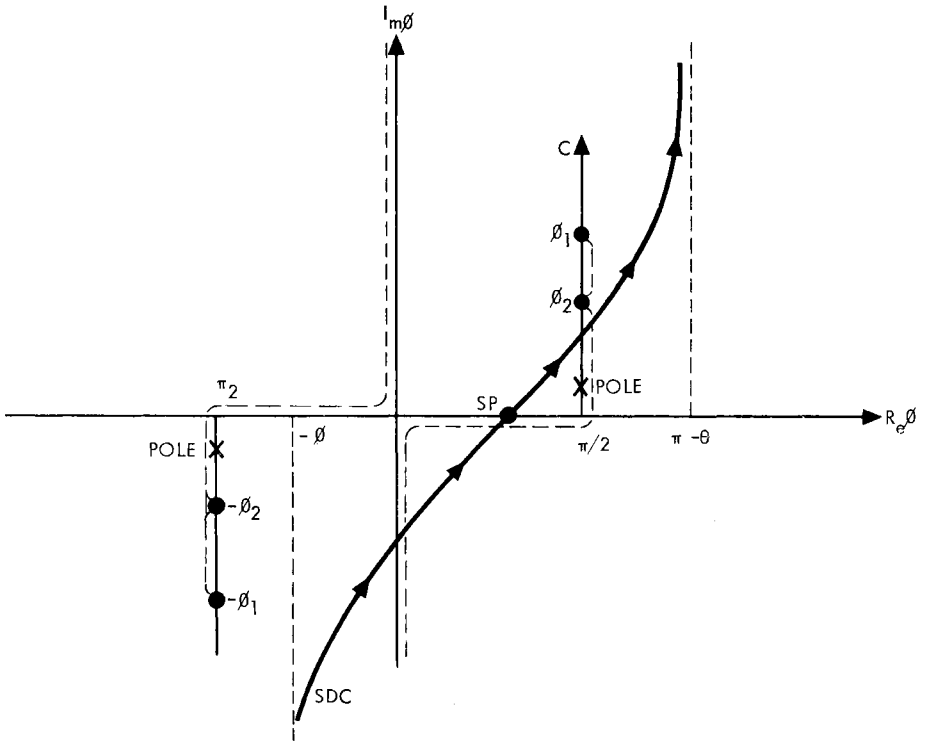

Figure 11. Φ-plane for Optical Mode Integration

Because all branch cuts are crossed twice before the SDC encounters the saddle point, all terms of the form $(K^2-\lambda^2)^{\frac{1}{2}}$ have a positive sign.

Here the saddle point result is

$$\Pi(R,\theta) = -i\left[\frac{\pi K_o}{2R}\right]^{\frac{1}{2}} \cdot$$

$$\frac{C_3 \sin\theta (K_1^2-K_o^2\cos^2\theta)^{\frac{1}{2}}(K_2^2-K_o^2\cos^2\theta)^{\frac{1}{2}} e^{-iK_oR} e^{i\pi/4}}{C_1K_o^2\cos^2\theta(K_1^2-K_o^2\cos^2\theta)^{\frac{1}{2}}+C_2K_o^2\cos^2\theta(K_2^2-K_o^2\cos^2\theta)^{\frac{1}{2}}+C_3K_o\sin\theta(K_1^2-K_o^2\cos^2\theta)^{\frac{1}{2}}(K_2^2-K_o^2\cos^2\theta)^{\frac{1}{2}}}$$

which is valid except for $\theta \approx 0$.

Writing $\Pi(R,\theta) = F_o(R,\theta)\,\frac{e^{-iK_oR}}{R^{\frac{1}{2}}}$ we will determine the Poynting vector for the optical mode. Recall that we constructed the solution TE to z, so $\vec{\Pi} = \Pi\hat{u}_z$

$$\vec{E}_o = -\nabla\times\vec{\Pi} \quad , \quad \vec{H}_o = -i\omega\epsilon\vec{\Pi} + \frac{1}{i\omega\mu_o}\nabla(\nabla\cdot\vec{\Pi})$$

Because $\vec{\Pi}$ has only a z component and no z-variation,

$$\vec{E}_o = -\nabla\times\vec{\Pi} \quad , \quad \vec{H}_o = -i\omega\epsilon\vec{\Pi} \quad , \quad \epsilon = \epsilon_o(1 - x_e - x_i)$$

In cylindrical coordinates, the radiation zone fields may be shown to be

$$\vec{E}_o = \frac{\partial\Pi}{\partial R}\,\hat{u}_\theta$$

$$\vec{H}_o = -i\omega\epsilon\Pi\hat{u}_z$$

According to Poynting's theorem, the time-average power density vector is

$$\vec{S}_o = \tfrac{1}{2}R_e(\vec{E}_o\times\vec{H}_o^*)$$

Since we have

$$\Pi = F_o(K,\theta)\,\frac{e^{-iK_oR}}{R^{\frac{1}{2}}}$$

the Poynting vector becomes

$$\vec{S}_o = \frac{\omega\epsilon K_o}{2}\,|F_o|^2\,\frac{1}{R}\,\hat{u}_c$$

4.3 The Radiation Patterns - Numerical Results

The formal solutions for the radiation patterns were evaluated on a digital computer for conditions approximating a dense reentry sheath. The parameters used in the computations were:

$$T = 10{,}000 \text{ K}$$

$$u_e^2 = 2 \times 10^{11} \text{ m}^2/\text{sec}^2$$

$$u_i^2 = 2 \times 10^{7} \text{ m}^2/\text{sec}^2$$

$$M_i = 2.34 \times 10^{-26} \text{ kg (oxygen)}$$

$$N_o = 1.5 \times 10^{14} \text{ cm}^{-3}$$

$$E_o = 2\pi \text{ v/m (excitation)}$$

Radiation patterns were computed for a number of frequencies above and below the critical frequency ω_{pe}. Although the ion mode radiation for $\omega < \omega_{pe}$ is the only item of interest in the practical ion mode communication system, numerous patterns for all three modes are given in the following pages, both for academic interest and to demonstrate that the computed results are physically reasonable. All power levels are referred to 1 watt/m^2.

The optical mode patterns shown in Figures 12 through 16 are all isotropic. Moreover, the intensity of the radiation increases with increasing signal frequency above ω_{pe}. Although the patterns are not given here, it was also shown that the optical mode radiation approaches zero as ω approaches ω_{pe} from above. These results correspond well with the radiation from an infinitesimal slot into a semi-infinite region of dielectric of permittivity $\epsilon = \epsilon_o(1 - x_e - x_i)$. Therefore, the solution for the optical mode seems reasonable.

To assist in considering the patterns for the electroacoustic modes recall that the so-called "electron" and "ion" modes are actually linear combinations of both particle motions, i.e.

$$\begin{bmatrix} P_e \\ P_i \end{bmatrix} = \begin{bmatrix} m_{11} & m_{12} \\ m_{21} & m_{22} \end{bmatrix} \begin{bmatrix} P_1 \\ P_2 \end{bmatrix}$$

One may show formally that for $\omega \ll \omega_{pe}$, the ion mode is composed of both P_e and P_i with equal amplitudes. However, for $\omega \to \infty$ the electron mode is due only to P_e, and the ion mode to P_i. Therefore, one might reasonably expect that the character of the radiation patterns would be different for the two limiting values of signal frequency. Further, because both modes are essentially due to pressure of a single specie of particle for high ω, one would expect the electron and ion mode patterns to have the same characteristics for $\omega \gg \omega_{pe}$.

The ion mode patterns are shown in Figures 17 through 27. For signal frequencies less than ω_{pe}, a very substantial broadside lobe occurs near $\theta = \pi/2$ with a sharp null at $\theta = \pi/2$. This is in the range of frequencies where the ion mode is composed of both particle pressures. As ω approaches ω_{pe} from below, the lobe becomes much sharper and the rest of the pattern, nearly isotropic; this reflects the approaching resonance condition at ω_{pe}. Finally, as ω increases through ω_{pe}, the sharp lobe disappears, and the pattern is nearly isotropic with the exception of a null at $\theta = \pi/2$. The overall intensity of the ion mode radiation is much greater for $\omega < \omega_{pi}$ where both particle species may easily follow variations in the applied fields. The intensity decreases for increasing ω, except for a local increase or "hump" for ω slightly greater

than ω_{pe}.

The patterns for the electron mode appear in Figures 28 through 32. Note that the electron mode intensity also exhibits a hump for ω slightly greater than ω_{pe}. This hump is characteristic of the resonance at ω_{pe}, and has been demonstrated in a number of compressible plasma problems, e.g., Cook and Edgar (1966) considering a cylindrical dipole and Wait (1965) on the slotted sphere. As ω increases still further, the electroacoustic radiation decreases monotonically due to the effects of particle inertia. The substantially uniform amplitude over a broad range of angles with a null at broadside agrees in character with the ion mode patterns for $\omega > \omega_{pe}$.

Having established the physical plausibility of the numerical results of the solution for slot radiation into a two-fluid plasma halfspace, the results will be combined in the final chapter with those on mode conversion at the shock front to support engineering recommendations for the ion mode reentry communication system.

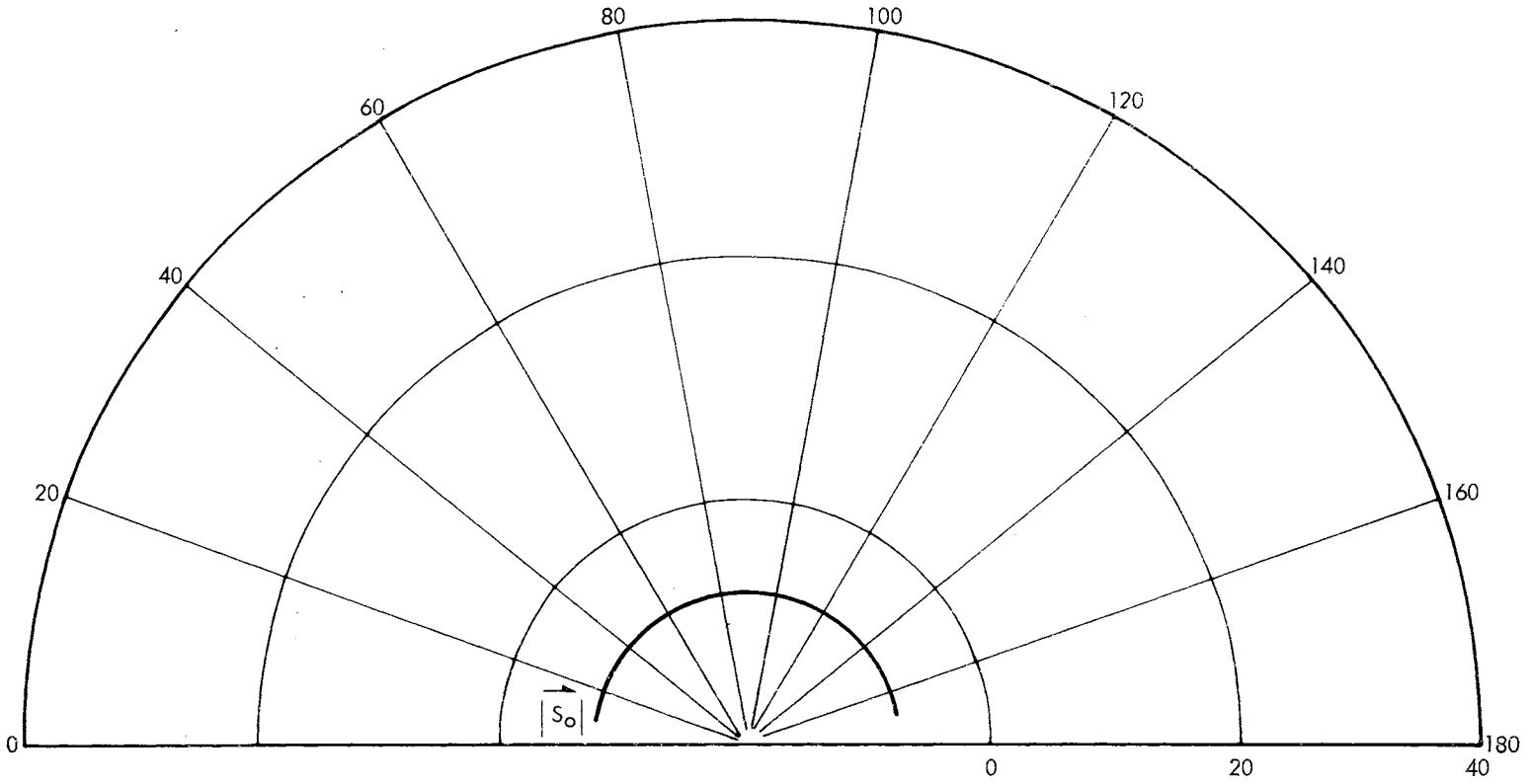

Figure 12. Optical Mode Pattern

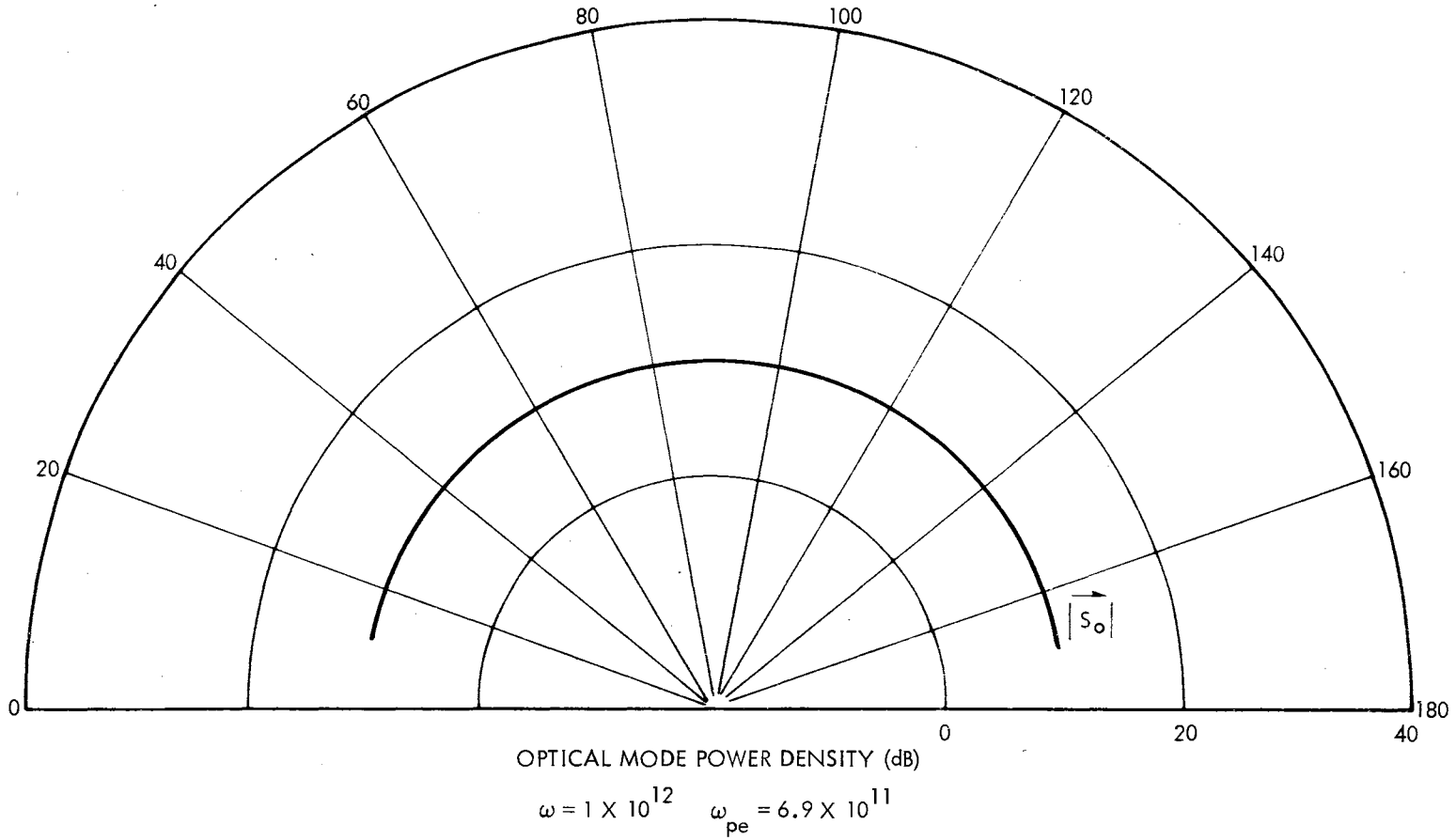

Figure 13. Optical Mode Pattern

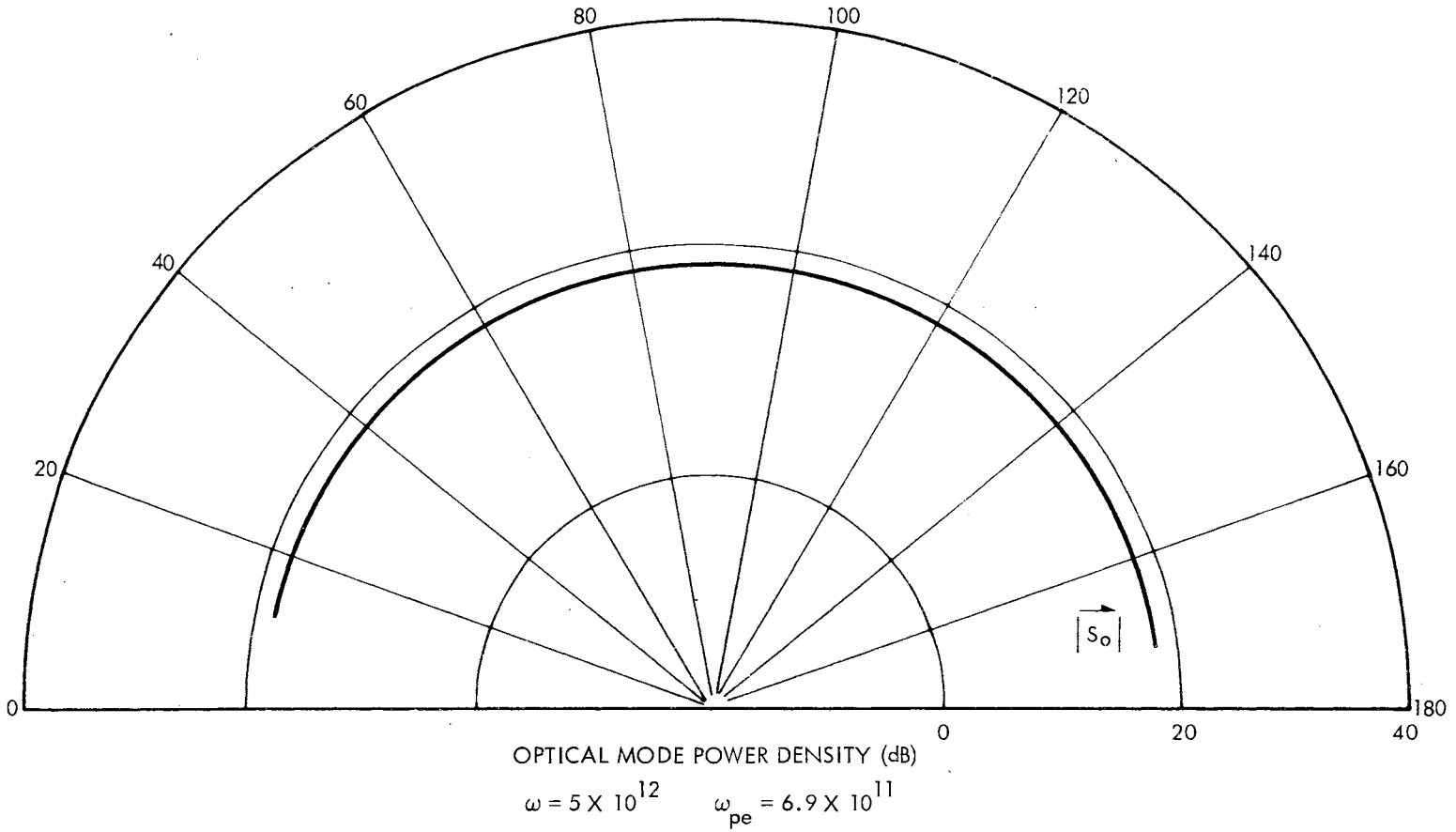

Figure 14. Optical Mode Pattern

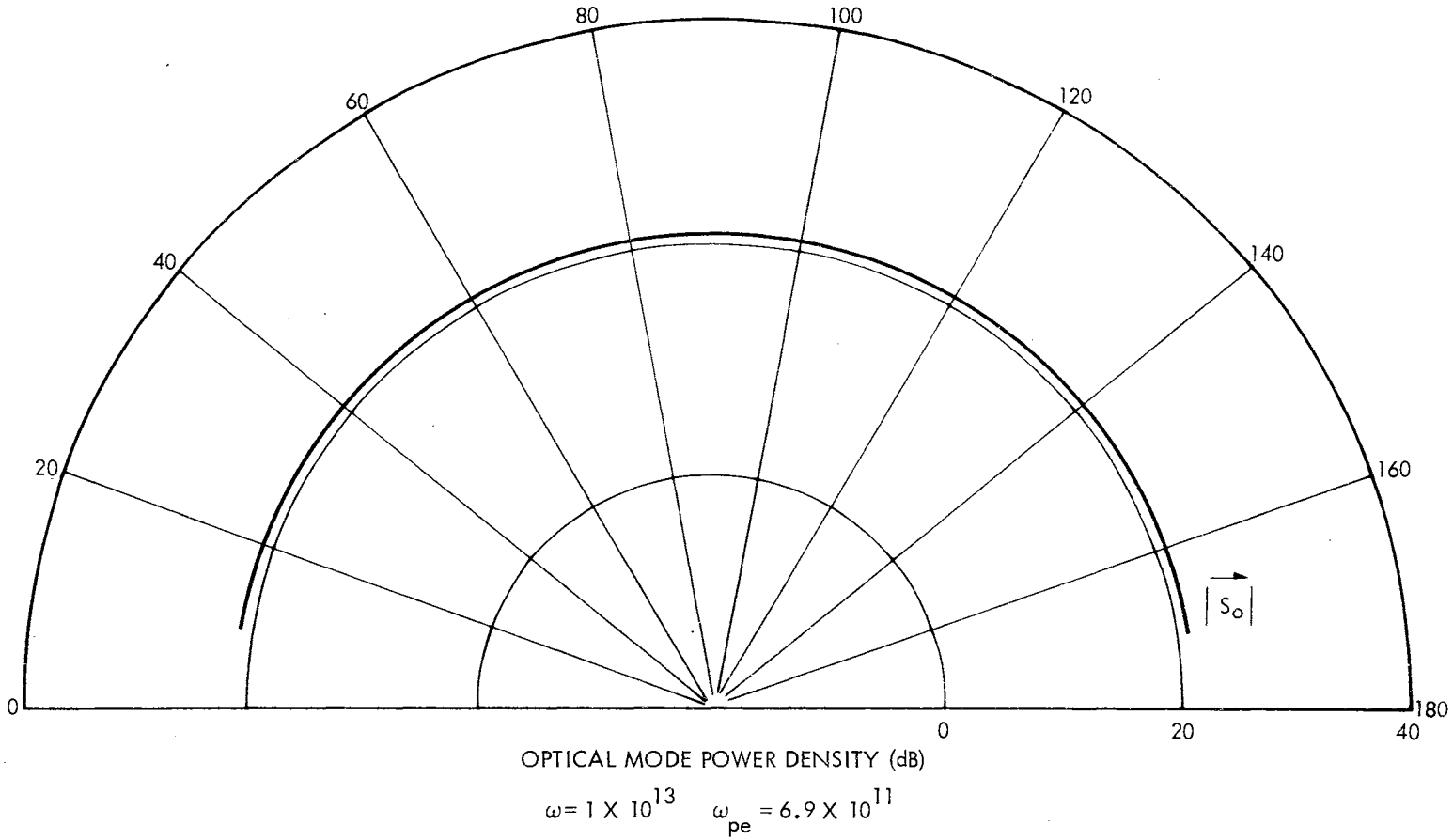

Figure 15. Optical Mode Pattern

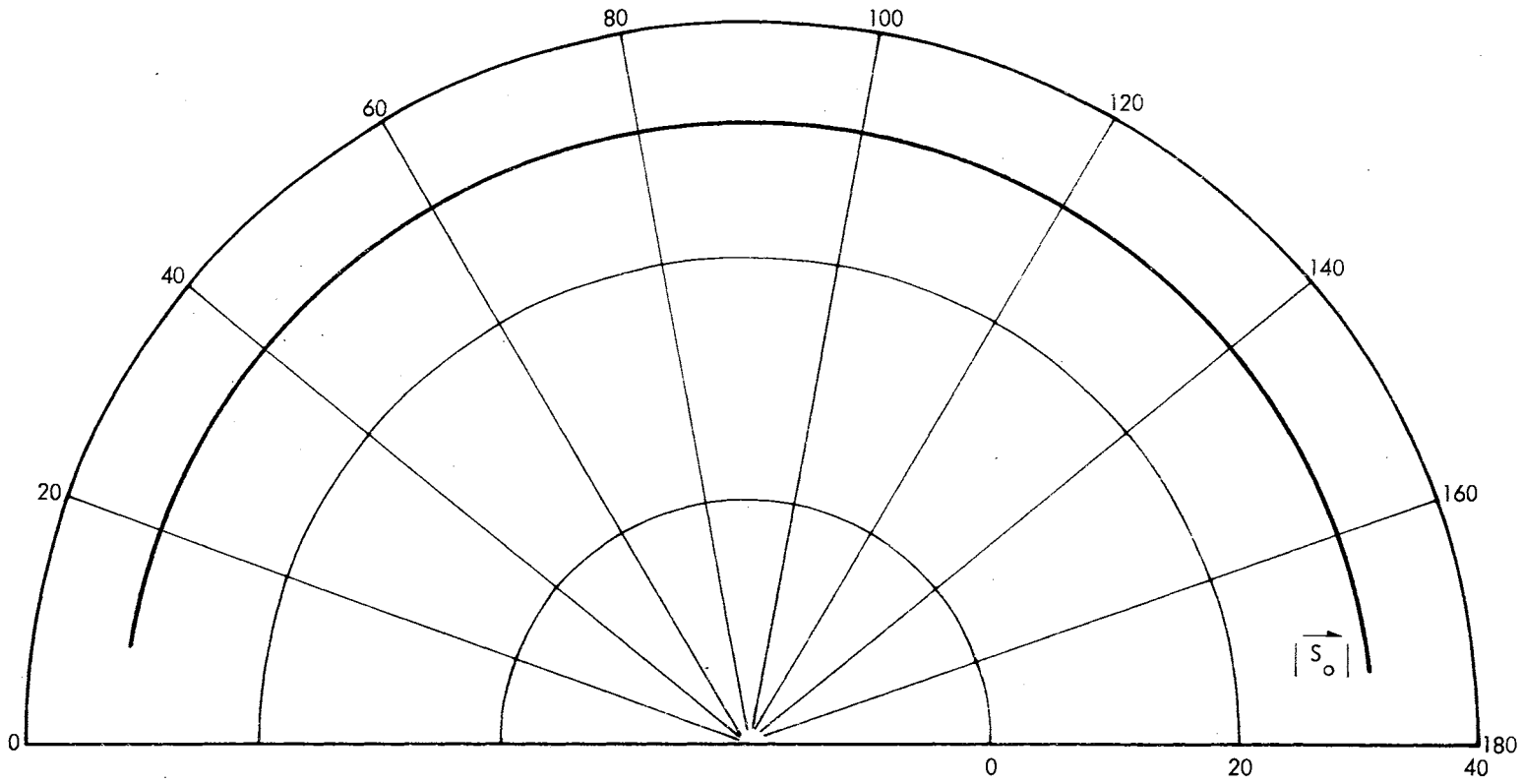

Figure 16. Optical Mode Pattern

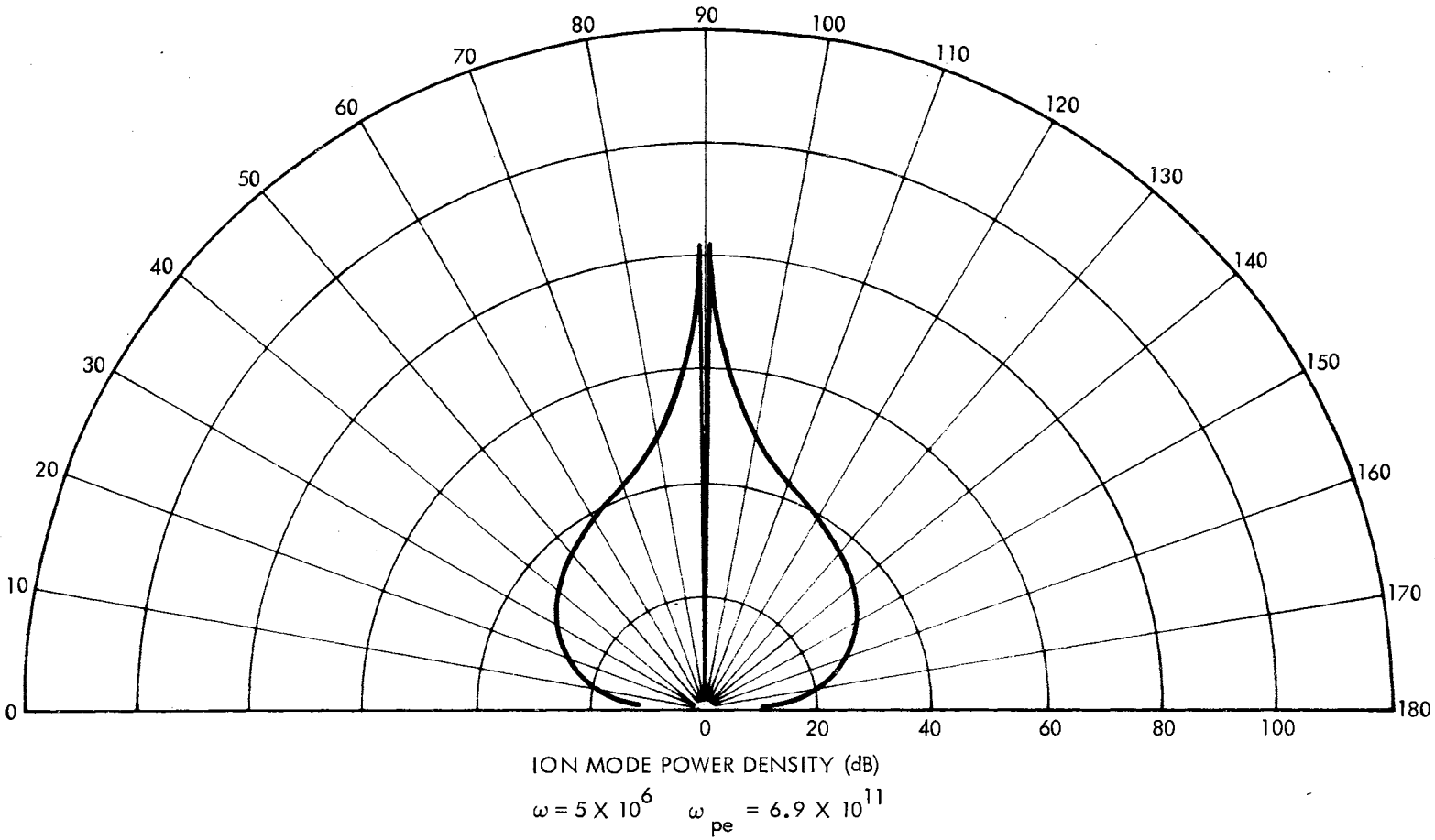

Figure 17. Ion Mode Pattern

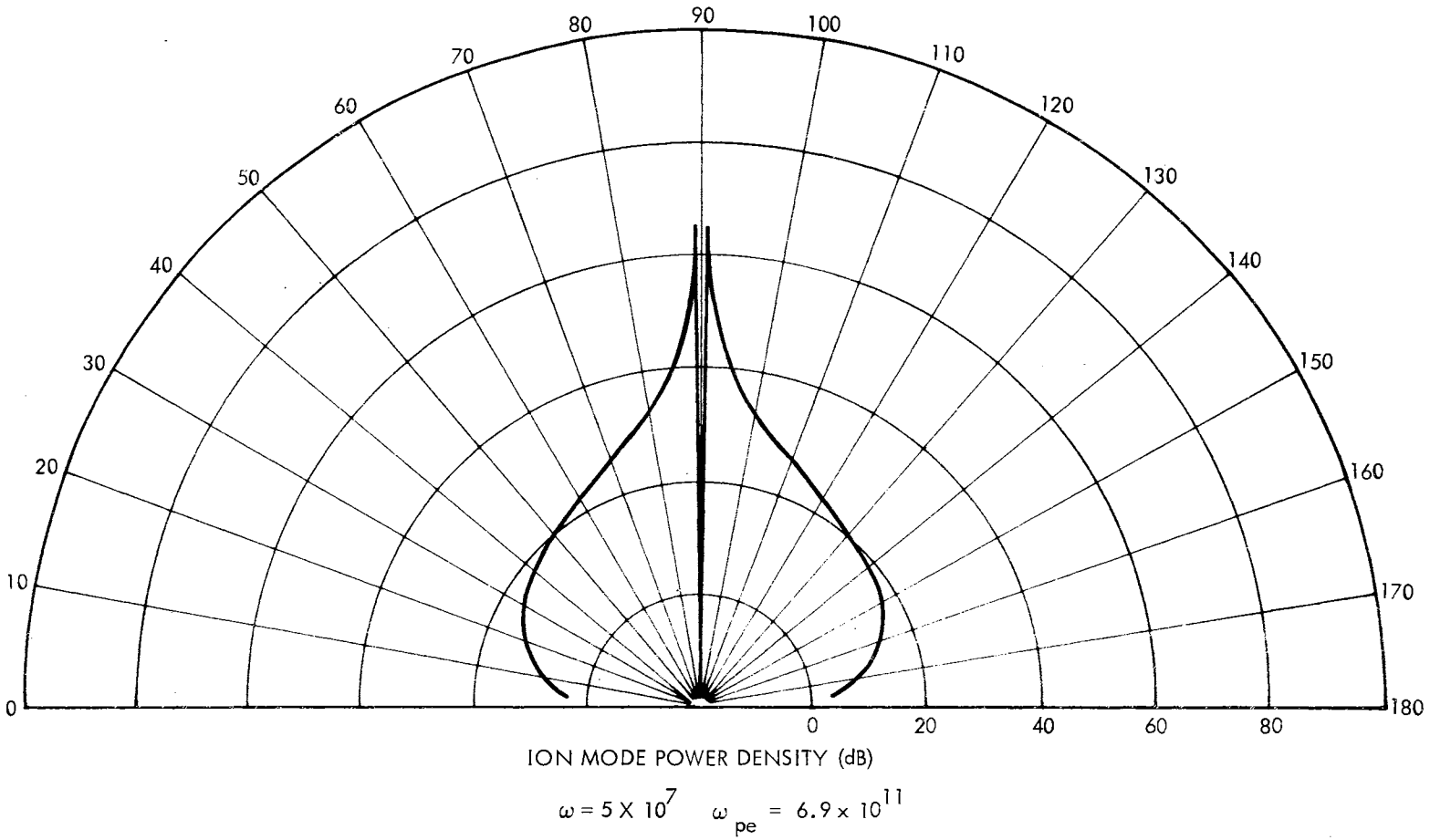

Figure 18. Ion Mode Pattern

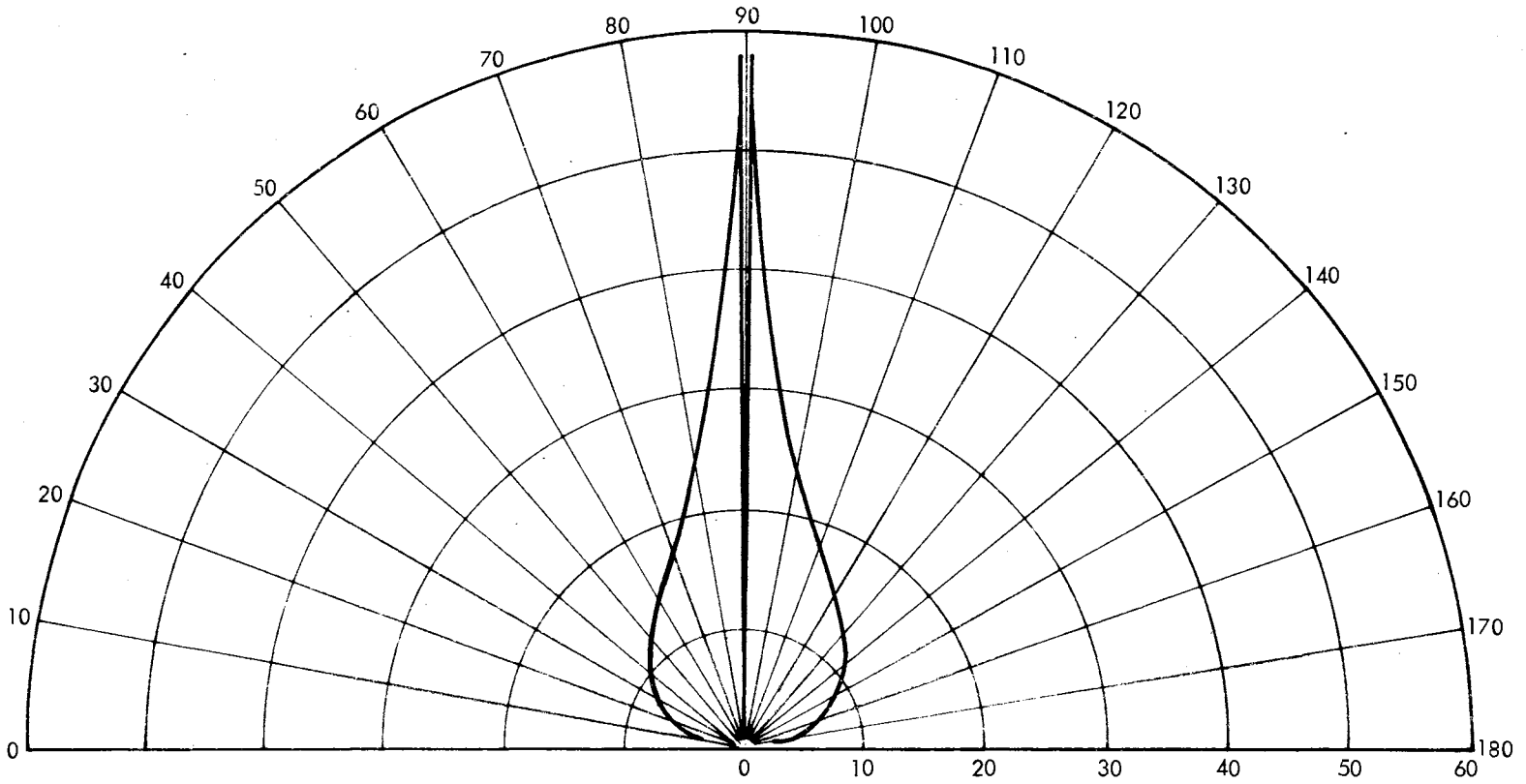

Figure 19. Ion Mode Pattern

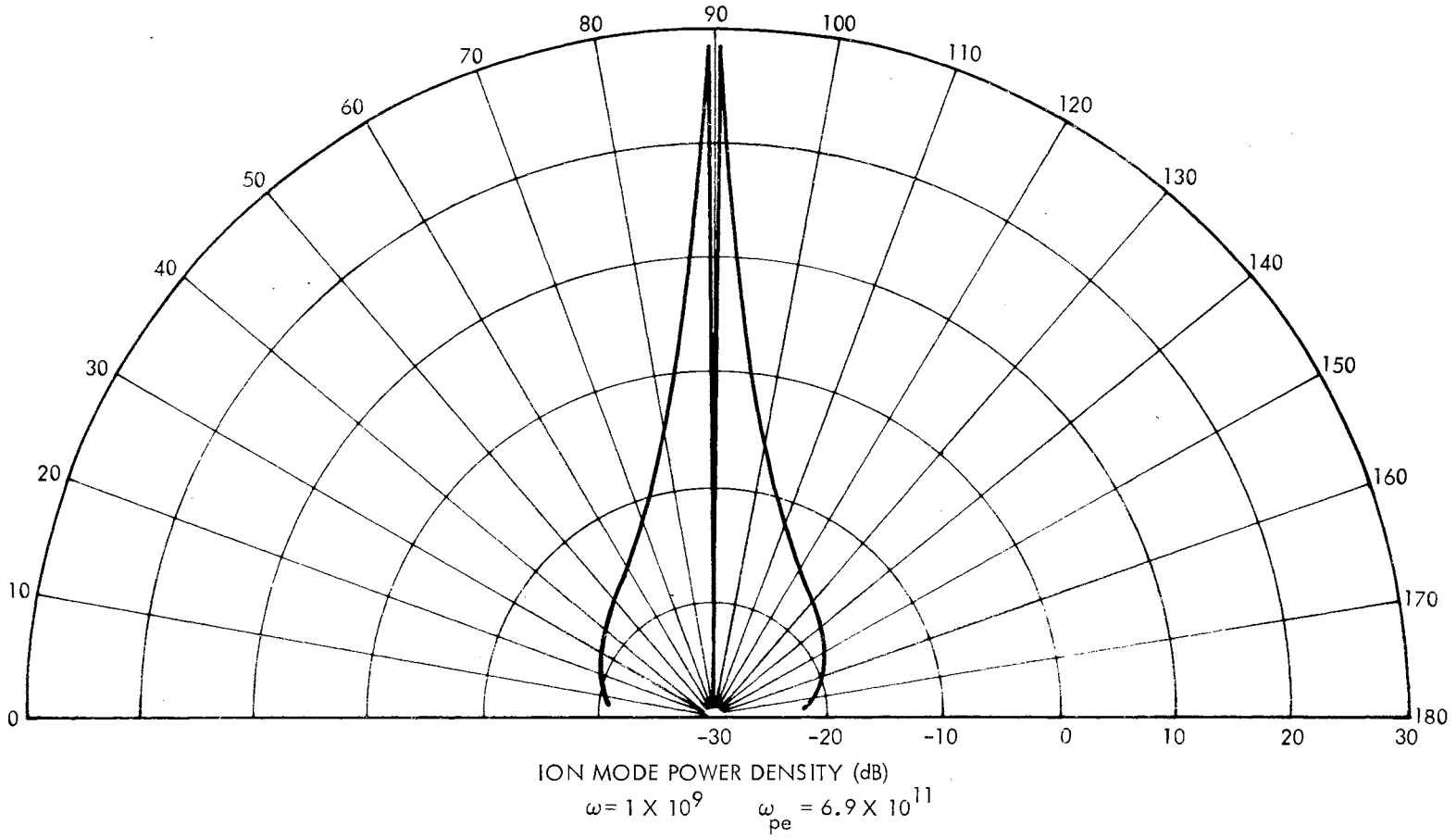

Figure 20. Ion Mode Pattern

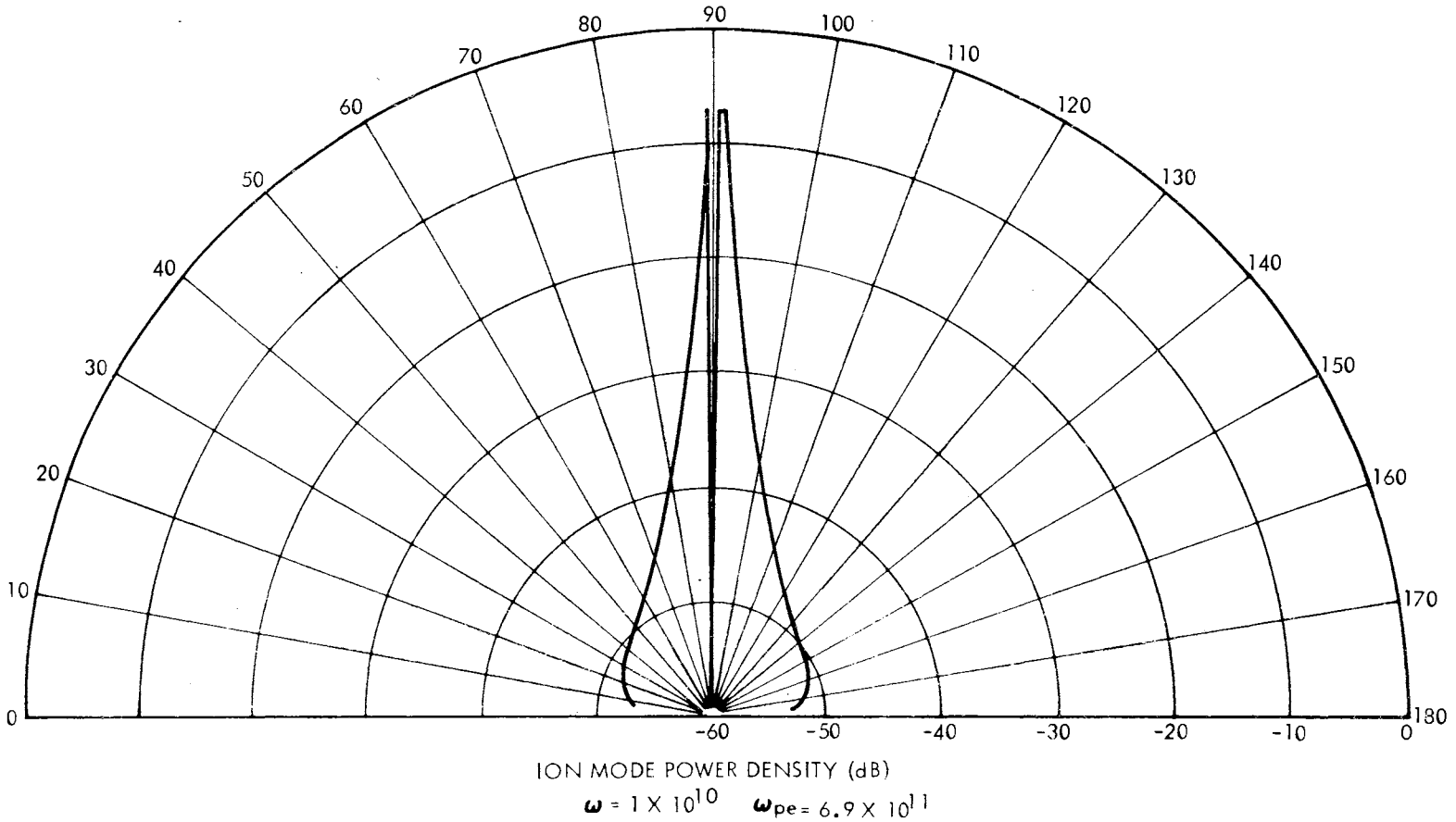

Figure 21. Ion Mode Pattern

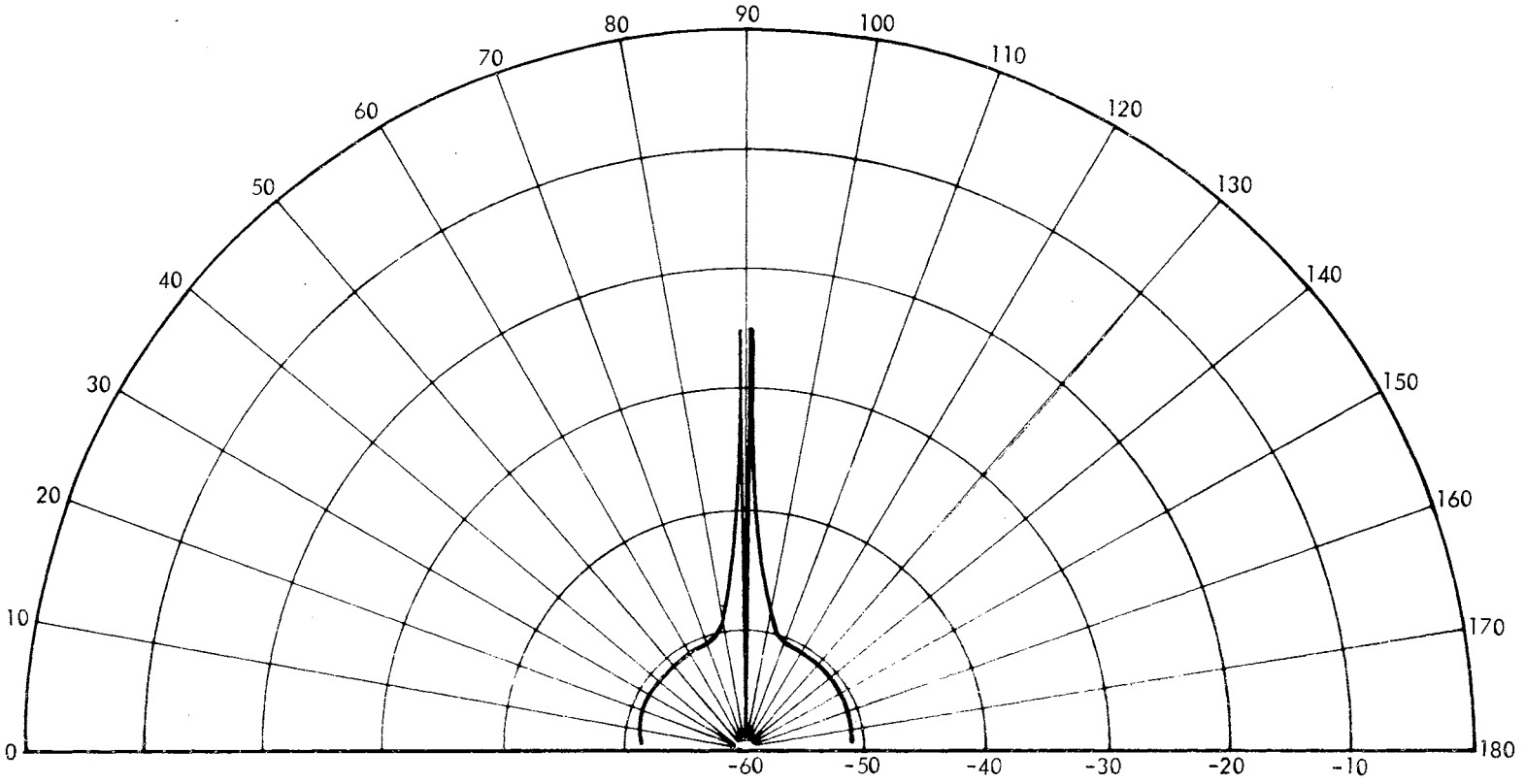

Figure 22. Ion Mode Pattern

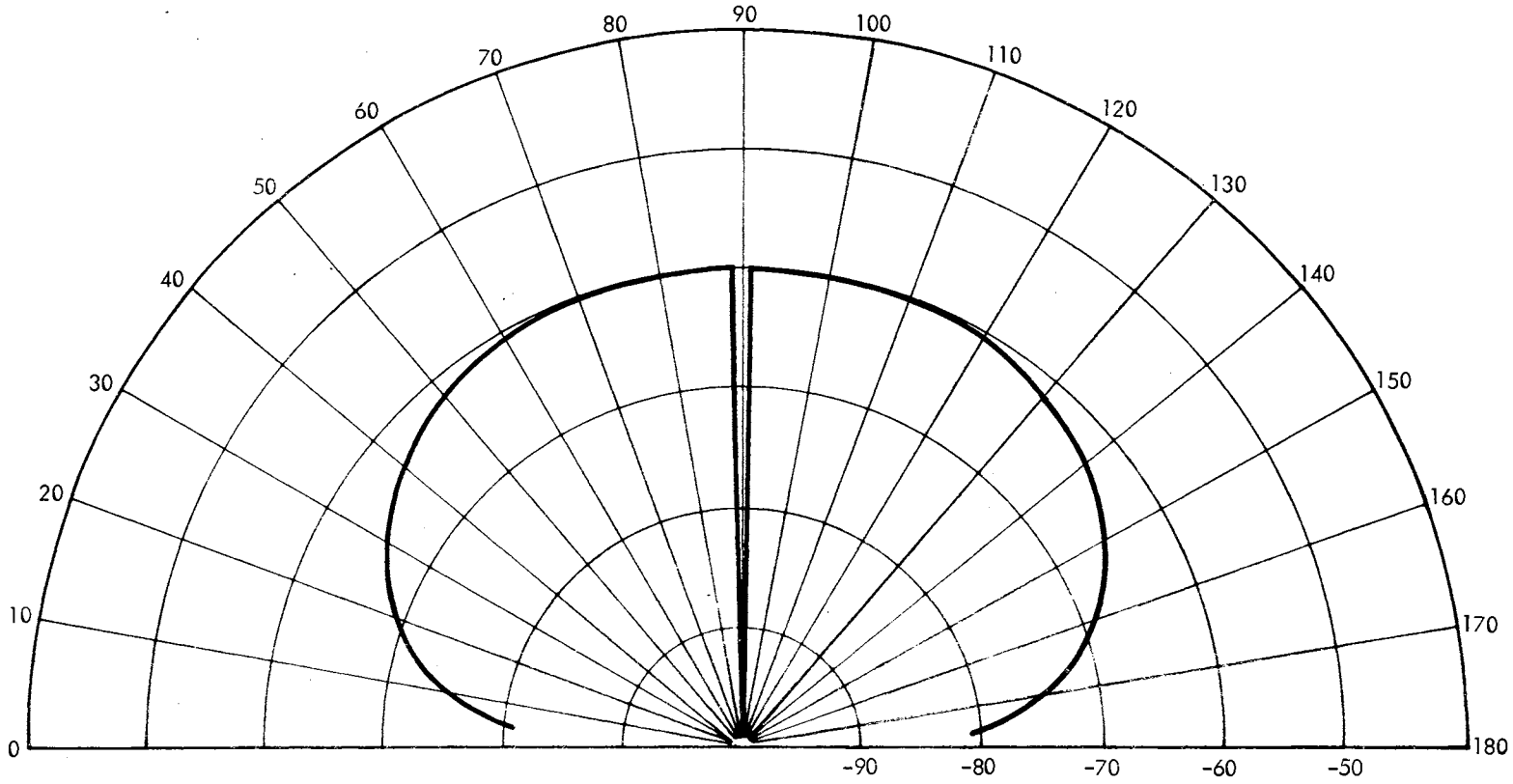

Figure 23. Ion Mode Pattern

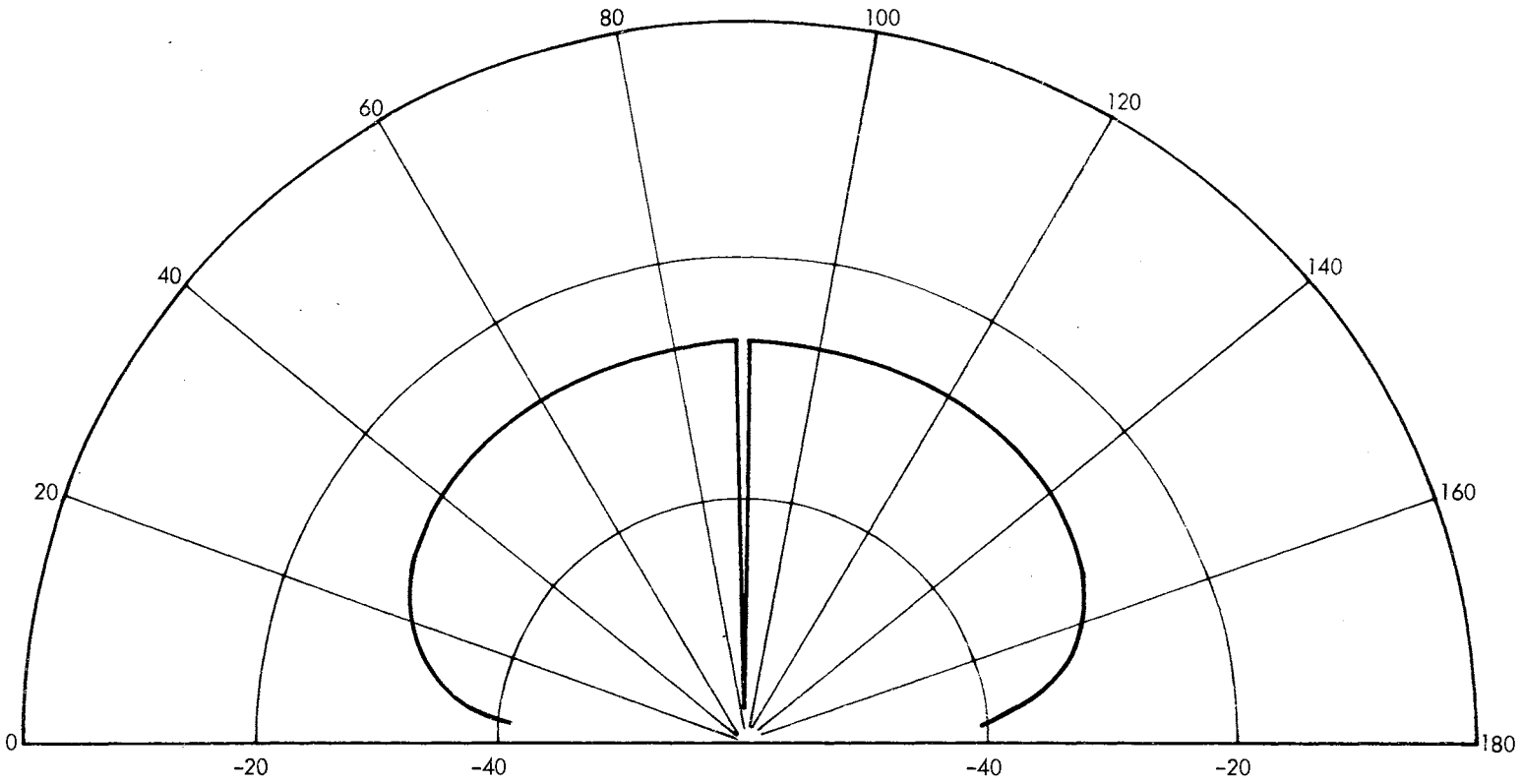

Figure 24. Ion Mode Pattern

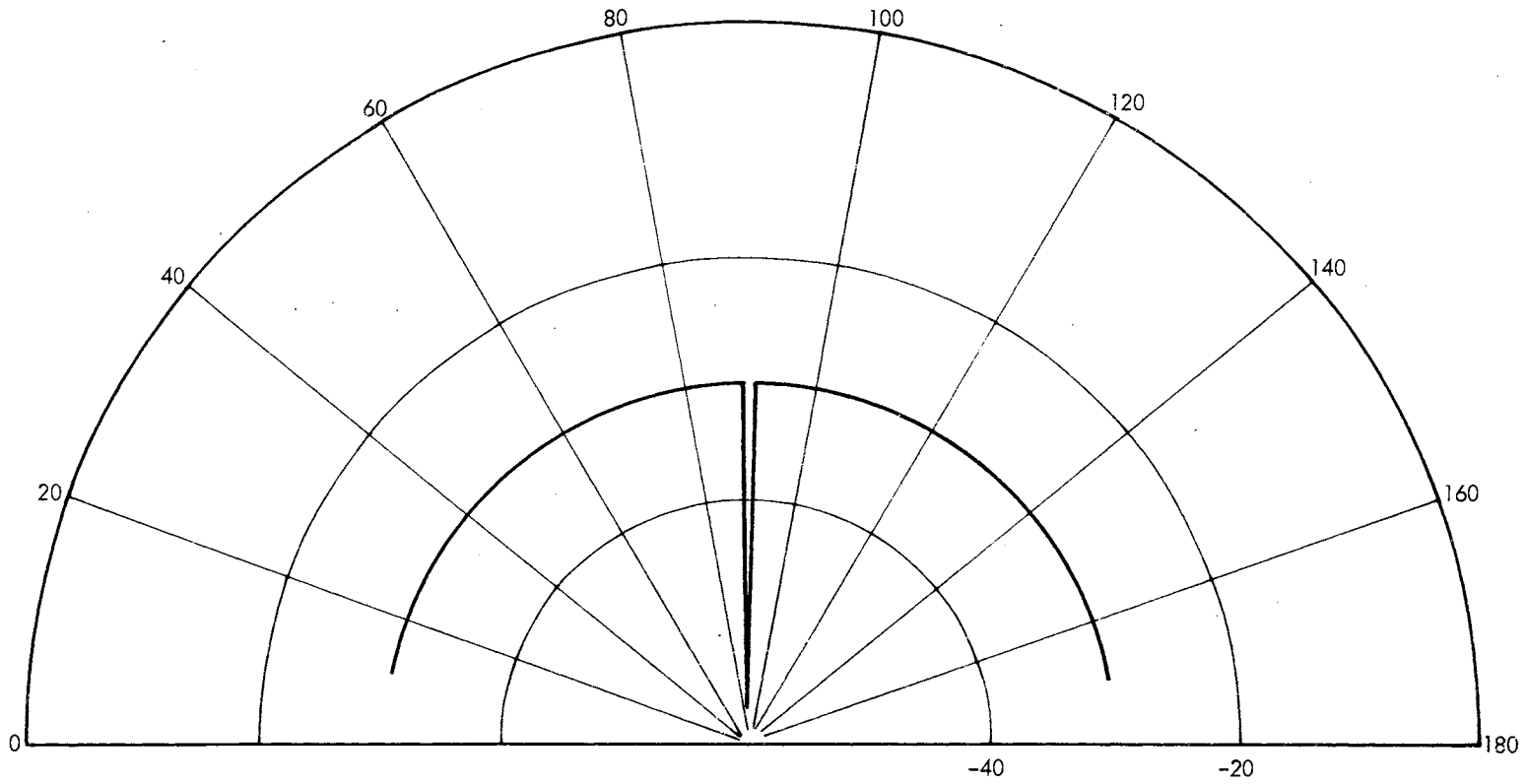

Figure 25. Ion Mode Pattern

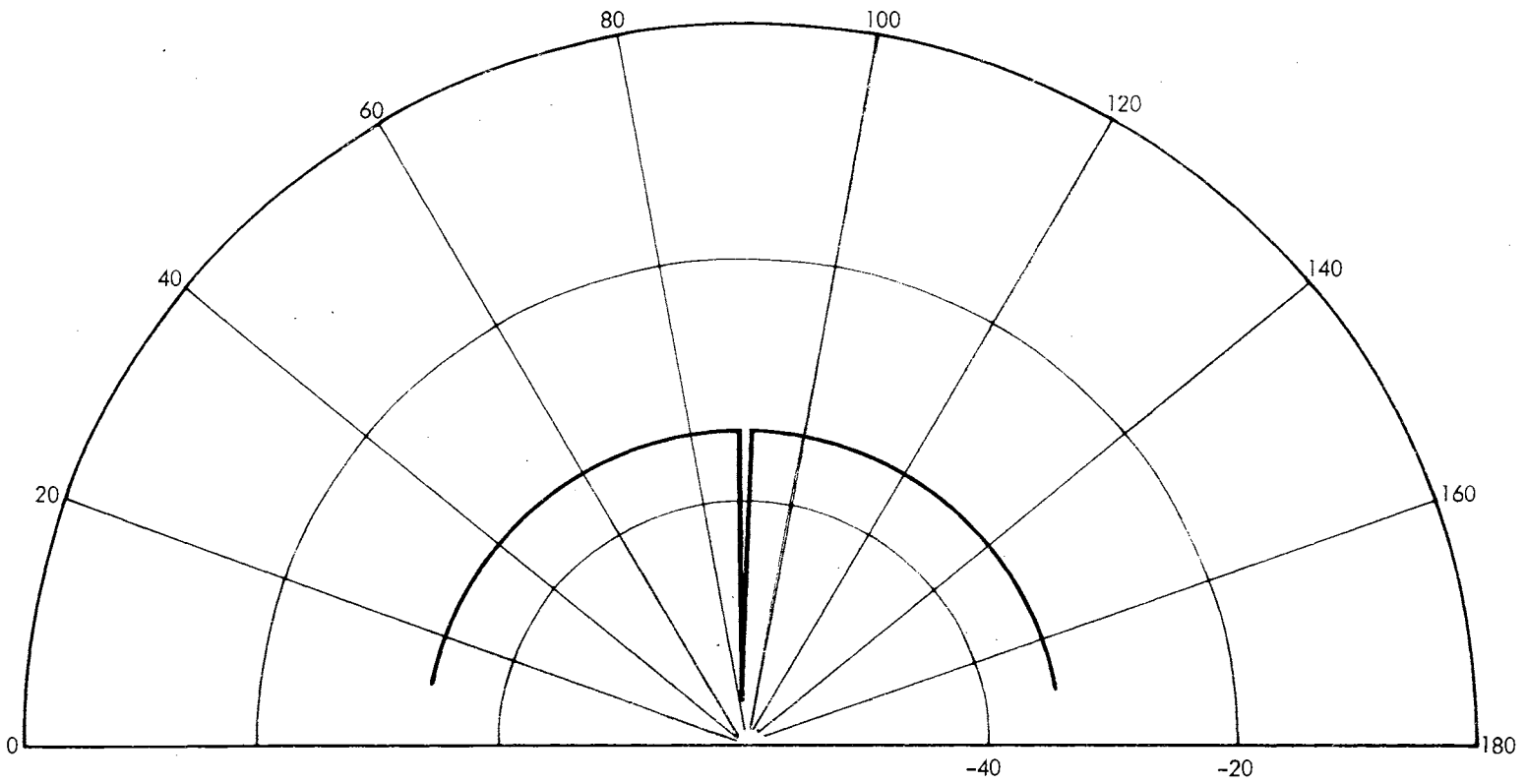

Figure 26. Ion Mode Pattern

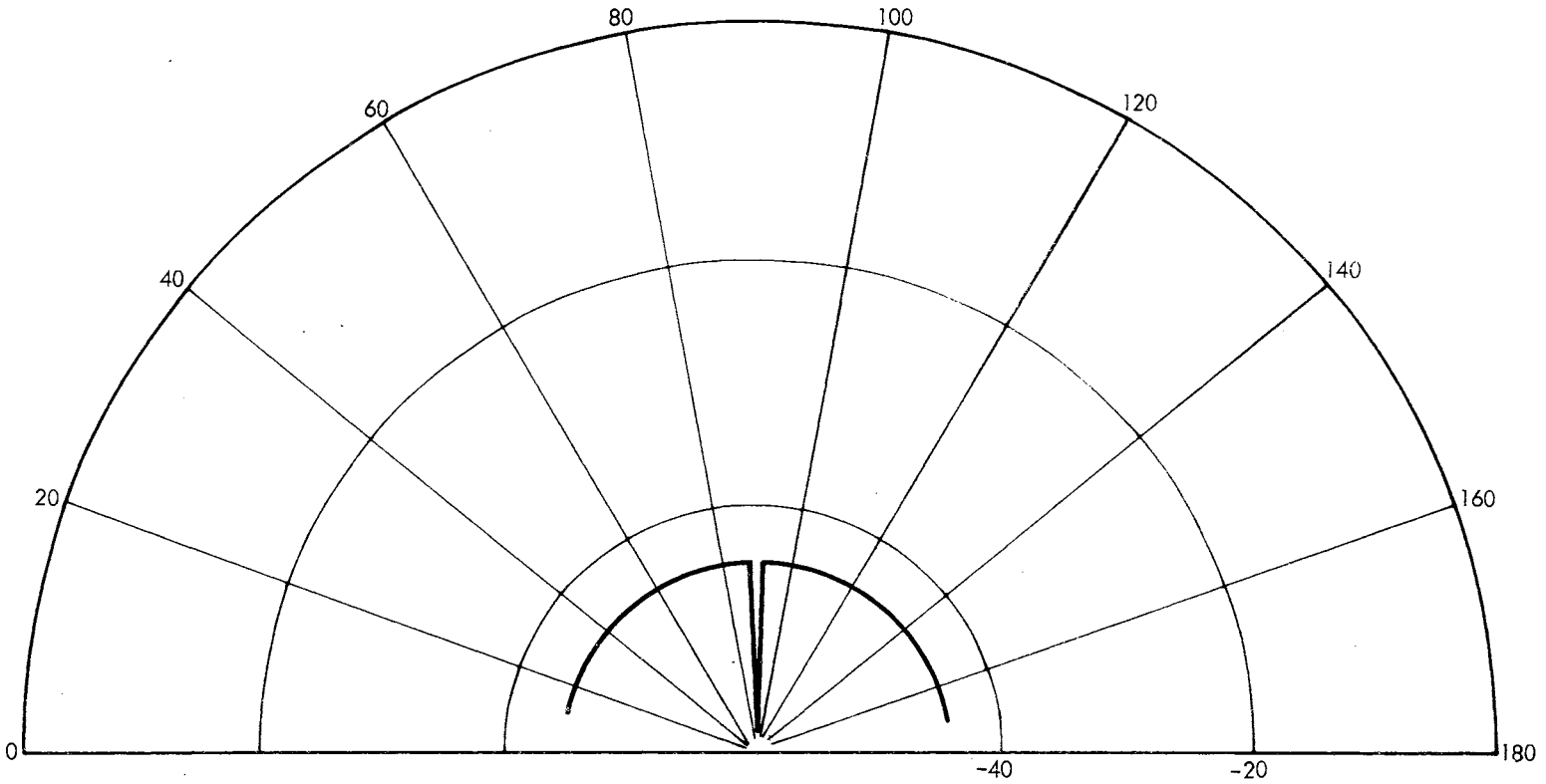

Figure 27. Ion Mode Pattern

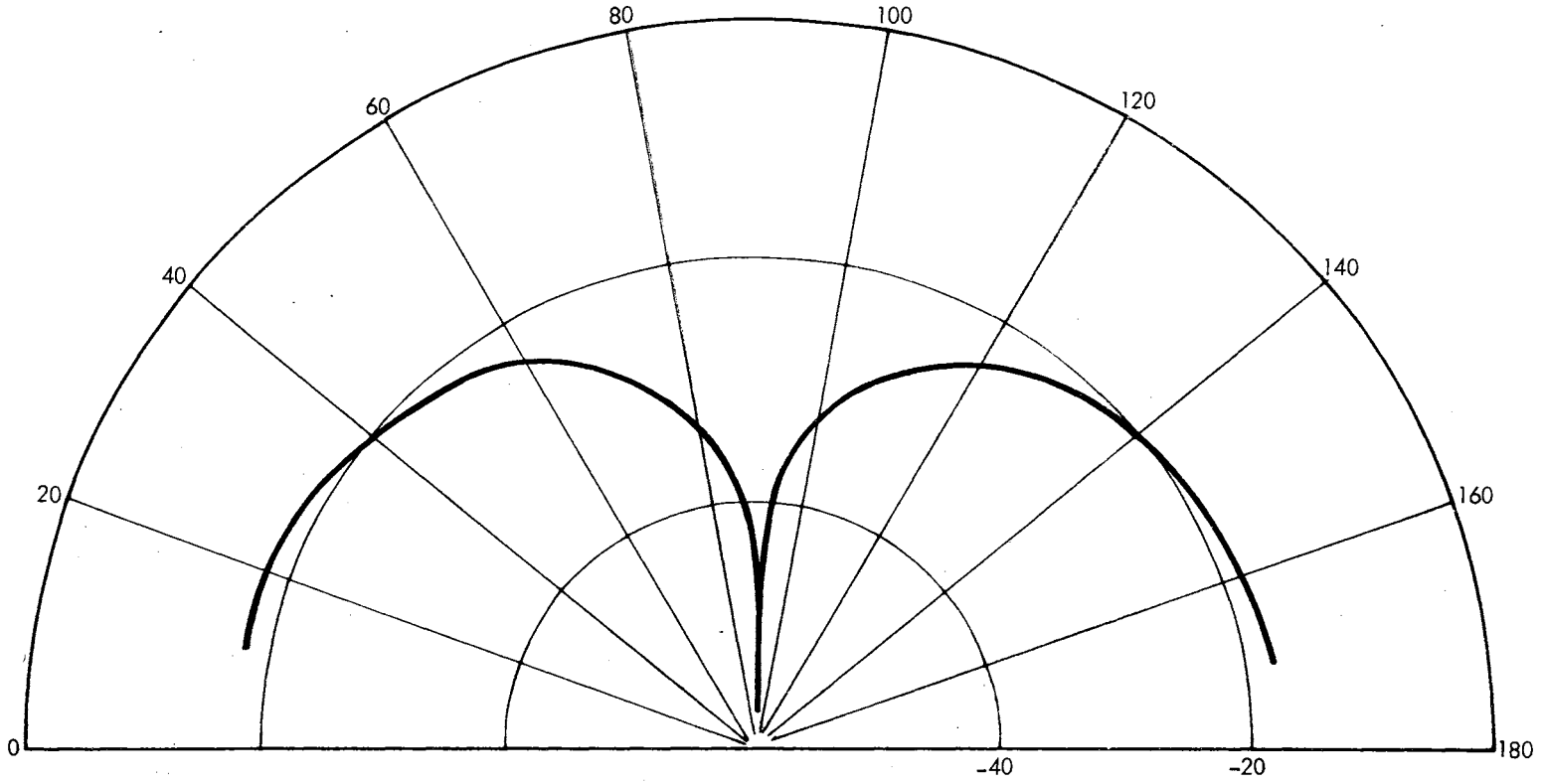

Figure 28. Electron Mode Pattern

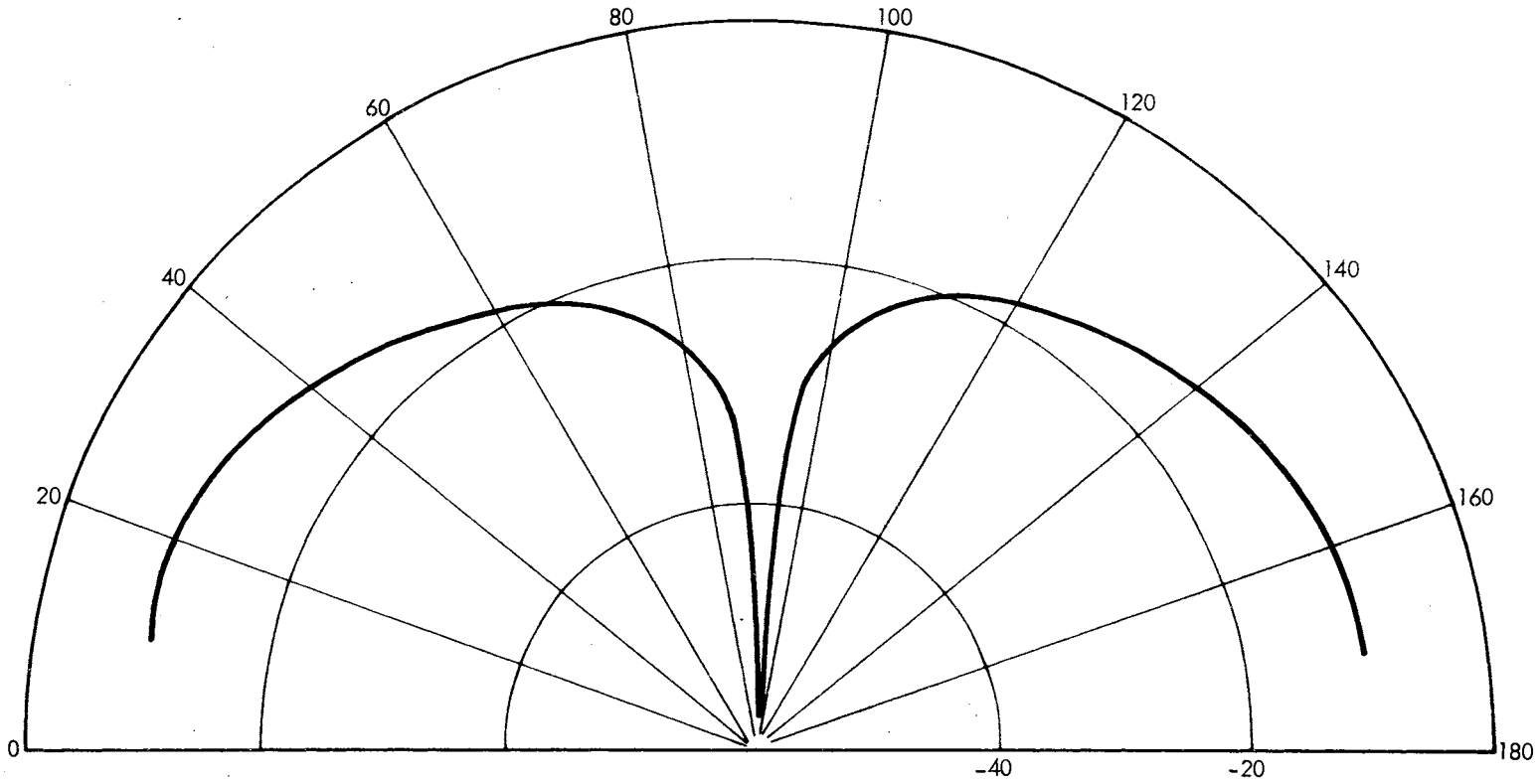

Figure 29. Electron Mode Pattern

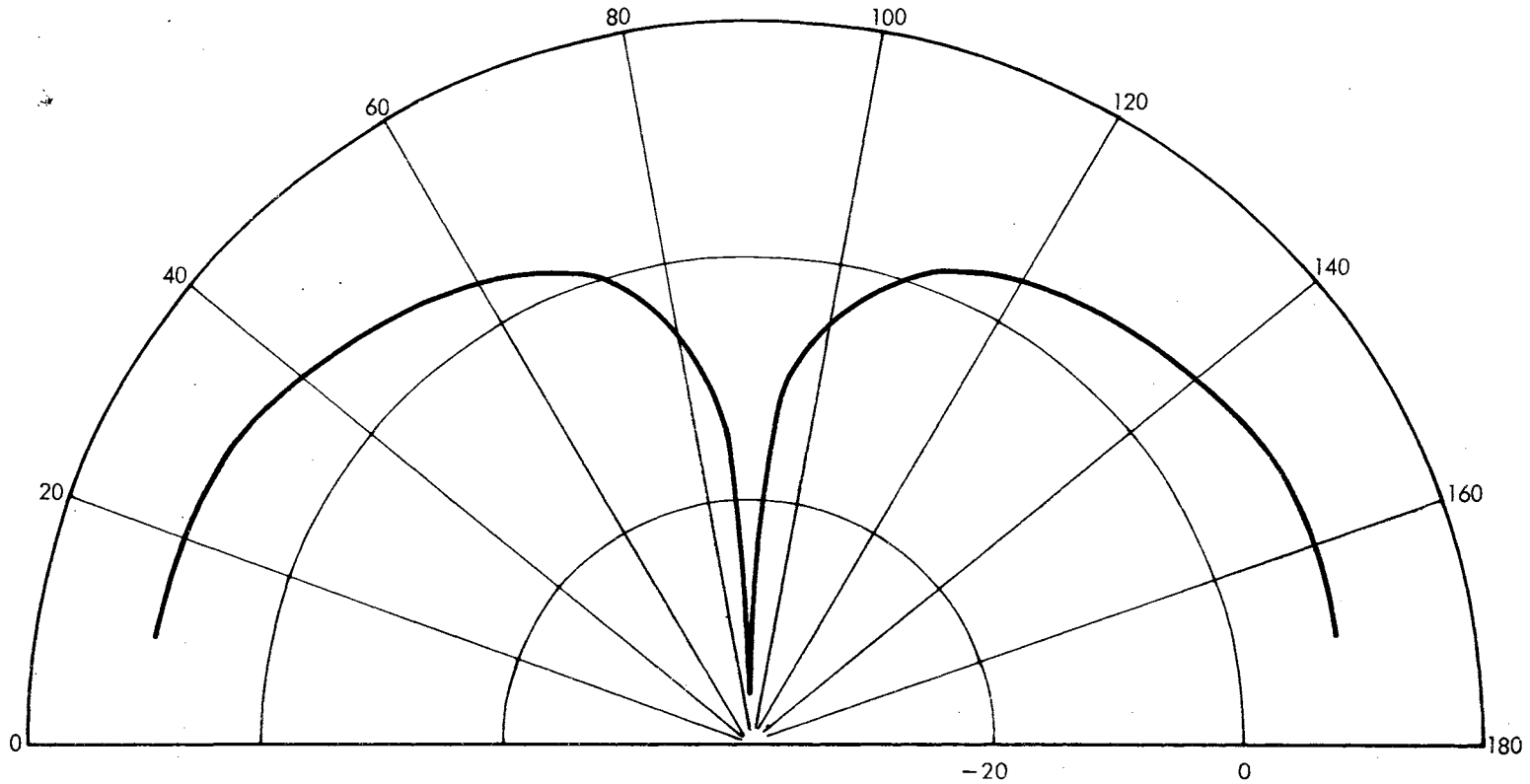

Figure 30. Electron Mode Pattern

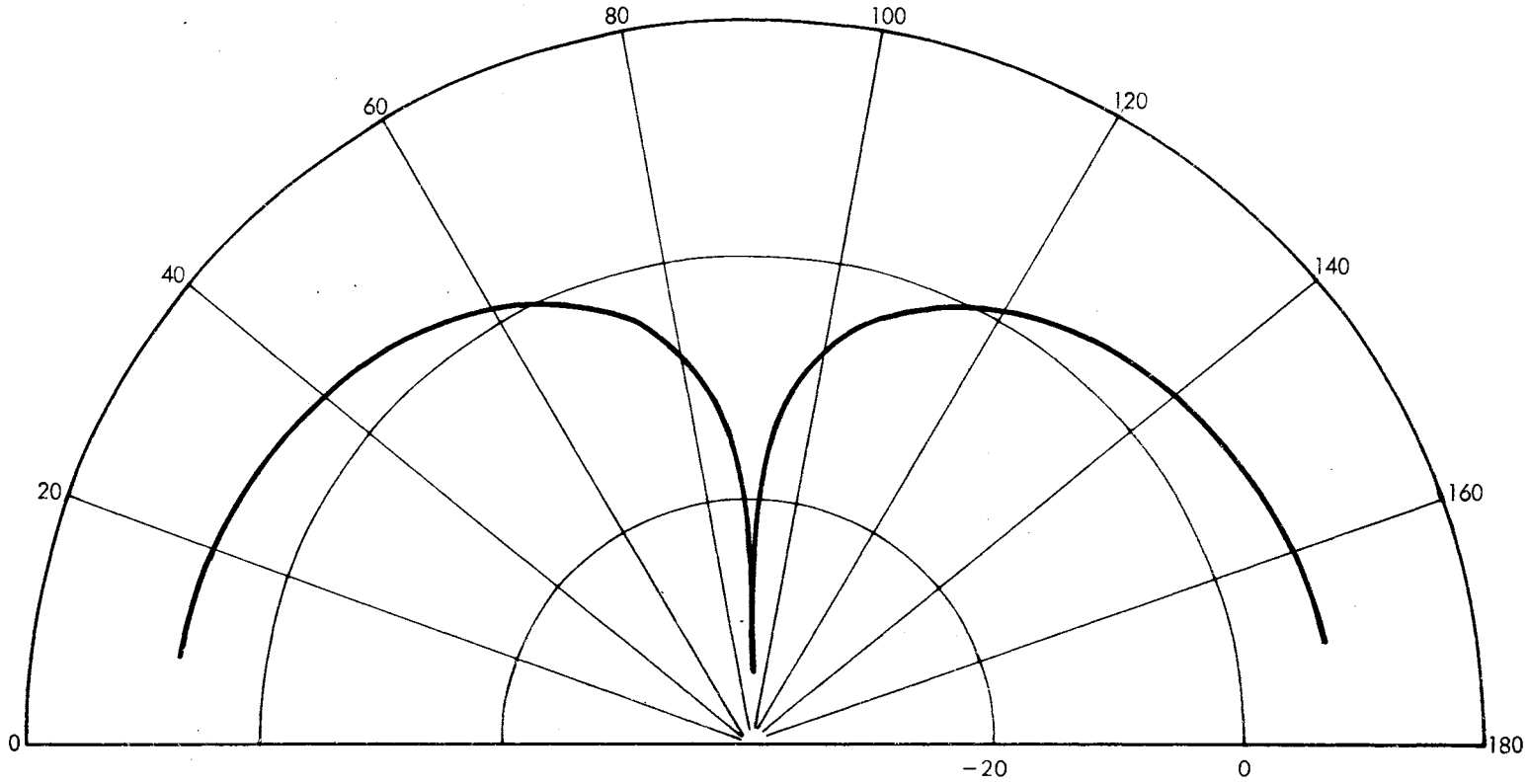

Figure 31. Electron Mode Pattern

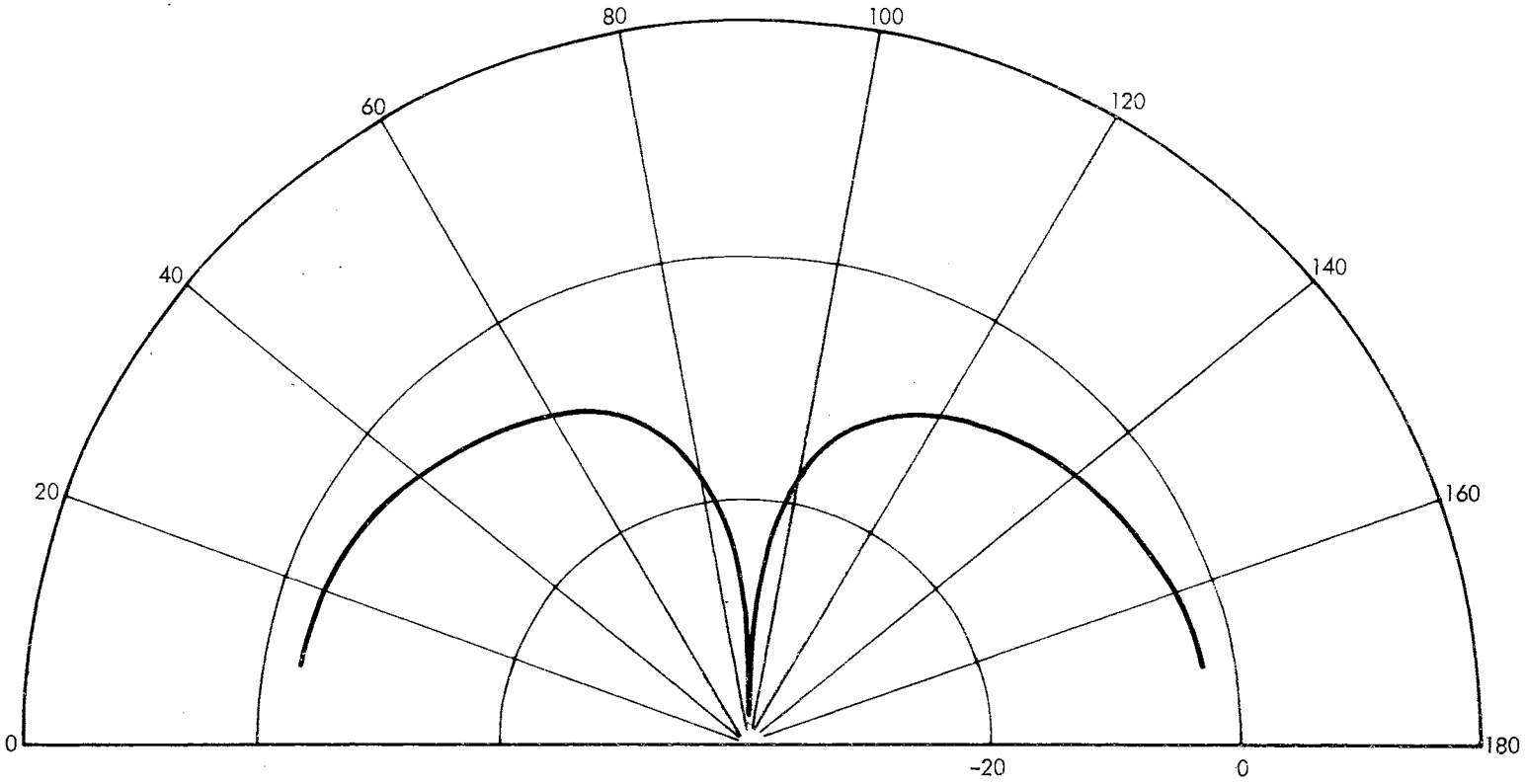

Figure 32. Electron Mode Pattern

CHAPTER V

BOUNDARY PROCESSES AT THE SHOCK FRONT

5.1 Background and Technical Approach

It is apparent from the study of the slotted ground plane that the ion mode may be used for transmitting a signal to the shock front forming the outer boundary of the reentry sheath. Recent studies such as Field (1956), Gallawa (1965), and Dunphy, Kahn, and Mintzer (1967) have shown that an electroacoustic wave may be partially converted into an electromagnetic wave at a discontinuity in plasma density. These studies have employed the condition of a rigid boundary, i.e., the normal particle velocity is zero at the boundary. This does not seem to be completely realistic; unfortunately, there seems to be no satisfactory substitute.

In addition to the usual difficulties associated with a normal plasma discontinuity, the nonequilibrium flow of a real gas mixture across a hypersonic three-dimensional shock front is a vastly complicated process. Even if the complete thermodynamic properties of such a flow were known with precision, there could be major difficulty in solving the associated electromagnetics problem. Therefore, an accurate theoretical analysis of the conversion process at the boundary seems impossible at the present time.

Owing to this, a two-part study was made to hopefully distinguish

the qualitative features of the boundary process as a guide to later experimental work. The first part is an analysis of a sharp, rigid boundary between a hot, two-fluid plasma and free space. An ion mode plane wave is assumed to impinge on the boundary and the power transmitted in the optical mode is derived. The second part of the study involves: (1) a qualitative description of a real hypersonic shock front, (2) a discussion of gradient coupling vs. rigid-boundary coupling, and, (3) heuristic consideration of an ion mode wave incident on a real shock front with some experimental support.

5.2 Mode Conversion at a Rigid Boundary

Assume that a semi-infinite region of two-fluid compressible plasma is separated from a similar region of free space at a plane boundary and that an ion mode wave is incident upon the boundary. Coupling between the various modes occurs at the rigid boundary so that the incident ion mode plane wave may cause transmitted and reflected optical mode waves and reflected electron and ion mode waves. The transmitted optical mode is of special interest here. The geometry of the problem is shown in Figure 33.

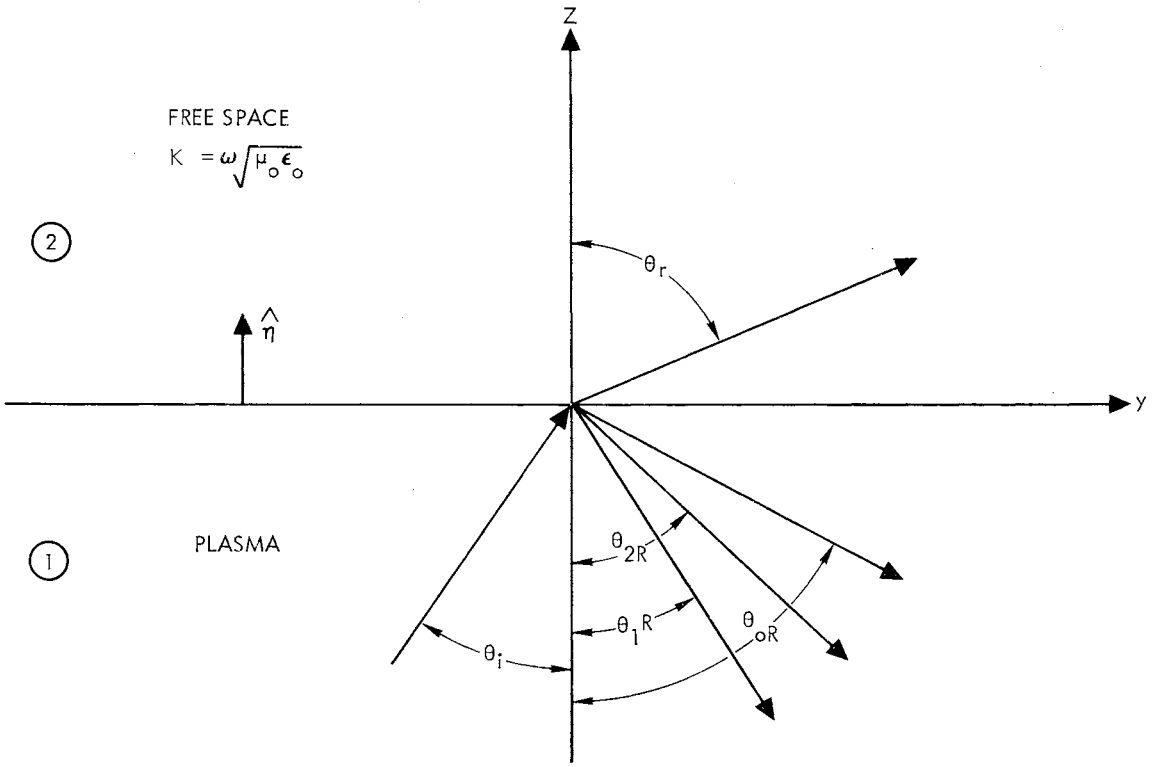

Figure 33. Coordinate System Showing the Two Media

By employing simplifications discussed in Appendix B, the following linearized boundary conditions apply to a sharp, rigid boundary between two contiguous compressible plasmas.

$$\hat{n}x(\vec{E}_1 - \vec{E}_2) = 0$$

$$\hat{n}x(\vec{H}_1 - \vec{H}_2) = 0$$

$$\hat{n}\cdot(N_{o1}\vec{v}_{11} - N_{o2}\vec{v}_{12}) = 0$$

The field quantities are represented in terms of the optical and plasma mode structures as before:

$$\vec{E} = \vec{E}_o + \vec{E}_p$$

$$\vec{H} = \vec{H}_o$$

$$\vec{v}_e = \vec{v}_{oe} + \vec{v}_{pe}$$

$$\vec{v}_i = \vec{v}_{oi} + \vec{v}_{pi}$$

$$\nabla^2\vec{E}_o + K_o^2\vec{E}_o = 0$$

$$\nabla^2 P_{1,2} + K_{1,2}^2 P_{1,2} = 0$$

Recalling that the so-called ion and electron modes (P_1 and P_2) are actually hybrid modes, we have

$$\vec{E}_p = \alpha_1 \nabla P_1 - \alpha_2 \nabla P_2$$

$$\vec{v}_{pe} = \beta_{11} \nabla P_1 + \beta_{12} \nabla P_2$$

$$\vec{v}_{pi} = \beta_{21} \nabla P_1 + \beta_{22} \nabla P_2$$

$$\vec{v}_{oe} = \frac{ie\vec{E}_o}{\omega m_e}$$

$$\vec{v}_{oi} = -\frac{ie\vec{E}_o}{\omega m_i}$$

The plasma modes are represented in terms of the scalar pressures P_1 and P_2. The optical mode will be represented in terms of the potential functions $\vec{\Pi}_{oe}$ and $\vec{\Pi}_{om}$. In a homogeneous, source-free region with $e^{i\omega t}$ supressed

$$\vec{E}_o = -\nabla \times \vec{\Pi}_{oe} + \frac{1}{i\omega\epsilon\mu_o} \nabla \times \nabla \times \vec{\Pi}_{om}$$

$$\vec{H}_o = \nabla x \vec{\Pi}_{om} + \frac{1}{i\omega\mu_o} \nabla x \nabla x \vec{\Pi}_{oe}$$

where, after the Lorentz gauge

$$\nabla^2 \vec{\Pi}_{oe} + K_o^2 \vec{\Pi}_{oe} = 0$$

$$\nabla^2 \vec{\Pi}_{om} + K_o^2 \vec{\Pi}_{om} = 0$$

Because TE modes are not coupled to plasma modes at such a boundary (Gallawa, 1965), the potentials must be chosen to represent a field TM to z. Thus, $\vec{\Pi}_{oe} = 0$

$$\vec{\Pi}_{om} = \Pi_{om} \hat{u}_z$$

Expanding the resulting field expressions in rectangular coordinates

$$E_{ox} = \frac{1}{i\omega\epsilon\epsilon_o} \frac{\partial^2 \Pi_{om}}{\partial x \partial z} = 0$$

$$E_{oy} = \frac{1}{i\omega\epsilon\epsilon_o} \frac{\partial^2 \Pi_{om}}{\partial y \partial z}$$

$$E_{oz} = \frac{1}{i\omega\epsilon\epsilon_o} \left(\frac{\partial^2}{\partial z^2} + K_o^2\right) \Pi_{om}$$

$$H_{ox} = \frac{\partial \Pi_{om}}{\partial y}$$

$$H_{oy} = H_{oz} = 0$$

Now, let

$$\vec{\Pi}_{om} = \Pi_{om} e^{i(\omega t - \vec{K}_o \cdot \vec{r})} \hat{u}_z$$

$$P_1 = \psi_1 e^{i(\omega t - \vec{K}_1 \cdot \vec{r})}$$

$$P_2 = \psi_2 e^{i(\omega t - \vec{K}_2 \cdot \vec{r})}$$

where

$\vec{K}_o = K_o \hat{u}_o$

$\vec{K}_1 = K_1 \hat{u}_1$ $\quad$ $\hat{u}_o$, $\hat{u}_1$, and $\hat{u}_2$ are unit vectors in the direction of propagation.

$\vec{K}_2 = K_2 \hat{u}_2$

We may now determine the field structures in each region.

Incident Longitudinal Wave. Since the incident field is assumed to have only the ion mode structures, P_2 and Π_{om} are zero and

$$\vec{E}_p^i = \alpha_1 \nabla P_1^i = \alpha_1 K_1 (\sin \theta_i \hat{u}_y + \cos \theta_i \hat{u}_z) P_1^i$$

$$\vec{v}_{pe} = \beta_{11} \nabla P_1^i = \beta_{11} K_1 (\sin \theta_1 \hat{u}_y + \cos \theta_i \hat{u}_z) P_1^i$$

$$\vec{v}_{pi} = \beta_{21} K_1 (\sin \theta_1 \hat{u}_y + \cos \theta^i \hat{u}_z) P_1^i$$

Reflected Fields.

$$\vec{E}_p^R = \alpha_1 \nabla P_1^R - \alpha_2 \nabla P_2^R$$

$$= (\alpha_1 K_1 \sin \theta_{1R} P_1^R - \alpha_2 K_2 \sin \theta_{2R} P_2^R)\hat{u}_y - (\alpha_1 K_1 \cos \theta_{1R} P_1^R - \alpha_2 K_2 \cos \theta_{2R} P_2^R)\hat{u}_z$$

$$\vec{v}_{pe}^R = (\beta_{11} K_1 \sin \theta_{1R} P_1^R + \beta_{12} K_2 \sin \theta_{2R} P_2^R)\hat{u}_y$$

$$- (\beta_{11} K_1 \cos \theta_{1R} P_1^R + \beta_{12} K_2 \cos \theta_{2R} P_2^R)\hat{u}_z$$

$$\vec{v}_{pi}^R = (\beta_{21} K_1 \sin \theta_{1R} P_1^R + \beta_{22} K_2 \sin \theta_{2R} P_2^R)\hat{u}_y$$

$$- (\beta_{21} K_1 \cos \theta_{1R} P_1^R + \beta_{22} K_2 \cos \theta_{2R} P_2^R)\hat{u}_z$$

$$\vec{E}_o^R = -\frac{iK_o^2}{\omega\epsilon\epsilon_o} \sin\theta_{OR}[\cos\theta_{OR}\hat{u}_y + \sin\theta_{OR}\hat{u}_z]\prod_{om}^R$$

$$\vec{H}_o^R = -iK_o \sin\theta_{OR}\prod_{om}^R \hat{u}_x$$

$$\vec{v}_{oe}^R = \frac{eK_o^2}{\omega^2 m_e \epsilon\epsilon_o} \sin\theta_{OR}[\cos\theta_{OR}\hat{u}_y + \sin\theta_{OR}\hat{u}_z]\prod_{om}^R$$

$$\vec{v}_{oi}^R = -\frac{eK_o^2}{\omega^2 m_i \epsilon\epsilon_o} \sin\theta_R[\cos\theta_{OR}\hat{u}_y + \sin\theta_{OR}\hat{u}_z]\prod_{om}^R$$

Transmitted Fields. Here, plasma modes are absent. Let $K^2 = \omega^2\mu_o\epsilon_o$.

$$\vec{E}^T = \frac{iK^2 \sin\theta_{OT}}{\omega\epsilon_o}[\cos\theta_{OT}\hat{u}_y - \sin\theta_{OT}\hat{u}_z]\prod_{om}^T$$

$$\vec{H}^T = -iK \sin\theta_{OT}\prod_{om}^T \hat{u}_x$$

Application of Boundary Conditions. Boundary conditions will now be applied to obtain an expression from which the transmitted power can be determined. From continuity of tangential $\vec{E}$,

$$\alpha_1 K_1 \sin\theta_i \psi_1^i + \alpha_1 K_1 \sin\theta_{1R}\psi_1^R - \alpha_2 K_2 \sin\theta_{2R}\psi_2^R - \frac{iK_o^2}{\omega\epsilon\epsilon_o}\sin\theta_{OR}\cos\theta_{OR}\prod_{om}^R$$

$$= -\frac{iK^2}{\omega\epsilon_o}\sin\theta_{OT}\cos\theta_{OT}\prod_{om}^T$$

From continuity of tangential $\vec{H}$,

$$-iK_o \sin\theta_{OR}\prod_{om}^R = -iK \sin\theta_{OT}\prod_{om}^T$$

From the normal electron velocity condition,

$$\beta_{11}K_1\cos\theta_i\psi_1^i - \beta_{11}K_1\cos\theta_{1R}\psi_1^R - \beta_{12}K_2\cos\theta_{2R}\psi_2^R + \frac{eK_o^2}{\omega^2 m_e \epsilon\epsilon_o}\sin^2\theta_{OR}\Pi_{om}^R = 0$$

And, from the normal ion velocity condition,

$$\beta_{21}K_1\cos\theta_i\psi_1^i - \beta_{21}K_1\cos\theta_{1R}\psi_1^R - \beta_{22}K_2\cos\theta_{2R}\psi_2^R - \frac{eK_o^2}{\omega^2 m_i \epsilon\epsilon_o}\sin^2\theta_{OR}\Pi_{om}^R = 0$$

Because the potential functions have exponential variation at z = 0, in order to meet the boundary conditions for all y,

$$K_1\sin\theta_i = K_1\sin\theta_{1R} = K_2\sin\theta_{2R} = K_o\sin\theta_{OR} = K\sin\theta_{OT}$$

which is a form of Snell's Law. By using these equations, considerable simplification may be achieved. We find that

$$\Pi_{om}^R = \Pi_{om}^T$$

Revising the symbolism to

$$\Pi_{om}^R = \Pi_{om}^T = \Pi^T$$

$$\psi_1^i = \psi^i$$

we may write

$$\begin{bmatrix} -\alpha_1 & \alpha_2 & i\left(\frac{K_o \cos\theta_{OR}}{\omega\epsilon\epsilon_o} + \frac{K\cos\theta_{OT}}{\omega\epsilon_o}\right) \\ \beta_{11}K_1\cos\theta_{1R} & \beta_{12}K_2\cos\theta_{2R} & -\frac{eK_o^2\sin^2\theta_{OR}}{\omega^2 m_e \epsilon\epsilon_o} \\ \beta_{21}K_1\cos\theta_{1R} & \beta_{22}K_2\cos\theta_{2R} & \frac{eK_o^2\sin^2\theta_{OR}}{\omega^2 m_i \epsilon\epsilon_o} \end{bmatrix} \times \begin{bmatrix} \psi_1^R \\ \psi_2^R \\ \Pi^T \end{bmatrix}$$

$$= \psi^i \begin{bmatrix} \alpha_1 \\ \beta_{11}K_1\cos\theta_i \\ \beta_{21}K_1\cos\theta_i \end{bmatrix}$$

The solution for the transmitted field in terms of the incident field is now straightforward, but messy. The final result is

$$\frac{\Pi^T}{\psi^i} = \frac{2\omega^2\epsilon\epsilon_o\alpha_1K_1K_2\cos\theta_i\cos\theta_{2R}(\beta_{11}B_{22} - \beta_{12}\beta_{21})}{A + iB}$$

where

$$A = -eK_o^2\sin^2\theta_{OR}\left[\alpha_1K_1\cos\theta_{2R}\left(\frac{\beta_{12}}{m_i} + \frac{\beta_{22}}{m_e}\right) + \alpha_2K_1\cos\theta_i\left(\frac{\beta_{11}}{m_i} + \frac{\beta_{21}}{m_e}\right)\right]$$

$$B = \omega K_1K_2\cos\theta_i\cos\theta_{2R}(K_o\cos\theta_{OR} + \epsilon K\cos\theta_{OT})(\beta_{11}\beta_{22} - \beta_{12}\beta_{21})$$

Because of the complexity of the preceding expression, one is forced to use numerical methods. The fact that the ion mode wave number exceeds the wave number of free space by a great deal means that transmission through the sharp boundary will take place within a very small cone of incidence angles; otherwise, total reflection occurs. Therefore, it will be more convenient to study the conversion in terms of the

angle of transmission, meanwhile realizing that the incident ion mode is nearly normal to the boundary. Using the Snell's Law relations, the preceding equation may be rewritten entirely in terms of the transmission angle with the substitutions

$$\theta = \theta_{0T}$$

$$\cos \theta_{0R} = \left[1 - \left(\frac{K}{K_o} \sin \theta\right)^2\right]^{\frac{1}{2}}$$

$$\cos \theta_{2R} = \left[1 - \left(\frac{K}{K_2} \sin \theta\right)^2\right]^{\frac{1}{2}}$$

$$\cos \theta_{i} = \left[1 - \left(\frac{K}{K_1} \sin \theta\right)^2\right]^{\frac{1}{2}}$$

$$\sin \theta_{0R} = \frac{K}{K_o} \sin \theta$$

Power Relationships. Recall from the ground plane study that, if $P_1 = \psi_1 e^{-i\vec{K}_1 \cdot \vec{r}}$, the power density for the ion mode is

$$|\vec{S}_1| = \frac{\omega |\psi_1|^2}{u_e^2 m_e N_o K_1}$$

The Poynting vector for the optical mode is

$$\vec{S}_o = \tfrac{1}{2} R_e[\vec{E}_o x \vec{H}^*]$$

Here, in the vacuum region

$$\vec{E}_o = \frac{iK^2 \sin \theta_{0T}}{\omega \varepsilon_o} [\cos \theta_{0T} \hat{u}_y - \sin \theta_{0T} \hat{u}_z] \Pi^T$$

$$\vec{H} = -iK \sin \theta_{0T} \Pi^T \hat{u}_x$$

Therefore, the normal component of power flow for the optical mode is

$$|S_{oz}| = \frac{K^3 \sin^2\theta_{0T} \cos\theta_{0T}}{\omega\epsilon_o} |\Pi^T|^2$$

Recalling that θ_i is very small, the ratio of normal power components is approximately

$$\left|\frac{S_o^T}{S_1^i}\right| \cong \frac{K^3 \sin^2\theta_{0T} \cos\theta_{0T} u_e^2 m_e N_o K_1}{\omega^2 \epsilon_o} \left|\frac{\Pi^T}{\psi^i}\right|^2$$

Numerical Results. The ratio of incident ion mode power to transmitted optical mode power was computed using plasma parameters that are somewhat typical of the stagnation region of a blunt body during high velocity reentry. These parameters were

$$u_e^2 = 2 \times 10^{11} \text{ m}^2/\text{sec}^2$$

$$u_i^2 = 2 \times 10^{7} \text{ m}^2/\text{sec}^2$$

$$m_e = 9.1 \times 10^{-31} \text{ kg}$$

$$m_i = 2.34 \times 10^{-26} \text{ kg (oxygen)}$$

$$N_o = 1.5 \times 10^{14} \text{ cm}^{-3}$$

Under these conditions the electron plasma frequency is

$$f_{pe} = 1.1 \times 10^{11} \text{ Hz}$$

The power conversion ratio was computed versus transmission angle for a number of frequencies, and Figures 34 through 39 were chosen as illustrative of the basic trends.

The first thing one notes about the rigid boundary results is that the magnitude of power conversion is quite low. This is in qualitative agreement with the results of Gallawa (1966) for a one-fluid plasma and with Dunphy, Kahn and Mintzer (1967) for a two-fluid plasma. Generally speaking, the overall conversion magnitude increases with increasing frequency until ω is of the same order as the ion plasma frequency (10^9). The power conversion increases several orders of magnitude as the transmission angle approaches 90 degrees, but never increases above 10^{-8}. As the signal frequency increases still further, a peak in the transmission pattern appears near 90 degrees and moves toward 0 degrees for increasing frequency; the overall conversion magnitude decreases with increasing frequency. This trend continues as ω increases.

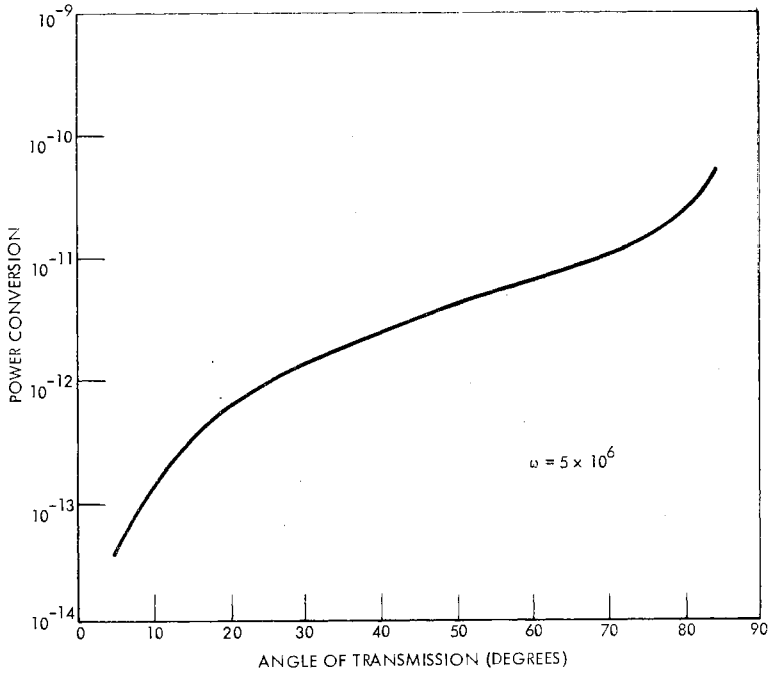

Figure 34. Power Conversion Vs. Angle of Transmission

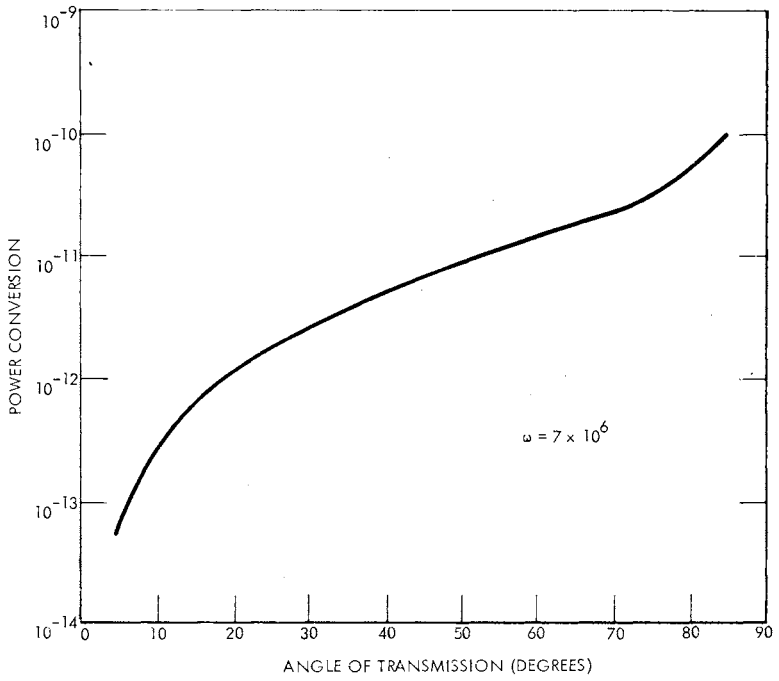

Figure 35. Power Conversion Vs. Angle of Transmission

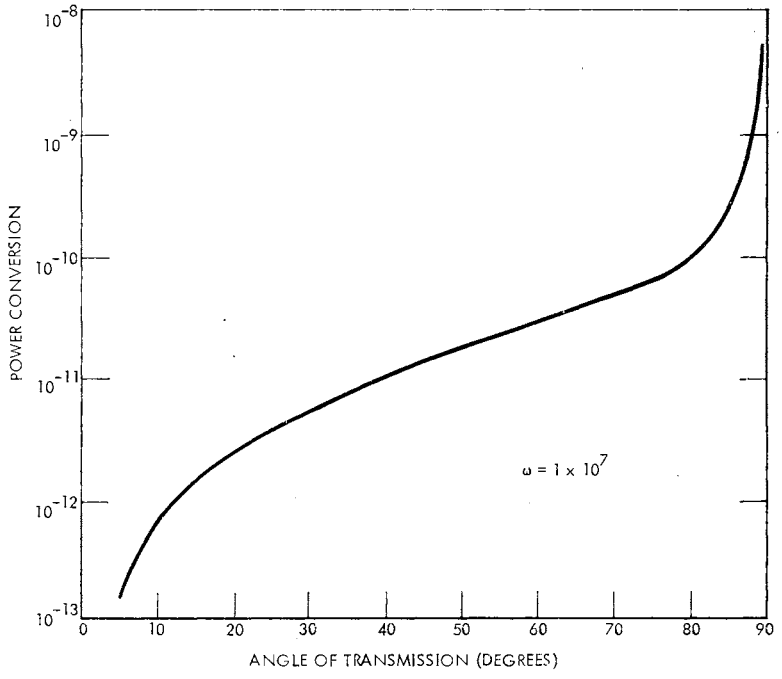

Figure 36. Power Conversion Vs. Angle of Transmission

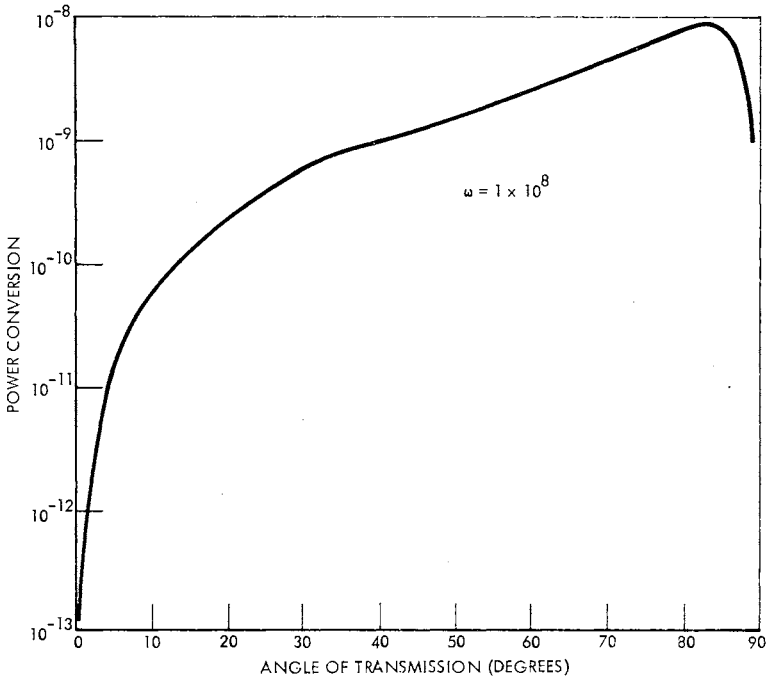

Figure 37. Power Conversion Vs. Angle of Transmission

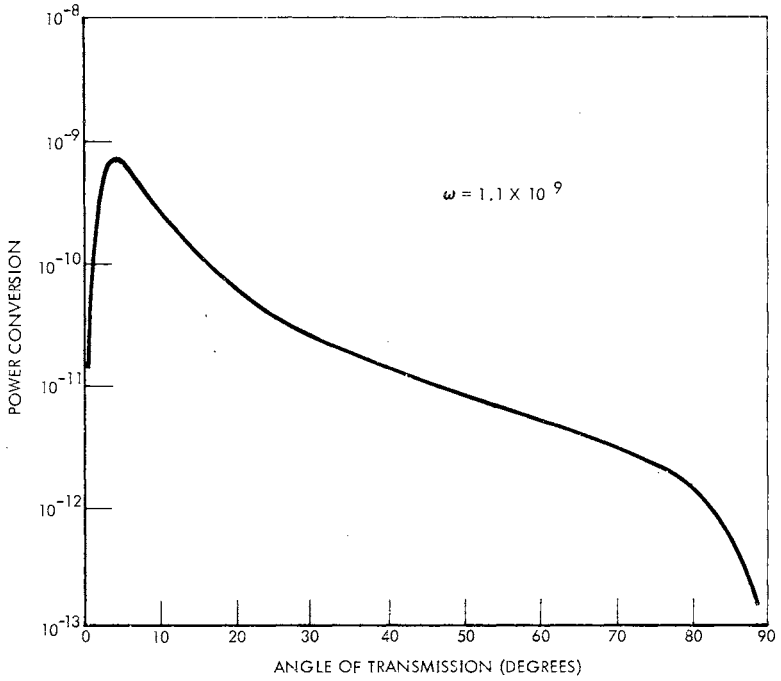

Figure 38. Power Conversion Vs. Angle of Transmission

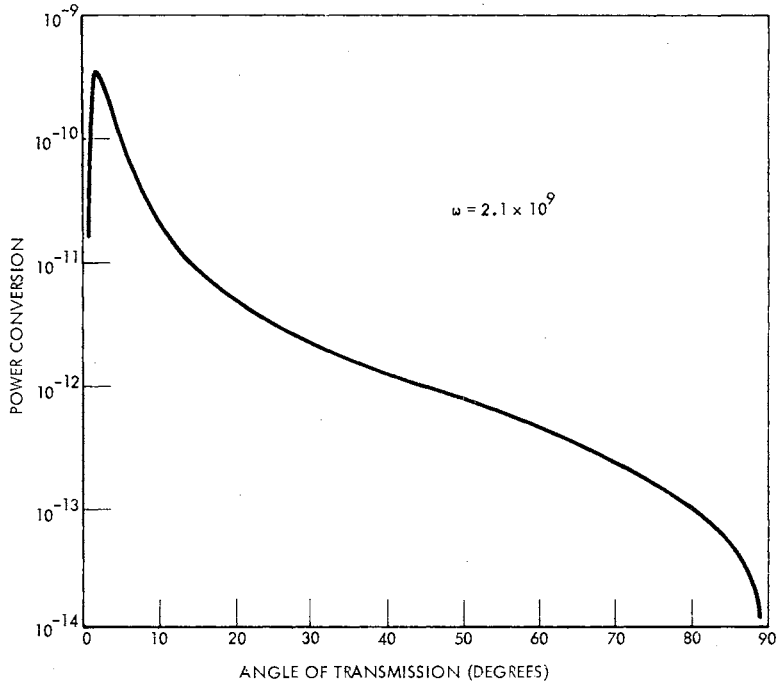

Figure 39. Power Conversion Vs. Angle of Transmission

5.3 Mode Conversion at a Hypersonic Shock Front

The preceding analysis concerned a sharp discontinuity in an equilibrium plasma with uniform temperature and density. This section will present some basic material which suggests that the sharp boundary model is inappropriate for the shock front and that better conversion from ion to optical mode radiation might be found in the real shock front.

A shock wave is a discontinuous change in velocity, pressure, density, etc. of a supersonic gas; the velocity entering the shock is supersonic, and that leaving is subsonic. The temperature, pressure, and density in the subsonic region can be obtained from those in the supersonic region by the Rankine-Hugoniot relations. The characteristic

of greatest importance here is that much of the energy of the supersonic flow goes into an instantaneous rise in temperature behind the shock wave; this increase in temperature occurs within about two collision lengths behind the shock and increases with increasing gas velocity relative to the shock.

For an ideal gas, the change in thermodynamic properties is instantaneous and predictable; however, many phenomena occur in a real gas with high internal energy that are not predicted by ideal gas theory. For temperatures below about 1000 °K, most of the internal energy is in translation and rotational states. However, as temperatures increase, progressively more and more of the energy goes into vibration, dissociation, electronic excitation, and ionization of the real gas molecules. These new energy states require an increasing number of collisions for adjustment, and both thermodynamic and ionization characteristics will vary with position behind the shock until relaxation is completed and thermodynamic equilibrium is established. The region between the start of the shock and the point of thermodynamic equilibrium behind the shock is called the "shock front." Because the shock front forms the real boundary which the ion mode signal encounters, the properties in the front are of intense interest. The following material on relaxation in shock fronts has been extracted from a paper by Shkarofsky, Johnston, and Bachynski (1959); the reader wishing a more complete discussion than that given here should consult their work.

The variation in gas temperature across the front will be considered first. When a shock wave impinges upon air, some of the shock's translational motion is converted into random translational motion of the molecules behind the shock; this amounts to an instantaneous rise in

temperature of the gas. If the thermal energy subsequently goes into other modes such as dissociation, the gas temperature falls. Because of large differences in the amount of time required for the various processes to reach equilibrium, they may be assumed to occur separately and consecutively. The gas temperature profile in the shock front may now be represented as in Figure 40.

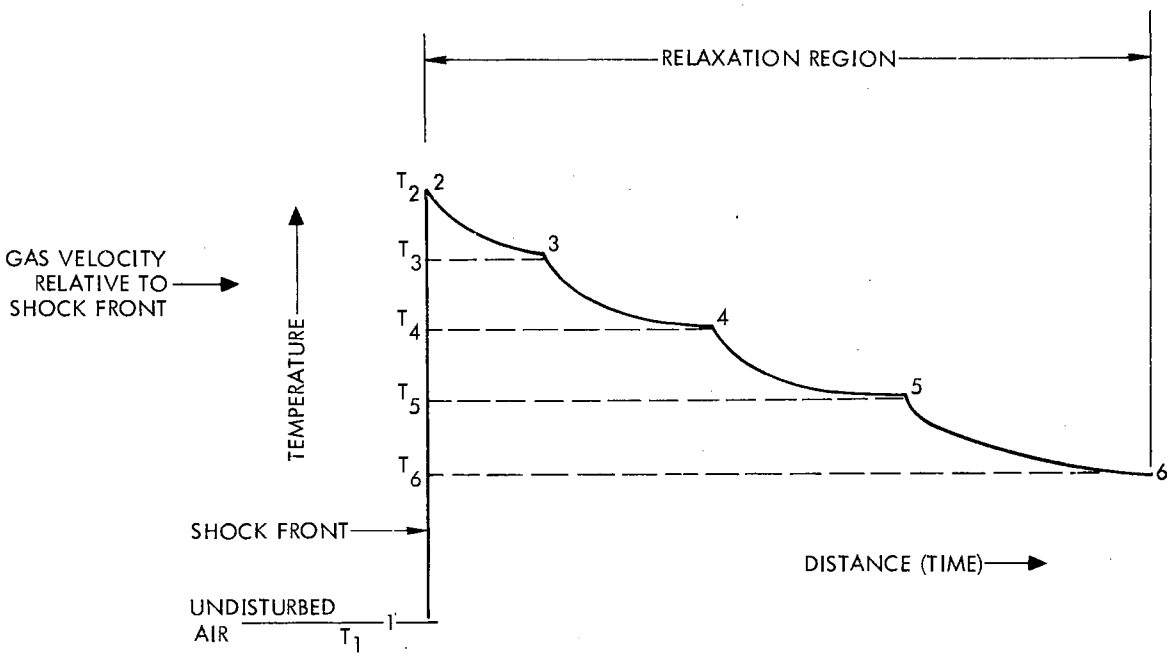

Figure 40. Temperature Profile Behind a Hypersonic Shock Front

Station 1 represents free-stream conditions ahead of the shock where translation and rotation are in equilibrium. Station 2 represents conditions behind, but very close to the shock wave where translation and rotation are again in equilibrium; however, vibration is just beginning to be excited. Dissociation of oxygen molecules occurs between Station 3 and 4. Nitrogen dissociates between Stations 4 and 5. At Station 5 the ionization of oxygen and nitrogen atoms becomes significant until the gas reaches thermodynamic equilibrium at Station 6.

The region of increasing ionization and decreasing gas temperature between Station 5 and 6 forms the boundary of the plasma sheath. Some ionization occurs prior to Station 5 because of atom-atom collisions. This process is important in that it governs the subsequent rate of ionization. However, at Station 5 ionization by electron-atom collisions becomes the dominant mechanism and rapidly overwhelms the atom-atom ionization. After some detailed considerations, Shkarofsky, Johnston, and Bachynski present the following electron density profile in the shock front (see Figure 41).

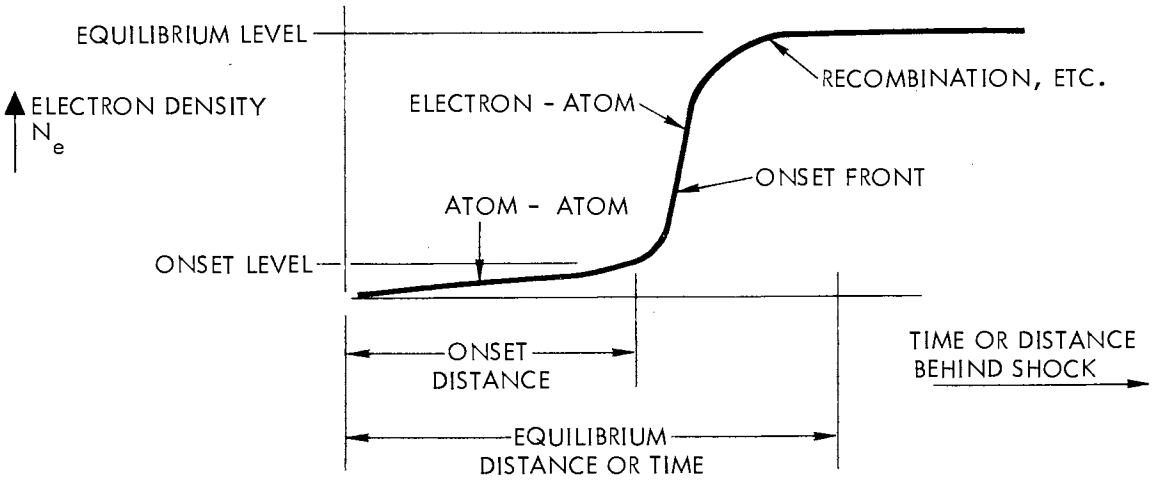

Figure 41. Electron Density Profile Behind a Hypersonic Shock Front

The electrons created by the ionization process initially have a relatively low temperature, whereas the gas temperature is high. However, equipartition of energy takes place between electrons, ions, and atoms by elastic collisions of electrons with the atoms and ions; therefore, the electron temperature will increase with increasing distance from the shock.

The qualitative nature of the plasma in a shock front may now be sketched as in Figure 42. Here T is the gas (ion) temperature and T_e is the electron temperature. The drop in gas temperature due to ionization is ΔT_I and ΔT_{μ_e} is the further drop required to bring the electron

temperature up to equilibrium.

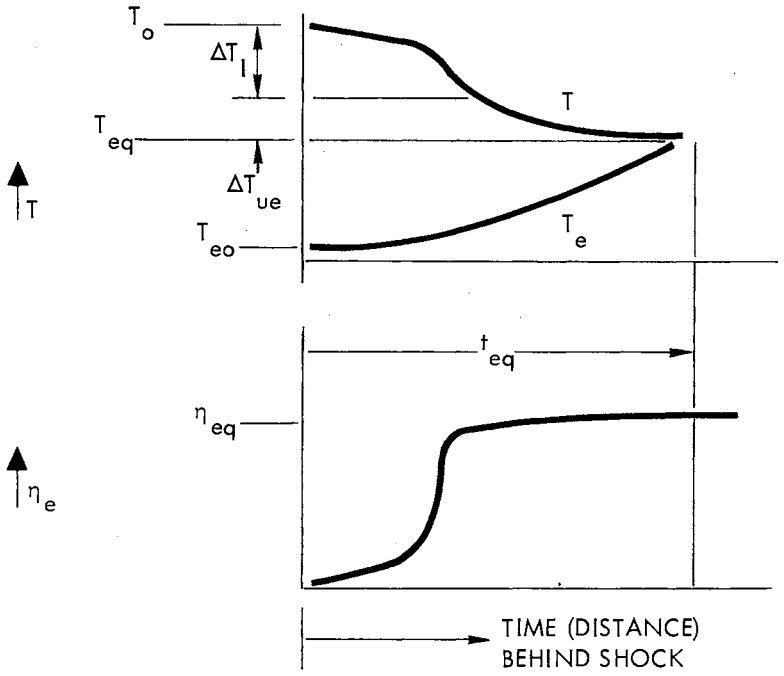

Figure 42. Comparison of Temperature and Electron Density Behind a Shock Front

We have now seen that the shock front as seen by an impinging ion mode wave is a nonequilibrium region of continuously decreasing electron density and electron temperature and continuously increasing ion temperature. Because the wave number of the ion mode is typically much greater than the free space wave number of the optical mode, the change in density and temperature may occur over many ion mode wavelengths. Since

the wave number of the ion mode depends on the densities and temperatures of the plasma, the index of refraction of the ion mode may be a continuous, slowly-varying function of position. Under these conditions the path of propagation curves smoothly as the ray moves through the front.

However, it appears difficult to say just how the wave number varies. To illustrate, recall the expression for K_1^2 derived earlier.

$$K_1^2 = \frac{\omega^2 m_i}{2u_e^2}\left\{\frac{1 - x_e}{m_i} + \frac{1 - x_i}{m_e} + \left[\left(\frac{1 - x_e}{m_i} + \frac{1 - x_i}{m_e}\right)^2 - \frac{4(1 - x_e - x_i)}{m_e m_i}\right]^{\frac{1}{2}}\right\}$$

The x_e and x_i terms are the normalized plasma frequencies and depend on the density of charged particles, which has been established relatively well. However, the difficulty occurs with the term representing the mean thermal velocity of the electrons

$$u_e^2 = \frac{3kT_e}{m_e} \qquad k = \text{Boltzmann Constant}$$

The assumption that electron and ion temperatures were equal, i.e.,

$$T_e = T_i = T$$

was implicit in the derivation of the electron and ion mode wave numbers; the relation $u_e^2 m_e = u_i^2 m_i = 3kT$ was employed at several steps in the derivation. This is clearly not the case in the shock front. Moreover, since the so-called ion mode is a hybrid combination of electron and ion particle pressures, it is not apparent at this point just what temperature should be used in the expression for the ion mode wave number. If $\omega >> \omega_{pe}$, the ion mode becomes essentially an ion particle

pressure wave, and one would heuristically expect that the ion temperature would be appropriate in such a case. However, in the blackout spectrum, electron and ion pressures are combined equally in the ion mode and probably neither T_e nor T_i is the correct temperature. A further complication is that the plasma in the front is not in equilibrium which contradicts assumptions used in deriving the basic plasma equations.

From the preceding discussion, it is apparent that the index of refraction for the ion mode wave varies continuously, if unpredictably, through the shock front profile. Field (1956) has shown that a gradient of the index of refraction in a compressible plasma produces coupling between the electroacoustic and optical modes. The reason for the coupling can be seen from the definition of the fields.

$$\vec{E} = \vec{E}_o + \vec{E}_p$$

where

$$\nabla \times \vec{E}_p = 0 \qquad \nabla \cdot \vec{E}_p \neq 0$$

$$\nabla \cdot \vec{E}_o = 0 \qquad \nabla \times \vec{E}_o \neq 0$$

Physically, the gradient in the index of refraction produces a bending in the lines of force (unless propagation is along the gradient), and thus a curl in the $\vec{E}$ field. Since $\nabla \times \vec{E}_p = 0$, the $\nabla \times \vec{E}$ produced is associated with an optical mode and mode conversion occurs as the electroacoustic mode propagates through the region.

Field (1956) comments that the mathematical procedure for treating small gradients in a one-fluid electron plasma is very involved. Such a

treatment of a two-fluid plasma would probably be quite formidable and inconclusive in view of the paucity of knowledge concerning the ion mode wave number in a real shock front.

Lacking an accurate mathematical description of mode conversion in a two-fluid diffuse boundary, some speculative statements can be made to compare sharp and diffuse boundary effects. When an ion mode wave impinges on a sharp boundary, most of the energy is reflected in the ion mode and very little is transmitted. Because the ion mode wave number is ordinarily several orders of magnitude greater than the free space wave number, the low transmission coefficient is not too surprising. In fact, electromagnetics is not the only realm in which waves incident upon a sharp boundary separating media of quite different intrinsic properties are almost totally reflected. This situation is contrasted with the one where the properties of the supporting media vary slowly with distance and reflection is greatly reduced. In view of this, it is not implausible that an ion mode wave may propagate through the shock front with little reflection and transfer energy into the optical mode with reasonable efficiency. Considering theoretical difficulties, conclusive statements will probably require experimental work.

Although definitive experimental work is lacking, some support for reasonable conversion efficiency may be drawn from the literature. Chen (1965) has theoretically shown that electroacoustic waves excited by a space vehicle in the ionosphere produce an enhancement of radar scattering which resembles the unusual observations of the CW reflected HF signal from satellites reported by Kraus, et al (1958a, 1958b, 1960). The sharp spikes observed in satellite radar cross section are apparently not predicted by conventional EM scattering theory, whereas the spikes

do appear if an electroacoustic wave is considered. If the efficiency of mode conversion were very small at the lower boundary of the ionosphere, one would expect that the contribution from the electroacoustic mode would not be apparent to an observer on the ground. The radar return would be almost entirely due to the optical mode alone. Therefore, this work provides some indication of a relatively efficient conversion process.

Further support comes from an experiment by Chen, Judson, and Lin (1967) which measured the input impedance and radiation pattern of a monopole immersed in a glass-enclosed plasma. Both the impedance and radiation patterns agreed well with the theoretical predictions and provided strong indications of the excitation of the electroacoustic mode. Although it was not stated in their paper, the experimental setup (see Figure 43) used in the study also indicates a reasonable mode conversion efficiency.

Theoretically, it can be demonstrated that if an electroacoustic wave is excited by the monopole, the radiation pattern will be end-fire, i.e. directed primarily along the antenna axis. This is in contrast with the broadside pattern of the optical mode. For ω slightly greater than ω_{pe}, the radiation patterns reported by Chen, et al, do have an end-fire lobe which is about 20 dB below the level of the broadside lobes, and the end-fire lobe is identified with an electroacoustic wave.

The significant idea here is that the electroacoustic wave must convert to an optical mode at the boundary of the plasma defined by the walls of the glass jar before it is observed by the receiving antenna. If something were known about the amplitude of the electroacoustic wave at the boundary, the magnitude of the mode conversion could be

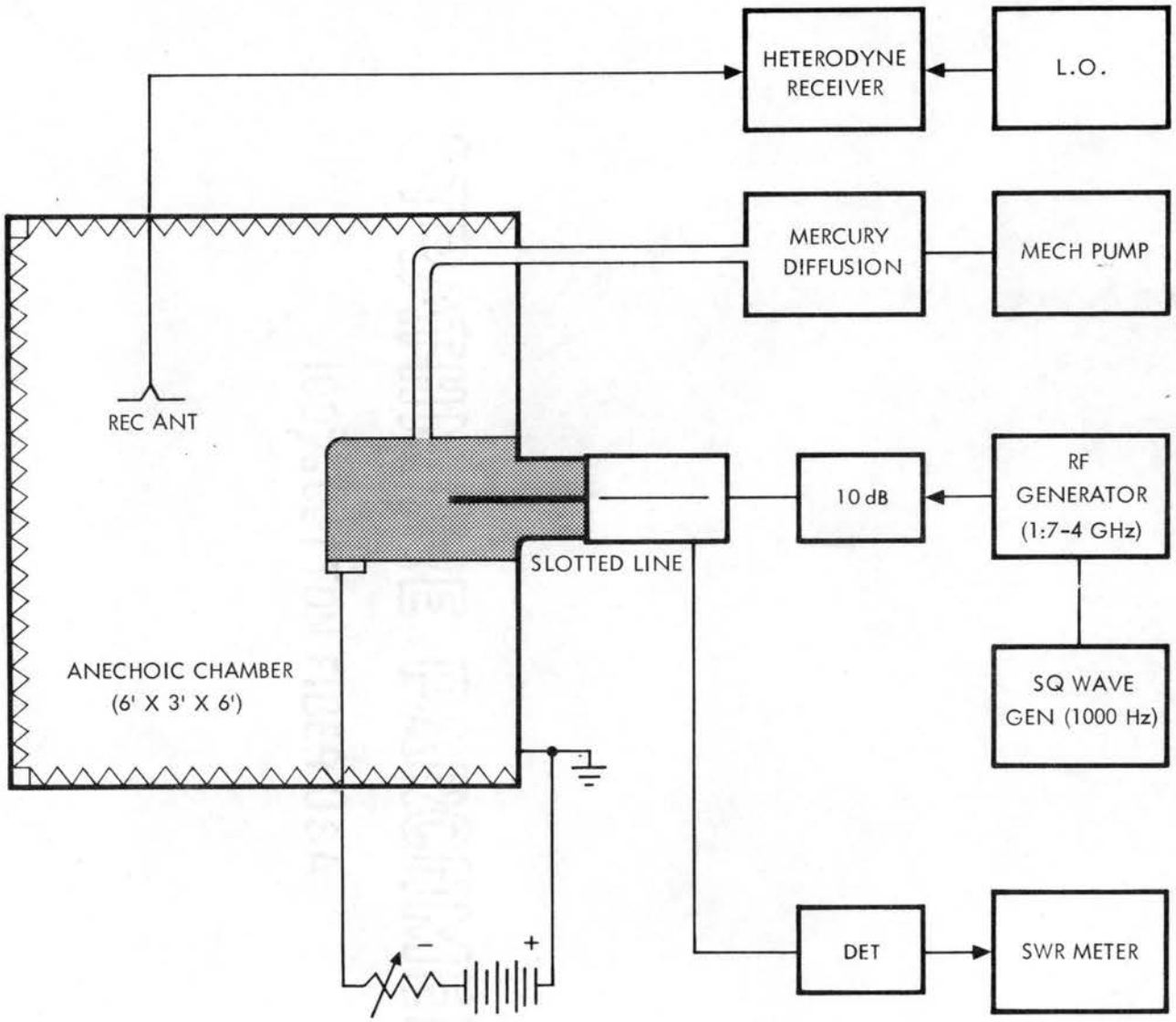

Figure 43. The Experimental Setup

estimated. As a first step in obtaining such information, it is noted that the radiation resistance measurements from this experiment are in close agreement with the theory by Chen (1964). According to this theory, for $0.7 < \left(\frac{\omega_p}{\omega}\right)^2 < 1.0$ the radiation resistance due to plasma mode radiation is greater than that due to the optical mode, but of the same order of magnitude. Other studies have predicted that the coupling into EA modes would be substantially larger; however, real-plasma effects such as the Debye sheath, absorption at the antenna surface, etc. have been ignored to reduce the complexity of the problem. Differences in theory notwithstanding, for the particular experimental conditions being discussed here, the radiation resistance is closely predicted by combining the usual radiated EM power from a cylindrical dipole with an electroacoustic power a few times larger. Keeping in mind that only a rough estimate of mode conversion efficiency is desired, assume that the EA power density leaving the vicinity of the monopole is a few times greater than the EM power density. Because the peak of the EA lobe was measured to be about 20 dB below the level of the EM lobes, it would appear that the loss in mode conversion is only about 25 dB, rather than the 80 dB or so from rigid boundary theory.

Further, before arriving at the outer boundary of the plasma, the EA wave must propagate for many wavelengths. During this time, one would expect the amplitude to decrease due to collisional losses and Landau damping. It is very difficult to say just how much loss is incurred over the propagation path; however, because the radiated EA power appears comparable with the EM power, any plasma mode losses present in the experiment would indicate a better conversion efficiency at the boundary. This is because the amplitude of the incident EA wave is

decreased relative to the incident EM wave.

Thus, it is seen that there are at least two experiments which support to some extent the statement that mode conversion at a plasma boundary may be a good deal greater than that predicted by the theory for a sharp, rigid plasma boundary. In the first experiment, the boundary was the lower side of the ionosphere; and in the second experiment, a plasma terminated at a glass wall. Probably neither boundary duplicates conditions in a shock front; however, the fact that an appreciable mode conversion is indicated at these diffuse boundaries offers some hope that conversion in the shock front will also be appreciable.

CHAPTER VI

SUMMARY AND ENGINEERING RECOMMENDATIONS

6.1 Summary

Chapter II discusses the basic properties of the hot two-fluid plasma model which is used to describe the electromagnetic characteristics of a reentry sheath. Plane wave dispersion relations are developed from the basic plasma equations; and, it is shown that the plasma will support a hybrid longitudinal or electroacoustic mode which will, in theory, propagate regardless of the charge density in the sheath. This mode is called the "ion mode". Examination of the boundary conditions at a sharp boundary indicates that an ion mode signal impinging upon a plasma discontinuity such as the outer boundary of the sheath will be partially converted into an electromagnetic mode which may propagate outside the sheath. Finally, the assumptions used in applying the two-fluid model to a reentry sheath are justified.

Chapter III discusses the theory of operation of the ion mode reentry communication system. In particular, the important questions of which type of antenna to use and where to place it are considered. Survivability considerations indicate that an aperture type antenna should be used, and propagation characteristics of the ion mode require that the antenna be placed in the stagnation region at the bow of the reentry vehicle. After discussing the theory of operation of the system, a

theoretical model is formulated to study the system characteristics.

The model considered first is a slab of plasma over a perfectly-conducting ground plane with an infinitesimal slot. However, because of the very burdensome algebra involved in the solution of this problem, further approximations are made. It is shown that conditions in an actual reentry sheath support to some extent the division of the slab problem into two simpler problems: (1) radiation by a slot into a plasma half space, and (2) mode conversion at a plasma-vacuum boundary. The approach taken in evaluating the practicality of the system then involves solving the ground plane problem to determine the ion mode radiation characteristics of an aperture, and considering the efficiency of conversion from ion mode to EM mode at the shock front.

Chapter III also outlines a method for approximating the EM radiation field by combining the results of the two simpler problems with proper phase and amplitude bookkeeping. This was not done, because the mathematical theory developed for mode conversion at a plasma boundary was felt to be inadequate to describe the processes at a real hypersonic shock front. Some justification for this is given in Chapter V.

Chapter IV is the solution for the radiation from a slotted ground plane into a two-fluid compressible plasma half space. The formal solution of the three simultaneous Helmholtz equations is carried out using Fourier transform techniques with the rigid boundary condition $\vec{v}\cdot\hat{n} = 0$. The resulting integrals are evaluated approximately by saddle point techniques to determine the fields in the radiation zone.

The discrete spectrum of the integrals was also considered to some extent. The complicated nature of the characteristic equation forced the use of numerical techniques. Computation of the poles of the

integrand for a signal frequency near the ion plasma frequency revealed the possibility of a surface wave with propagation constant slightly greater than the ion mode wave number. For the computed example, the amplitude of the surface wave was severely attenuated at typical shock detachment distances; this indicates that the illumination of the shock front will be almost entirely due to ion mode radiation. However, the large number of variables in a plasma sheath make it risky to conclude that the surface wave will be sufficiently attenuated in all reentry plasmas. Indeed, there is also the possibility of surface modes bound to the outer boundary at the shock front; this phenomena was obscured by the division of the slab problem into the two subproblems. Therefore, one of the criticisms of the analysis is the difficulty in dealing with surface modes.

The formal solutions for all three radiated modes were evaluated on a digital computer and a number of the computed radiation patterns are given in the text. Although numerous electron and optical mode patterns were included to demonstrate the reasonability of the computed results, the ion mode patterns for $\omega < \omega_{pe}$ are of greatest interest for the reentry communication system. The ion mode patterns show a pronounced broadside lobe which increases a great deal in intensity as signal frequency passes below the ion plasma frequency. The ion mode radiation is much smaller than the other modes for ω above the electron plasma frequency. The rigid boundary problem of Chapter V indicates that the ion mode radiation from the aperture is properly directed for greatest mode conversion efficiency.

Chapter V discusses mode conversion processes at a hypersonic shock front. A theoretical analysis of mode conversion at a sharp, rigid

boundary is presented first. The usual techniques for boundary value problems are employed to arrive at a formal solution, and the numerical results agree in character with those of other workers considering similar problems. Although the predicted conversion efficiencies were quite low, in the blackout spectrum the peak conversion efficiencies occur for transmission angles almost parallel to the boundary, i.e. almost normal to the velocity vector of the reentry craft. This would offer some hope of a peak in the radiation pattern in the direction of ground stations. If this were the case, a single ion mode aperture antenna would produce a wide-angle cone of EM radiation which could be linked with ground stations even for a spinning reentry body.

Chapter V goes on to explain some aspects of the physical processes inside an actual hypersonic shock front, and it is noted that the real boundary is diffuse rather than sharp and rigid. After a short discussion of gradient mode coupling versus rigid-boundary coupling, heuristic arguments are presented to support much better mode conversion efficiency at the real boundary. Although definitive experimental work is lacking, related experiments in the literature are drawn upon to give a much more optimistic picture than that resulting from rigid-boundary theory. Lack of an adequate mathematical theory of electromagnetic processes at a plasma discontinuity is a serious weakness in present knowledge; careful experiments will probably offer the best hope in this area for some time to come.

In defense of the approach taken in analyzing the ion mode system, by considering the aperture radiation, propagation, and mode conversion problems separately, one obtains a more detailed physical insight into the various processes involved in the system operation than that offered

by the slab problem, although at the expense of not having an entirely accurate picture of the overall radiation. It might be argued, though, that a solution of the much more burdensome problem of a plasma slab over a ground plane with a rigid-boundary condition might give a false feeling of accuracy in view of the serious weaknesses in modeling the processes at the shock front.

The theoretical analysis of the separated problem has indicated that: (1) an aperture antenna will radiate significant amounts of properly directed ion mode radiation for frequencies lower than the ion plasma frequency, which may be in the microwave spectrum for a dense sheath; and (2) the mode conversion at the outer boundary of the sheath may be reasonably efficient and provide a radiation pattern which allows the use of a single antenna on a spinning reentry body.

The remaining link in the theoretical evaluation of system practicality is the study of propagation losses for the ion mode in the reentry sheath. As noted in Chapter II, the losses were ignored in the basic equations to allow the diagonalization of an otherwise non-Hermitian matrix. Generally speaking, propagation losses will occur as Landau damping or collisional losses. For short wavelengths, Landau damping will predominate; whereas for long wavelengths, collisional attenuation will be the primary mechanism. This places an upper and lower bound on the operating frequency of the ion mode system. From a practical standpoint, one would like to operate at lower frequencies; this makes collision loss the main problem.

6.2 Engineering Recommendations

Based on the theoretical results of this investigation, the following approach is recommended for alleviating communications blackout during reentry of a blunt vehicle into an atmosphere.

The primary communication system should be an ordinary EM system operating from antennas located such that the onset of blackout is delayed as long as possible. For typical blunt reentry bodies, this is probably in the aft region to allow maximum reduction in charge density due to volumetric expansion, recombination, and electron attachment. The ion-mode aperture antenna should operate into the bow stagnation region with the axis of the aperture normal to the detached bow shock. By the time that the charge density in the aft portion of the sheath has increased sufficiently to create blackout for the primary antennas, the much higher charge density in the stagnation region should allow the aperture in the bow to operate near or below the ion plasma frequency for that region. As noted earlier, this is the condition for substantial ion mode radiation. The reverse process occurs as the vehicle slows down and sheath ionization abates. By the time that the aperture in the bow is operating well above the ion plasma frequency, the primary antennas should be out of blackout again.

A sketch of the total system concept is shown in Figure 44. The primary system consists of four apertures mounted at equal intervals around the aft section of the reentry body; this will tend to eliminate loss of radio contact due to spinning. The ion mode aperture is mounted in the bow. From the boundary studies of Chapter V, it may be cautiously stated that there is some hope for a wide-angle cone of EM radiation

from the ion mode antenna; such a cone would allow contact with ground stations even with spinning.

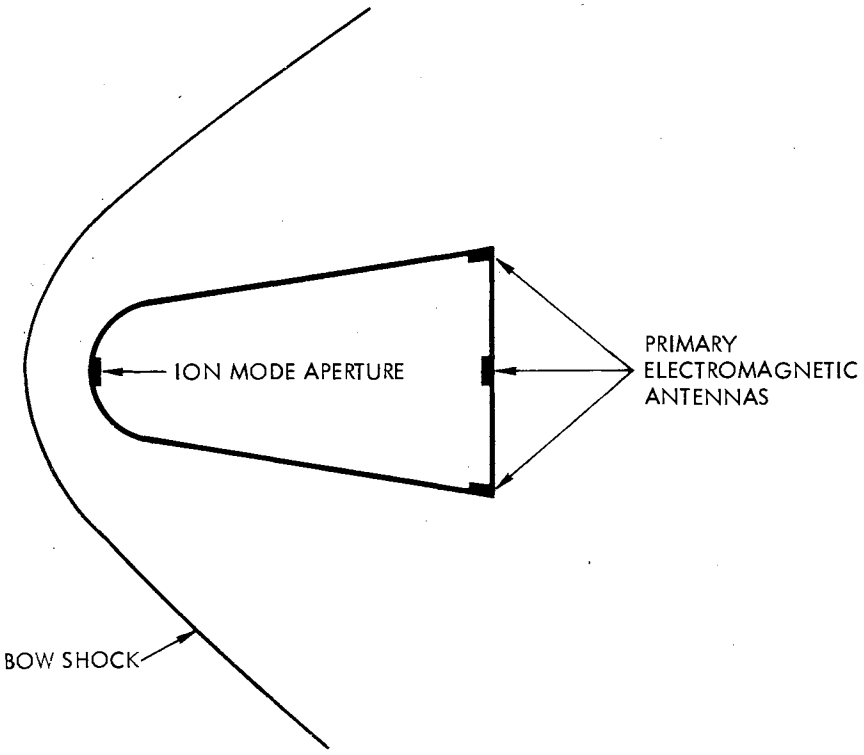

Figure 44. The Total System Concept

The choice of operating frequency should be based upon knowledge of mode propagation characteristics in the expected plasma for specific reentry missions. A substantial amount of both theoretical and experimental work is needed to adequately define this area for engineering purposes.

The vast number of papers and reports in the last decade related to reentry blackout indicates the intense interest generated by this problem. Discussions of the blackout problem have even reached the popular news media. It would seem that the particular merits of this thesis lie in the proposal of a novel approach for alleviating blackout and in the theoretical analysis of its practicality. In addition to this, the solution of the radiation problem in Chapter IV may be of some interest outside the reentry problem.

Finally, a great deal of work still remains, notably in the areas of electroacoustic mode propagation in real plasmas and mode conversion at a diffuse plasma boundary such as a shock front. Because of the complexity of these problems, an empirical approach, supported by theory where possible, seems to offer the best hope for a partial solution. Such research could have widespread implications, not only for the reentry problem, but also in the areas of telecommunications and astrophysics.

A SELECTED BIBLIOGRAPHY

Aksornkitti, S., H. C. S. Hsuan, and K. E. Lonngren (1967). "Properties of Ion Acoustic Waves in Mercury-Vapor Plasmas." 1967 IEEE G-AP International Symposium Digest, October, 1967, 164-165.

Caron, P. R., and G. E. Stewart (1964). "Radiation from a Line Source in a Ground Plane Covered by a Warm Plasma Slab." Aerospace Corporation, General Research Report No. ATN-64(9230)-3.

Chen, K. M., H. Judson, and C. C. Lin (1967). "Experimental Study on the Input Impedance and the Radiation Field of Cylindrical Antennas in a Compressive Plasma--Search for Electroacoustic Wave." 1967 IEEE G-AP International Symposium Digest, October 1967, 153-156.

Chen, Kun-Mu (1964). "Interaction of a Radiating Source with a Plasma." Proceedings of the IEE (London), 111, No. 10 (1964), 1668-1678.

Chen, Kun-Mu (1965). "Electroacoustic Waves Excited by a Space Vehicle in Ionized Atmosphere and Its Effect on Radar Return." Radio Science, 69D, No. 2 (February, 1965), 235-241.

Cohen, M. H. (1961). "Radiation in a Plasma I, Cerenkov Effect." Physical Review, 123 (1961), 711-715.

Cook, K. R. and B. C. Edgar (1966). "Current Distribution and Impedance of a Cylindrical Antenna in an Isotropic Compressible Plasma." Radio Science, Vol. 1 (January, 1966), 13-19.

Dunphy, K. H., D. Kahn, and D. Mintzer (1967). "Energy Coupling at a Two-Fluid Plasma Density Discontinuity." Physics of Fluids, 10, No. 1 (January, 1967), 162-171.

Felsen, L. B. and N. Marcuvitz (1959). "Modal Analysis and Synthesis of Electromagnetic Fields." Electrophysics Group Report R-776-59, PIB-705. Microwave Research Institute, Polytechnic Institute of Brooklyn, Brooklyn, New York, 1959.

Field, G. B. (1956). "Radiation by Plasma Oscillations." Astrophysics Journal, 124, No. 3, 555-570.

Friedman, B. (1956). Principles and Techniques of Applied Mathematics. New York: John Wiley, 1956.

Gallawa, R. L. (1965). "Propagation of Waves Across a Magnetoplasma-Vacuum Boundary." Radio Science, 69D, No. 6 (June, 1965), 807-817.

Gallawa, R. L. (1966). "Power Flow From a Plasma Having Complex Electroacoustic-Wave Impedance." Proceedings IEE (London), 113, No. 12 (December, 1966), 1927-1933.

Harrington, R. F. (1961). Time-Harmonic Electromagnetic Fields. New York: McGraw-Hill 1961.

Hessel, A., N. Marcuvitz, and J. Shmoys (1962). "Scattering and Guided Waves at an Interface Between Air and a Compressible Plasma." IEEE Transactions on Antennas and Propagation, AP-10, No. 1, 48-54.

Hodara, H. (1961). "The Use of Magnetic Fields in the Elimination of the Re-Entry Radio Blackout." Proceedings of the IRE, 49, No. 12 (December, 1961), 1825-1830.

Huber, P. W. and T. E. Sims (1964). "The Entry-Communications Problem." Astronautics and Aeronautics, Vol. 2, No. 10 (October, 1964), 30-40.

Kraus, J. D. (1958). "Detection of Sputnik I and II by CW Reflection." Proceedings of the IRE, 46, 611-612.

Kraus, J. D., R. C. Higgy, and W. R. Crone (1960). "The Satellite Ionization Phenomenon." Proceedings of the IRE, 48, 672-678.

Kraus, J. D., R. C. Higgy, and J. S. Albus (1958), "Observation of the U. S. Satellites Explorers I and III by CW Reflection." Proceedings of the IRE, 46, 1534.

Kritz, A. H. and D. Mintzer (1960). "Propagation of Plane Waves Across a Density Discontinuity." Physical Review, 117, No. 2, 382-386.

Lin, S. C. (1959). "Thermal Ionization Behind Shock Waves in Air." Electromagnetic Radiation in Hypersonic Environment, Pergamon Press.

Oster, L. (1960). "Linearized Theory of Plasma Oscillations." Review of Modern Physics, 32, No. 1, 141-168.

Pope, A. and K. L. Goin (1965). High-Speed Wind Tunnel Testing. Wiley: 1965.

Ridyard, H. W. (1959). "A Comparison of the Ionized Shock Layer About Two and Three Dimensional Blunt Shapes at Hypersonic Speeds." Electromagnetic Radiation in Hypersonic Environment, Pergamon Press.

Samaddar, S. N. (1964). "Excitation of Electro-acoustical Waves in a Two Fluid Compressible Plasma." Journal of Electronics and Control, 17, 267-272.

Seshadri, S. R. (1965). "Infinite Cylindrical Antenna Immersed in a Warm Plasma." Research Report Number 440. Applied Research Laboratory, Sylvania Electronic Systems. Waltham, Massachusetts: January 6, 1965.

Seshadri, S. R. (1965). "Radiation from Electromagnetic Sources in a Plasma." IEEE Transactions on Antennas and Propagation, January 1965.

Sessler, G. M. (1967). "Excitation and Measurement of Acoustic Ion Waves." Journal of the Acoustical Society of America, 42, No. 2 (August 1967), 360-366.

Shkarofsky, L. P., T. W. Johnston, and M. P. Bachynski (1959). "Relaxation Phenomena in Shock Fronts (A Review)." AFCRC-TR-60-108(I) (Unclassified). Electronics Research Directorate, Air Force Cambridge Research Center, Air Research and Development Command.

Spencer, D. F. (1964). "An Evaluation of the Communication Blackout Problem for a Blunt Mars-Entry Capsule and a Potential Method for Elimination of Blackout." Technical Report No. 32-594, Jet Propulsion Laboratory: April 15, 1964.

Stratton, J. A. (1941). Electromagnetic Theory. New York: McGraw-Hill, 1941.

Uman, M. A. (1964). Introduction to Plasma Physics. New York: McGraw-Hill, 1964.

Wait, J. R. (1964). "On the Theory of Reflection of Electromagnetic Waves from the Interface Between a Compressible Magneto-Plasma and a Dielectric." Radio Science, 68D, No. 11, 1187-1191.

Wait, J. R. (1964a). "Theory of a Slotted-Sphere Antenna Immersed in a Compressible Plasma." Part I. Radio Science, Vol. 1 (October, 1964), 1127-1136.

Wait, J. R. (1964b). "Theory of a Slotted-Sphere Antenna Immersed in a Compressible Plasma." Part II. Radio Science, Vol. 1 (October, 1964), 1137-1143.

Whale, H. A. (1963). "Excitation of Electroacoustic Waves by Antenna in the Ionosphere." Journal of Geophysical Research, 68, 415-422.

Whale, H. A. (1964). "Ion Sheath Effects Near Antennas Radiating Within the Ionosphere." Journal of Geophysical Research, 69, 447-455.

APPENDIX A

LINEARIZATION OF THE BASIC PLASMA EQUATIONS

The basic equations governing wave motion in an isotropic compressible plasma containing ℓ species of charged particles are:

$$\nabla\times\vec{H} - \epsilon_o \frac{\partial\vec{E}}{\partial t} = \sum_{i=1}^{\ell} N_i q_i \vec{V}_i \tag{A.1}$$

$$\nabla\times\vec{E} + \mu_o \frac{\partial\vec{H}}{\partial t} = 0 \tag{A.2}$$

$$\frac{\partial N_i}{\partial t} + \nabla\cdot(N_i\vec{V}_i) = 0 \tag{A.3}$$

$$N_i m_i\left[\frac{\partial V_i}{\partial t} + (\vec{V}_i\cdot\nabla)\vec{V}_i\right] = N_i q_i[\vec{E} + \mu_o(\vec{V}_i\times\vec{H})] - \nabla P_i \tag{A.4}$$

where

P_i = the ith specie pressure,

N_i = the ith specie density,

q_i = the ith specie charge,

$\vec{V}_i$ = the ith specie velocity,

m_i = the ith specie mass,

$\vec{E}$, $\vec{H}$ = the electric and magnetic field.

In the above form, the basic equations are nonlinear partial differential equations, and are virtually intractable. However, if it is assumed that the impressed electromagnetic fields are of small amplitude

linearization may be achieved.

Employing a perturbation approach, assume that the ith particle specie density and velocity may be expressed as the sum of a steady state value and a small amplitude time function. Thus

$$\begin{aligned} N_i &= N_{oi} + n_i \\ \vec{V}_i &= \vec{V}_{oi} + \vec{V}_{1i} \end{aligned} \tag{A.5}$$

$$\frac{\partial N_{oi}}{\partial t} = 0 \qquad \frac{\partial \vec{V}_{oi}}{\partial t} = 0$$

where

$$|N_{oi}| \gg |n_i| \qquad |\vec{V}_{oi}| \gg |\vec{V}_{1i}|$$

Invoking the ideal gas laws subject to adiabatic conditions,

$$P_i = N_i kT \qquad T = T_o \left(\frac{N_i}{N_o}\right)^{\gamma-1}$$

where

T = temperature of the plasma,

T_o = steady state plasma temperature,

γ = specific heat ratio,

k = gas constant.

More simply,

$$P_i = N_i kT_o \left(\frac{N_i}{N_{oi}}\right)^{\gamma-1} \tag{A.7}$$

Substituting the perturbation relations of Equation A.5 into Equations A.1, A.2, A.3, and A.7 and neglecting as small all nonlinear terms containing products of $\vec{V}_{1i}$ and n_i, we find

$$\nabla\times\vec{H} - \epsilon_o \frac{\partial\vec{E}}{\partial t} = \sum_{i=1}^{\ell} [N_{oi} q_i \vec{V}_{1i} + n_i q_i \vec{V}_{oi}] \tag{A.8}$$

$$\frac{\partial n_i}{\partial t} + N_{oi} \nabla\cdot\vec{V}_{1i} = 0 \tag{A.9}$$

$$N_{oi} m_i \frac{\partial\vec{V}_{1i}}{\partial t} = N_{oi} q_i \vec{E} - \nabla P_i \tag{A.10}$$

$$P_i = N_{oi} kT_o \left(1 + \frac{n_i}{N_{oi}}\right)^{\gamma-1} \tag{A.11}$$

Since by A.6

$$\left|\frac{n_i}{N_{oi}}\right| \ll 1$$

Equation A.11 may be approximated by

$$\begin{aligned} P_i &\doteq N_{oi} kT_o (1 + \gamma n_i / N_{oi}) \\ &= N_{oi} kT_o + \gamma n_i KT_o \end{aligned} \tag{A.12}$$

If the dynamic perturbation fields have three degrees of freedom, then $\gamma = 3$. Using the mean square thermal velocity for the ith particle specie

$$u_{oi}^2 = \frac{3kT_o}{m_i} \tag{A.13}$$

we have

$$P_i = N_{oi} kT_o + m_i u_{oi}^2 n_i \tag{A.14}$$

Since we have assumed that the plasma is described by Maxwell-Boltzmann

statistics, the drift velocity is zero. Therefore, the linearized basic equations are

$$\nabla \times \vec{H} - \epsilon_o \frac{\partial \vec{E}}{\partial t} = \sum_{i=1}^{\ell} N_{oi} q_i \vec{V}_{1i}$$

$$\nabla \times \vec{E} + \mu_o \frac{\partial \vec{H}}{\partial t} = 0$$

$$\frac{\partial n_i}{\partial t} + N_{oi} \nabla \cdot \vec{v}_{1i} = 0$$

$$m_i N_{oi} \frac{\partial V_{1i}}{\partial t} = N_{oi} q_i \vec{E} - m_i u_{oi}^2 \nabla n_i$$

$$P_i = N_{oi} K T_o + m_i u_{oi}^2 n_i$$

The first two equations are the source-free Maxwell equations, the third is the equation of continuity, the fourth is the force equation for a plasma fluid particle, and the last expression is the linearized equation of state.

APPENDIX B

BOUNDARY CONDITIONS AT A PLASMA DISCONTINUITY

(Rigid Boundary)

A derivation of the boundary conditions at a sharp, rigid interface between a plasma and air will be developed using the geometry in Figure B-1. It will be assumed that the interface separates warm plasmas of different densities; and the result for a plasma-air boundary follows by taking $N_1 = 0$.

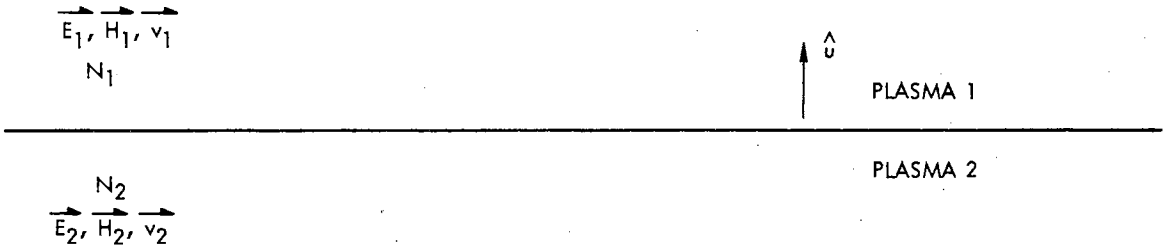

Figure B-1. A Discontinuity Separating Plasma Half-Space

From Appendix A, the linearized basic equations are

$$\nabla\times\vec{H} - i\omega\varepsilon_o\vec{E} = Ne(\vec{v}_i - \vec{v}_e) \tag{B.1}$$

$$\nabla\times\vec{E} + i\omega\mu_o\vec{H} = 0 \tag{B.2}$$

$$i\omega n_i + N_{oi}\nabla\cdot\vec{v}_i = 0 \tag{B.3}$$

$$i\omega n_e + N_{oe}\nabla\cdot\vec{v}_e = 0 \tag{B.4}$$

$$im_e\omega N_o\vec{v}_e = -N_o e\vec{E} - m_e u_e^2\nabla n_e \tag{B.5}$$

$$im_i\omega N_o\vec{v}_i = N_o e\vec{E} - m_i u_i^2\nabla n_i \tag{B.6}$$

Consider the continuity Equation, B.4, integrated over a regular volume containing the plasma boundary

$$\int_V \nabla\cdot(N_o\vec{v}_e)\,dv = -i\omega\int_V n_e\,dv$$

and apply the divergence theorem to show

$$\int_S N_o\vec{v}_e\cdot\hat{u}_n\,da = -i\omega\int_V n_e\,dv$$

where $\hat{u}_n$ is a unit vector normal to the surface bounding the volume. Assume that the boundary is time-invariant, i.e. "rigid", and let the volume of integration be the classical pillbox shown in Figure B-2.

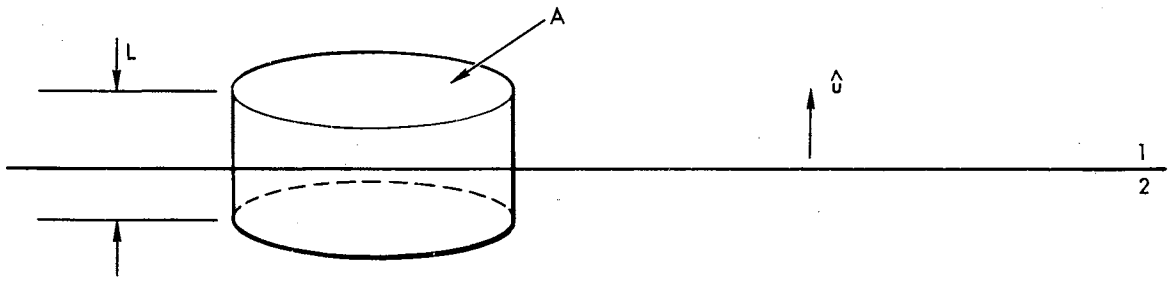

Figure B-2. The Volume of Integration

Allowing the dimension of the volume orthogonal to the boundary to approach zero, we have

$$\lim_{L\to 0} \int_S N_o \vec{v}_e \cdot \hat{u}_n \, da = -i\omega \lim_{L\to\infty} \int_V n_e \, dv$$

Because the electron density must be finite, the volume integral vanishes and

$$\hat{u} \cdot [N_{o1} \vec{v}_{e1} - N_{o2} \vec{v}_{e2}] = 0 \qquad \text{(B.7)}$$

An identical procedure starting with Equation B.3 yields

$$\hat{u} \cdot [N_{oi} \vec{v}_{i1} - N_{o2} \vec{v}_{i2}] = 0 \qquad \text{(B.8)}$$

where $\hat{u}$ is the unit normal vector from Region 2 to Region 1. Equations B.7 and B.8 describe continuity of mass flow across the boundary; this is contrasted with the continuity of velocity condition used by some writers.

Upon application of the classical technique of a contour integral of the Maxwell Equation B.1 about a rectangular path enclosing a length of the boundary as the height of the rectangle vanishes, we find

$$\hat{u}x[\vec{H}_1 - \vec{H}_2] = 0 \tag{B.9}$$

Likewise, from (2) the same procedure yields

$$\hat{u}x[\vec{E}_1 - \vec{E}_2] = 0 \tag{B.10}$$

where the boundary is assumed source-free.

If Region 1 is assumed to be neutral gas, $N_1 = 0$ and the linearized boundary conditions become

$$\begin{aligned} \hat{u}x[\vec{E}_1 - \vec{E}_2] &= 0 \\ \hat{u}x[\vec{H}_1 - \vec{H}_2] &= 0 \\ \hat{u}\cdot[N_{o1}\vec{v}_{e1} - N_{o2}\vec{v}_{e2}] &= 0 \\ \hat{u}\cdot[N_{o1}\vec{v}_{i1} - N_{o2}\vec{v}_{i2}] &= 0 \end{aligned} \tag{B.11}$$

The set of Equations B.11 provide a basis for dealing with propagation in warm plasma as a boundary value problem. However, it is not intuitively obvious that a real boundary between a plasma and air is indeed rigid. Moreover, for Equations B.11 to apply, the transition between plasma and air must occur over a distance that is short relative to any wavelength involved; due to the very short electroacoustic wavelengths, this may often be a serious limitation of the theory.

VITA

Robert Byron Buchanan

Candidate for the Degree of

Doctor of Philosophy

Thesis: AN ION MODE REENTRY COMMUNICATION SYSTEM

Major Field: Engineering

Biographical:

Personal Data: Born in Omaha, Nebraska on December 2, 1941, the son of Howard B. and Verna Buchanan.

Education: Attended numerous grade schools; graduated from Wichita High School West in 1959; received the Bachelor of Science degree from the Wichita State University, with a major in Electrical Engineering, in June, 1963; received the Master of Science degree from the Oklahoma State University, with a major in Electrical Engineering, in June, 1965; completed requirements for the Doctor of Philosophy degree in May, 1968.

Professional Experience: Entered the U. S. Marine Corps Reserve in 1961 and served as a radio repair instructor until discharge in 1967. Employed by the Department of Electrical Engineering of the Wichita State University as a departmental assistant during 1963. Employed by the King Radio Corporation during the summer of 1963. Employed by the Tulsa Division of the North American Rockwell Corporation since the summer of 1964.

Professional and Honorary Organizations: Member of Tau Beta Pi and Sigma Pi Sigma.